ACCEPTED MANUSCRIPT

Journal of Applied Physics

This is the author's peer reviewed, accepted manuscript. However, the online version of record will be different from this version once it has been copyedited and typeset.
PLEASE CITE THIS ARTICLE AS DOI: 10.1063/5.0081067

AIP Publishing

Laser-controlled ultrafast nonlinear optical responses of interacting e-h pairs in electromagnetically-coupled GaAs quantum dots

Xuejun Lu[1], Danhong Huang[2]*, and Jeremy R. Gulley[3]
[1] *Department of Electrical & Computer Engineering, Francis College of Engineering, University of Massachusetts Lowell, Lowell, Massachusetts 01854, USA*
[2] *US Air Force Research Laboratory, Space Vehicles Directorate (AFRL/RVSU), Kirtland Air Force Base, New Mexico 87117, USA*
[3] *Department of Physics, Kennesaw State University, Kennesaw, GA 30144, USA*
(Dated: January 14, 2022)

In this paper, by applying generalized density-matrix equations, we explore the ultrafast dynamics of photo-generated electron-hole pairs in the system composed of electromagnetically-coupled GaAs/AlGaAs quantum dots, and reveal the physics mechanism behind laser-controlled nonlinear-optical response of electron-hole pairs. For the single-dot system, we present numerical results to show the transient dependence of carrier occupations and induced quantum coherence of electron-hole pairs in the presence of either a single or double laser pulses, as well as for a step turning-on of laser field. For a dipole-radiation coupled double-dot system, we study numerically the time dependence of both intradot and interdot self-consistent depolarization fields within and between two dots, respectively. Meanwhile, we further demonstrate the significance of phase matching between induced depolarization fields and incident-laser pulse in order to maximize the stimulated transitions of electron-hole pairs and ensure non-quenched Rabi oscillations in each quantum dot. The employed theoretical model and associated numerical analysis method are expected to facilitate designing and developing artificial quantum molecules composed of arbitrarily dielectric-embedded quantum dots with non-local quantum interactions and entanglement, as well as optically manipulating electron states of artificial quantum molecules.

I. INTRODUCTION

Ultrafast and strong interactions of matter and electromagnetic field are of great interests in both theoretical physics and practical applications, including high-speed optically-controlled electron states, energy-level shift and modulation due to the strong light-matter interaction, as well as electromagnetic field-induced spatial quantum coherence and entanglement. In a previous study,[1] we have investigated the strong light and GaAs quantum dot interactions, which established a simple and transparent depolarization-field model, and then, applied it to study Rabi-oscillation dynamics[2] for level occupations and induced quantum coherence of electrons in both single and double quantum dots under laser irradiation. Here, in order to resolve the transient Rabi oscillations within the width of a laser pulse, the Rabi frequency, which is proportional to the laser-field strength, must be large enough so that its inverse becomes smaller than this pulse width. Meanwhile, the induced quantum coherence will be enhanced since it is proportional to the laser pulse intensity. However, this simplified model limits itself by treating both self-consistent depolarization field and dot-to-dot coupling phenomenologically. On the other hand, by combining with a self-consistent electric-dipole-radiation coupling model[3], we apply the generalized density-matrix equations (GDMEs)[4–10] in this work so as to evaluate accurately ultrafast field-interaction dynamics[9,11,12] of electron-hole pairs in multiple-quantum-dot systems. From this study, we demonstrate that bandedge[4–8] and optical[13–18] nonlinearities result from stimulated interband transition and from self-sustained depolarization field[19–24], respectively.

For a light-interacting semiconductor electronic system,[26] the presence of an interacting optical field can be treated either perturbatively[19–24] or self-consistently[4–8,10] for non-steady and non-equilibrium electron states. For the former, the *total electromagnetic field* interacting with electrons is simply taken as a given incident optical field.[23,24] For the latter, however, the total electromagnetic field must be included as a sum of the incident optical field and the undetermined induced depolarization field as well.[7,8] Such a self-sustaining depolarization field originates from the density fluctuations[22–24,27] in the system, and should be obtained self-consistently[7,28,29] from the induced charge-density fluctuations due to electron interaction with the total electromagnetic field. The self-consistent model offers a more accurate study of the system especially for strong interactions and non-equilibrium systems.

In order to find the induced depolarization field in the system, we usually employ a quantum-statistical theory[27,29] to associate a microscopic quantum coherence of electrons[4,5,8], i.e., the off-diagonal elements of a density matrix[29], with

* E-mail contact: danhong.huang@spaceforce.mil

ACCEPTED MANUSCRIPT
Journal of Applied Physics
AIP Publishing
This is the author's peer reviewed, accepted manuscript. However, the online version of record will be different from this version once it has been copyedited and typeset.
PLEASE CITE THIS ARTICLE AS DOI: 10.1063/5.0081067

a macroscopic optical-polarization field [3] introduced in the Maxwell's electromagnetic theory. Practically, by making use of a linear-response theory [27,29,30] to calculate the optical-polarization field as part of the total electromagnetic field, we are left with a self-consistent linear equation with respect to the total and incident electromagnetic fields. [7,28] Fundamentally, however, we should utilize GDMEs [8] to relate quantum-mechanically the induced optical-polarization field to the total electromagnetic field beyond the linear-response regime, even incorporating into a back action [8] of electrons in quantum dots exerted onto interacting laser photons, and vice versa.

In comparison with the conventional DMEs [4,5,9,11,12], the GDMEs [7,8] are a joint quantum-dynamical model to deal with both optical transitions [4,5] and the nonlinear transport [31–33] of electrons within the same frame. Here, this unified quantum-dynamical theory is applied to study strong interactions [8] between an ultrafast light pulse and drifting electrons in an electronic system beyond the perturbation scheme. It is found that the electron excitations in these systems are optically nonlinear [13–18], temporally non-adiabatic [34], and spatially non-local [27]. Furthermore, the electrons and holes are expected to stay in non-thermal states and are described by extreme non-equilibrium (or non-thermal) distributions. [8] In order to couple DMEs with Maxwell equations, both propagating transverse and localized longitudinal electric fields must be considered simultaneously. Moreover, the DMEs are generalized to account for the drifting of electrons under a net driving force including electron momentum dissipation [33,35,36] due to back-scattering [37] with impurities [38], lattice phonons [39] and other electrons [40] based on a linearized Boltzmman transport equation [41]. The theoretical model and the ultrafast study of the nonlinear, non-adiabatic and quantum interactions enable the design and development of artificial quantum molecules composed of arbitrarily located quantum dots with nonlocal quantum interactions and entanglement as well as optically manipulating the electron states of the artificial quantum molecules.

Density-matrix theory has widely been used to study linear-optical responses of electrons in low-dimensional semiconducting systems, including quantum dots, [42–44] quantum wires [19,45,46] and quantum wells [47–49]. For a quantum dot having a high spatial symmetry, such as a cubic (or a spherical) one, each discrete energy level can accommodate up to six energy-degenerate electrons with different spins and orbits in the absence of a magnetic field [50] and a spin-orbit coupling [51], giving rise to twelve e-h pairs totally in a two-level single quantum dot. To deal with this quasi-many-body system, however, the application of a density-matrix theory is usuall regarded as a practical approach for investigating very complex ultrafast electron dynamics either inside a tunneling structure [52] or under an ultrafast laser pulse [7] beyond the perturbation regime. Meanwhile, the screening of Coulomb interactions [27] between charged particles in quantum dots decreases in comparison with other low-dimensional quantum wire, quantum well and bulk systems acquiring continuous electronic bands, due to reduced number of available free electrons and holes inside a quantum dot. Therefore, the exciton binding energy in a quantum dot is expected enhanced for a colloidal CdSe quantum dot. [53], reaching as high as from 100 meV to 1000 meV. For a spherical GaAs semiconductor quantum dot, on the other hand, the exciton binding energy becomes much smaller on the order of ~ 8.7 meV. [54] As a result, exciton effect in GaAs quantum dots will be unresolved at room temperature. Correspondingly, we will neglect exciton effect thereafter. Although there are only few electrons in a quantum dot, the charge density for Coulomb interaction is still appreciable due to very small volume of a quantum dot. Moreover, in our generalized density-matrix theory, Hartree and exchange interactions are included semi-classically and quantum-mechanically in renormalized energies of electrons and holes by introducing a density-distribution function [19] at temperatures above 150 K, [25] along with energy relaxations of electrons and holes within the second-order Born approximation [7]. Particularly, the higher-order correlation effects of electrons and holes can further be taken into account while solving the time evolution of an off-diagonal density-matrix element by applying the self-consistent-field method [24,48] for an induced depolarization field as part of the total electromagnetic field [8] interacting strongly with non-equilibrium electrons in quantum dots.

The rest of paper is organized as follows. In Sec. II A, we put forward the GDMEs for a single QD interacting with a pulsed-laser field, including optical interaction exerted by a self-consistently induced depolarization field. Additionally, electromagnetic interdot coupling is also introduced self-consistently in Sec. II B for a multi-dot system. Numerical results based on our GDMEs are presented in Sec. III A for Rabi oscillations in occupation factors, induced quantum coherence and stimulated transition of single quantum dot, for transient energy-relaxation and spontaneous-emission rates, as well as for time-domain optical nonlinearity resulting from electromagnetic interdot coupling. The numerical results for effect of electromagnetic coupling of double quantum dots on ultrafast electron dynamics are also presented in Sec. III B for comparison. Finally, a brief summary is given in Sec. IV along with some remarks.

II. MODEL AND THEORY

In Sec. II A, we present the GDMEs for a single GaAs quantum dot (QD) to study ultrafast interaction and scattering dynamics of a photo-generated interacting e-h pairs in the presence of a femetosecond laser pulse. [7] Using calculated Coulomb-renormalized dynamical interband dipole-moment for a single GaAs dot, we further generalize single-dot

ACCEPTED MANUSCRIPT
Journal of Applied Physics
AIP Publishing
This is the author's peer reviewed, accepted manuscript. However, the online version of record will be different from this version once it has been copyedited and typeset.
PLEASE CITE THIS ARTICLE AS DOI: 10.1063/5.0081067

GDMEs by including multi-dot electric-dipole-radiation couplings in Sec. II B, which adds a self-consistent multi-dot depolarization field to the GaAs single-dot one.

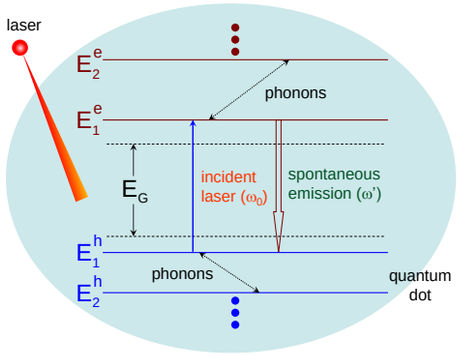

FIG. 1: Illustration for photo-generation of electron (e) and hole (h) pairs in a GaAs quantum dot by an incident laser field with a frequency ω_0 in resonance with the two lowest e and h energy levels in a four-level system. Here, $E_{\rm G}$ is the bandgap of host semiconductor, $E_\ell^{\rm e}$ and $E_j^{\rm h}$ stand for quantized electron (ℓ) and hole (j) energy levels with ℓ, $j = 1, 2$. Photons with frequency ω' are emitted between $\ell = 1$ and $j = 1$ energy levels. Meanwhile, the lower $\ell = 1$ and $j = 1$ levels are coupled, respectively, to the upper $\ell = 2$ and $j = 2$ levels by longitudinal-optical phonons in the system.

A. Single-Dot Generalized Density-Matrix Equations

As depicted in Fig. 1, we consider a four-level QD model for photo-generated electron ($E_{1,2}^{\rm e}$) and hole ($E_{1,2}^{\rm h}$) pairs, where an incident pulsed-laser field with its central frequency ω_0 couples $E_1^{\rm e}$ and $E_1^{\rm h}$ energy levels, and meanwhile, the spontaneously-emitted photons with frequency ω' appear between the same two levels. Furthermore, the emission and absorption of longitudinal-optical phonons at finite temperatures T facilitate the intraband energy relaxations of electrons ($E_{1,2}^{\rm e}$) and holes ($E_{1,2}^{\rm h}$).

For photo-excited spin-degenerated electrons in a QD with energy-level index $\ell = 1, 2$, GDMEs take the form [7,8,25]

$$\frac{dn_\ell^{\rm e}(t)}{dt} = \frac{2}{\hbar}\sum_{j=1}^{2}{\rm Im}\left\{\left[Y_\ell^j(t)\right]^*\widetilde{\mathcal{M}}_{\ell,j}^{\rm eh}(t)\right\} + \left.\frac{\partial n_\ell^{\rm e}(t)}{\partial t}\right|_{\rm rel} - \mathcal{R}_\ell^{\rm sp}(t)\,n_\ell^{\rm e}(t)\,n_\ell^{\rm h}(t)\ , \tag{1}$$

where $\widetilde{\mathcal{M}}_{\ell,j}^{\rm eh}(t) = \mathcal{M}_{\ell,j}^{\rm eh}(t) - Y_\ell^j(t)\,V_{\ell,j;j,\ell}^{\rm eh}(t)$ is the Coulomb-renormalized Rabi coupling, $\mathcal{R}_\ell^{\rm sp}(t)$ stands for the ℓth-level spontaneous-emission rate of e-h pairs, and $n_\ell^{\rm e}(t)$ and $n_j^{\rm h}(t)$ are the transient electron and hole level-occupation numbers. In Eq. (1), the first term on its right-hand-side corresponds to the stimulated transition [4] of electrons, whereas the term marked 'rel' refers to the non-radiative intraband energy relaxation [7] for $n_\ell^{\rm e}(t)$. The other quantities, such as $Y_\ell^j(t)$, $\mathcal{M}_{\ell,j}^{\rm eh}$ and $V_{\ell,j;j,\ell}^{\rm eh}$, will be defined later in the text.

Similarly, for spin-degenerate holes in a QD with energy-level index $j = 1, 2$, GDMEs give rise to [7,8,25]

$$\frac{dn_j^{\rm h}(t)}{dt} = \frac{2}{\hbar}\sum_{\ell=1}^{2}{\rm Im}\left\{\left[Y_\ell^j(t)\right]^*\widetilde{\mathcal{M}}_{\ell,j}^{\rm eh}(t)\right\} + \left.\frac{\partial n_j^{\rm h}(t)}{\partial t}\right|_{\rm rel} - \mathcal{R}_j^{\rm sp}(t)\,n_j^{\rm e}(t)\,n_j^{\rm h}(t)\ , \tag{2}$$

where the non-radiative intraband energy relaxation for $n_j^{\rm h}(t)$ is also included. From Eqs. (1) and (2), it is clear that

$$N_{\rm e}(t) = g_0\sum_\ell n_\ell^{\rm e}(t) = g_0\sum_j n_j^{\rm h}(t) = N_{\rm h}(t)\ , \tag{3}$$

where $g_0 = 2\times 3$ represents the total spin-orbit degeneracy, and $N_{\rm e}(t)$ and $N_{\rm h}(t)$ are the transient effective total numbers of photo-generated electrons and holes within a QD.

ACCEPTED MANUSCRIPT
Journal of Applied Physics
AIP Publishing
This is the author's peer reviewed, accepted manuscript. However, the online version of record will be different from this version once it has been copyedited and typeset.
PLEASE CITE THIS ARTICLE AS DOI: 10.1063/5.0081067

Finally, for a spin-averaged e-h pairs under the rotation-wave approximation, its induced interband quantum coherence $Y_\ell^j(t)$, introduced in Eqs. (1) and (2), with j, $\ell = 1, 2$ satisfies [7,8,25]

$$\begin{aligned} i\hbar\frac{d}{dt}Y_\ell^j(t) &= \left[E_{\rm G}(T)+E_\ell^{\rm e}+E_j^{\rm h}-\hbar(\omega_0+i\gamma_{\rm dp})\right]Y_\ell^j(t)+\left[1-n_\ell^{\rm e}(t)-n_j^{\rm h}(t)\right]\widetilde{\mathcal{M}}_{\ell,j}^{\rm eh}(t) \\ &+ Y_\ell^j(t)\left\{\sum_{j_1=1}^{2}n_{j_1}^{\rm h}(t)[V_{j,j_1;j_1,j}^{\rm hh}(t)-V_{j,j_1;j,j_1}^{\rm hh}(t)]-\sum_{\ell_1=1}^{2}n_{\ell_1}^{\rm e}(t)\,V_{\ell_1,j;j,\ell_1}^{\rm eh}(t)\right\} \\ &+ Y_\ell^j(t)\left\{\sum_{\ell_1=1}^{2}n_{\ell_1}^{\rm e}(t)[V_{\ell,\ell_1;\ell_1,\ell}^{\rm ee}(t)-V_{\ell,\ell_1;\ell,\ell_1}^{\rm ee}(t)]-\sum_{j_1=1}^{2}n_{j_1}^{\rm h}(t)\,V_{\ell,j_1;j_1,\ell}^{\rm eh}(t)\right\} \\ &\equiv \left[E_{\rm G}(T)+\overline{E}_\ell^{\rm e}(t)+\overline{E}_j^{\rm h}(t)-\hbar(\omega_0+i\gamma_{\rm dp})\right]Y_\ell^j(t)+\left[1-n_\ell^{\rm e}(t)-n_j^{\rm h}(t)\right]\widetilde{\mathcal{M}}_{\ell,j}^{\rm eh}(t)\ , \end{aligned} \tag{4}$$

where $E_{\rm G}(T) = E_{\rm G}(0) - 5.41\times10^{-4}\,T^2/(T+204)$ (in units of eV) is the temperature-dependent bandgap of host semiconductor, $\gamma_{\rm dp}$ stands for the diagonal dephasing rate [4,8], ω_0 is the pulsed-laser central frequency, and $E_\ell^{\rm e}$ and $E_j^{\rm h}$ are single-particle energy levels of e-h pairs in a QD [calculated in Eq. (A4)]. For single QD, we define $\delta_0 = [E_{\rm G}(T)+E_1^{\rm e}+E_1^{\rm h}-V_{1,1;1,1}^{\rm eh}]-\hbar\omega_0$ as frequency detuning and $\Delta(t) = \overline{E}_\ell^{\rm e}(t)+\overline{E}_j^{\rm h}(t)-(E_\ell^{\rm e}+E_j^{\rm h})$ is the Coulomb correction to δ_0. Here, $\delta_0<0$ and $\delta_0>0$ separately designate the above- and below-bandgap excitation. In addition, $\overline{E}_\ell^{\rm e}(t)$ and $\overline{E}_j^{\rm h}(t)$ in Eq. (4) represent the Coulomb-renormalized energy levels, given by

$$\overline{E}_\ell^{\rm e}(t) = E_\ell^{\rm e}+\sum_{\ell_1=1}^{2}n_{\ell_1}^{\rm e}(t)V_{\ell,\ell_1;\ell_1,\ell}^{\rm ee}(t)-\sum_{j_1=1}^{2}n_{j_1}^{\rm h}(t)\,V_{\ell,j_1;j_1,\ell}^{\rm eh}(t)-\sum_{\ell_1=1}^{2}n_{\ell_1}^{\rm e}(t)V_{\ell,\ell_1;\ell,\ell_1}^{\rm ee}(t)\ , \tag{5a}$$

$$\overline{E}_j^{\rm h}(t) = E_j^{\rm h}+\sum_{j_1=1}^{2}n_{j_1}^{\rm h}(t)V_{j,j_1;j_1,j}^{\rm hh}(t)-\sum_{\ell_1=1}^{2}n_{\ell_1}^{\rm e}(t)\,V_{\ell_1,j;j,\ell_1}^{\rm eh}(t)-\sum_{j_1=1}^{2}n_{j_1}^{\rm h}(t)V_{j,j_1;j,j_1}^{\rm hh}(t)\ , \tag{5b}$$

where the second and third terms on right-hand-sides of both equations correspond to Hartree energies between the e-e, h-h and e-h pairs, whereas the last terms represent the exchange energies for the e-e and h-h pairs. [42]. Here, the time-dependent Coulomb-renormalized energy levels $\overline{E}_\ell^{\rm e}(t)$ and $\overline{E}_j^{\rm h}(t)$ lead to a transient frequency detuning in Eq. (4). The initial conditions for Eqs. (1), (2) and (4) are set as: $n_\ell^{\rm e}(t=0) = n_j^{\rm h}(t=0) = Y_\ell^j(t=0) = 0$ with ℓ, $j = 1, 2$ for the absence of a laser field at beginning.

In Eqs.(5a) and (5b), we have defined three screened Coulomb-interaction matrix elements by

$$\begin{aligned} V_{\ell_1,\ell_2;\ell_3,\ell_4}^{\rm ee}(t) &= \int d^3\boldsymbol{r}\int d^3\boldsymbol{r}'\ \left[\psi_{\ell_1}^{\rm e}(\boldsymbol{r})\right]^*\left[\psi_{\ell_2}^{\rm e}(\boldsymbol{r}')\right]^*\frac{e^2}{4\pi\epsilon_0\epsilon_b|\boldsymbol{r}-\boldsymbol{r}'|\epsilon_s(\boldsymbol{r}-\boldsymbol{r}')}\,\psi_{\ell_3}^{\rm e}(\boldsymbol{r}')\,\psi_{\ell_4}^{\rm e}(\boldsymbol{r}) \\ &= \frac{e^2}{8\pi^3\epsilon_0\epsilon_b}\int d^3\boldsymbol{q}\,\mathcal{F}_{\ell_1,\ell_4}^{\rm e}(\boldsymbol{q})\,[\mathcal{F}_{\ell_3,\ell_2}^{\rm e}(\boldsymbol{q})]^*\left[\frac{1}{q^2+Q_s^2(t)}\right]\ , \end{aligned} \tag{6a}$$

$$\begin{aligned} V_{j_1,j_2;j_3,j_4}^{\rm hh}(t) &= \int d^3\boldsymbol{r}\int d^3\boldsymbol{r}'\ \left[\psi_{j_1}^{\rm h}(\boldsymbol{r})\right]^*\left[\psi_{j_2}^{\rm h}(\boldsymbol{r}')\right]^*\frac{e^2}{4\pi\epsilon_0\epsilon_b|\boldsymbol{r}-\boldsymbol{r}'|\epsilon_s(\boldsymbol{r}-\boldsymbol{r}')}\,\psi_{j_3}^{\rm h}(\boldsymbol{r}')\,\psi_{j_4}^{\rm h}(\boldsymbol{r}) \\ &= \frac{e^2}{8\pi^3\epsilon_0\epsilon_b}\int d^3\boldsymbol{q}\,\mathcal{F}_{j_1,j_4}^{\rm h}(\boldsymbol{q})\,[\mathcal{F}_{j_3,j_2}^{\rm h}(\boldsymbol{q})]^*\left[\frac{1}{q^2+Q_s^2(t)}\right]\ , \end{aligned} \tag{6b}$$

$$\begin{aligned} V_{\ell,j;j',\ell'}^{\rm eh}(t) &= \int d^3\boldsymbol{r}\int d^3\boldsymbol{r}'\ \left[\psi_\ell^{\rm e}(\boldsymbol{r})\right]^*\left[\psi_j^{\rm h}(\boldsymbol{r}')\right]^*\frac{e^2}{4\pi\epsilon_0\epsilon_b|\boldsymbol{r}-\boldsymbol{r}'|\epsilon_s(\boldsymbol{r}-\boldsymbol{r}')}\,\psi_{j'}^{\rm h}(\boldsymbol{r}')\,\psi_{\ell'}^{\rm e}(\boldsymbol{r}) \\ &= \frac{e^2}{8\pi^3\epsilon_0\epsilon_b}\int d^3\boldsymbol{q}\,\mathcal{F}_{\ell,\ell'}^{\rm e}(\boldsymbol{q})\,[\mathcal{F}_{j',j}^{\rm h}(\boldsymbol{q})]^*\left[\frac{1}{q^2+Q_s^2(t)}\right]\ , \end{aligned} \tag{6c}$$

where $\epsilon_s(\boldsymbol{r}-\boldsymbol{r}')$ refers to a static dielectric function of the system and ϵ_b is the average dielectric constant of host semiconductor. In Eqs.(6a)−(6c), the introduced static-screening wave number Q_s for a three-dimensional Coulomb interaction at high temperatures T is found to be [55]

$$Q_s^2(t) = \frac{e^2}{\epsilon_0\epsilon_b k_B T}\left[n_{\rm e}(t)+n_{\rm h}(t)\right] \approx \frac{12\,e^2}{\epsilon_0\epsilon_b k_B T\mathcal{V}_0} \equiv Q_0^2\ , \tag{7}$$

ACCEPTED MANUSCRIPT
Journal of Applied Physics
This is the author's peer reviewed, accepted manuscript. However, the online version of record will be different from this version once it has been copyedited and typeset.
PLEASE CITE THIS ARTICLE AS DOI: 10.1063/5.0081067
AIP Publishing

where $n_{\rm e,h}(t) = N_{\rm e,h}(t)/\mathcal{V}_0$ are the e-h volume densities of a QD and $\mathcal{V}_0$ is the QD volume.

Furthermore, $\psi^{\rm e}_{\ell}(\boldsymbol{r})$ and $\psi^{\rm h}_{j}(\boldsymbol{r})$ in Eqs.(6a)−(6c) stand for the e-h envelope wave functions for a QD [calculated in Eq. (A3)]. Meanwhile, the e-h form factors in Eqs.(6a)−(6c) due to QD confinement are defined by [calculated in Eqs. (A5) and (A6)]

$$\mathcal{F}^{\rm e}_{\ell,\ell'}(\boldsymbol{q}) = \int d^3\boldsymbol{r}\,[\psi^{\rm e}_{\ell}(\boldsymbol{r})]^*\exp(i\boldsymbol{q}\cdot\boldsymbol{r})\,\psi^{\rm e}_{\ell'}(\boldsymbol{r})\;, \tag{8a}$$

$$\mathcal{F}^{\rm h}_{j,j'}(\boldsymbol{q}) = \int d^3\boldsymbol{r}\,\left[\psi^{\rm h}_{j}(\boldsymbol{r})\right]^*\exp(i\boldsymbol{q}\cdot\boldsymbol{r})\,\psi^{\rm h}_{j'}(\boldsymbol{r})\;. \tag{8b}$$

On the other hand, the Coulomb-renormalized $\widetilde{\mathcal{M}}^{\rm eh}_{\ell,j}(t)$, which is used in Eqs. (1), (2) and (4) for the interaction between e-h pairs and external pulsed-laser field $\boldsymbol{\mathcal{E}}_{\rm ext}(\boldsymbol{r},t) = \Theta_0(t-t_0)\,\boldsymbol{\mathcal{E}}^{(0)}_{\rm ext}(t)\,\exp(i\boldsymbol{q}\cdot\boldsymbol{r})$, is calculated as

$$\widetilde{\mathcal{M}}^{\rm eh}_{\ell,j}(t) = -\boldsymbol{\mathcal{E}}^{\rm tot}_{\ell,j}(t)\cdot\boldsymbol{d}_{cv}(T) - Y^{j}_{\ell}(t)\,V^{\rm eh}_{\ell,j;j,\ell}(t)\;, \tag{9}$$

where t_0 is the field starting time and $\Theta_0(x)$ is a Heaviside function. The second term in Eq. (9) represents the correction from e-h interaction to the dipole moment. The static interband dipole-moment $\boldsymbol{d}_{cv}(T)$ in Eq. (9) is [calculated Eq. (A8)]

$$\boldsymbol{d}_{cv}(T) = d_{cv}(T)\,\hat{\boldsymbol{e}}_d = e\int\limits_{\mathbb{V}_{\rm c}} d^3\boldsymbol{r}\,[u_c(\boldsymbol{r})]^*\;\boldsymbol{r}\,u_v(\boldsymbol{r})\;, \tag{10}$$

where the volume integral is performed within a unit-cell $\mathbb{V}_{\rm c}$, $u_c(\boldsymbol{r})$ and $u_v(\boldsymbol{r})$ are the Bloch functions associated with conduction and valence bands at the $\boldsymbol{\Gamma}$-point within the first Brillouin zone of host semiconductor (e.g., GaAs). Moreover, the *effective* total optical field in Eq. (9) is defined as

$$\boldsymbol{\mathcal{E}}^{\rm tot}_{\ell,j}(t) = \int d^3\boldsymbol{r}\,[\psi^{\rm e}_{\ell}(\boldsymbol{r})]^*\;\left[\delta_{\ell,1}\delta_{j,1}\,\boldsymbol{\mathcal{E}}^{(0)}_{\rm ext}(t-t_0) + \boldsymbol{\mathcal{E}}_{\rm intra}(\boldsymbol{r},t\,|\,\omega_0)\right]\;\left[\psi^{\rm h}_{j}(\boldsymbol{r})\right]^*\;, \tag{11}$$

where $\mathcal{E}^{(0)}_{\rm ext}(t) = (\mathcal{E}_0/\sigma_0\sqrt{2\pi})\,\exp[-t^2/2\sigma_0^2]$ stands for a laser pulse with peak field $\mathcal{E}_0$ and pulse width $\sqrt{2}\sigma_0$, and it is in resonance with the energy separation between ground states of electrons and holes. In Eq. (11), $\mathcal{E}_{\rm intra}(\boldsymbol{r},t\,|\,\omega_0) \propto Y^1_1(t)$ represents a self-consistent depolarization field, [21–24] resulting from photo-excited interacting e-h pairs in a QD as presented in Eq. (23) below. The dependence of $\boldsymbol{\mathcal{E}}^{\rm tot}_{\ell,j}(t)$ on $\boldsymbol{\mathcal{E}}^{(0)}_{\rm ext}(t)$ in Eq. (11) leads to bandedge nonlinearity [4,7,8] ($\propto |\boldsymbol{\mathcal{E}}^{(0)}_{\rm ext}(t)|^2$, $|\boldsymbol{\mathcal{E}}^{(0)}_{\rm ext}(t)|^4$, $\cdots$ for level occupations) in Eqs. (1) and (2) through stimulated transitions. On the other hand, the dependence of $\boldsymbol{\mathcal{E}}^{\rm tot}_{\ell,j}(t)$ on $\boldsymbol{\mathcal{E}}_{\rm intra}(\boldsymbol{r},t\,|\,\omega_0)$ is responsible for optical nonlinearity [1] ($2\omega_R$, $4\omega_R$, $\cdots$ for oscillation frequencies of $Y^1_1(t)$) in Eq. (4), where ω_R represents the Rabi frequency $\omega_R = d_{cv}(T)\,\mathcal{E}^{(0)}_{\rm ext}/\hbar$. In addition, we have $\boldsymbol{\mathcal{E}}_{\rm intra}(\boldsymbol{r},t\,|\,\omega_0) \propto Y^1_1(t)$ as will be shown later in Eq. (23), and meanwhile, $Y^1_1(t) \propto \mathcal{M}^{\rm eh}_{1,1}(t) \propto \boldsymbol{\mathcal{E}}^{\rm tot}_{1,1}(t)$ as found from in Eq. (4) under the steady-state condition $dY^1_1(t)/dt = 0$. Therefore, Eq. (11) leads to a set of inhomogeneous linear equations with a source term $\boldsymbol{\mathcal{E}}^{(0)}_{\rm ext}(t)$ for $\boldsymbol{\mathcal{E}}^{\rm tot}_{\ell,j}(t)$ having different indexes $\{\ell,j\}$, and zero determinant of the coefficient matrix determines plasmon branches for a single QD.

Non-radiative energy relaxation process in GDMEs plays a key role on ultrafast non-equilibrium dynamics [8] of e-h pairs in a QD under a femetosecond laser pulse. The Boltzmann-type scattering term [37] for electron non-radiative energy relaxation in Eq. (1) can be formally written as

$$\left.\frac{\partial n^{\rm e}_{\ell}(t)}{\partial t}\right|_{\rm rel} = \mathcal{W}^{\rm (in)}_{\ell}(t)\,[1-n^{\rm e}_{\ell}(t)] - \mathcal{W}^{\rm (out)}_{\ell}(t)\,n^{\rm e}_{\ell}(t)\;, \tag{12}$$

where, after the Coulomb interaction between pairs of photo-generated carriers has been neglected for low densities and high temperatures, the microscopic scattering-in and scattering-out rates within the second-order Born approximation are calculated as

ACCEPTED MANUSCRIPT
Journal of Applied Physics
AIP Publishing
This is the author's peer reviewed, accepted manuscript. However, the online version of record will be different from this version once it has been copyedited and typeset.
PLEASE CITE THIS ARTICLE AS DOI: 10.1063/5.0081067

$$\mathcal{W}_{\ell}^{(\mathrm{in})}(t) = \frac{2\pi}{\hbar} \sum_{\ell'=1}^{2}{}' \left|V_{\ell,\ell'}^{\mathrm{ep}}(t)\right|^2 n_{\ell'}^{\mathrm{e}}(t) \Big\{ N_0(\Omega_0)\, \mathcal{L}_0(\overline{E}_{\ell}^{\mathrm{e}}(t) - \overline{E}_{\ell'}^{\mathrm{e}}(t) - \hbar\Omega_0, \hbar\Gamma_0) + [N_0(\Omega_0)+1]\, \mathcal{L}_0(\overline{E}_{\ell}^{\mathrm{e}}(t) - \overline{E}_{\ell'}^{\mathrm{e}}(t) + \hbar\Omega_0, \hbar\Gamma_0) \Big\} + \frac{2\pi}{\hbar} \sum_{\ell'=1}^{2}{}' \sum_{j,j'=1}^{2}{}' \left|V_{\ell,j;j',\ell'}^{\mathrm{eh}}(t)\right|^2 \times [1 - n_j^{\mathrm{h}}(t)]\, n_{j'}^{\mathrm{h}}(t)\, n_{\ell'}^{\mathrm{e}}(t)\, \mathcal{L}_0(\overline{E}_{\ell}^{\mathrm{e}}(t) + \overline{E}_{j}^{\mathrm{h}}(t) - \overline{E}_{\ell'}^{\mathrm{e}}(t) - \overline{E}_{j'}^{\mathrm{h}}(t), \hbar\gamma_0)\ , \tag{13a}$$

$$\mathcal{W}_{\ell}^{(\mathrm{out})}(t) = \frac{2\pi}{\hbar} \sum_{\ell'=1}^{2}{}' \left|V_{\ell,\ell'}^{\mathrm{ep}}(t)\right|^2 [1 - n_{\ell'}^{\mathrm{e}}(t)] \Big\{ N_0(\Omega_0)\, \mathcal{L}_0(\overline{E}_{\ell'}^{\mathrm{e}}(t) - \overline{E}_{\ell}^{\mathrm{e}}(t) - \hbar\Omega_0, \hbar\Gamma_0) + [N_0(\Omega_0)+1]\, \mathcal{L}_0(\overline{E}_{\ell'}^{\mathrm{e}}(t) - \overline{E}_{\ell}^{\mathrm{e}}(t) + \hbar\Omega_0, \hbar\Gamma_0) \Big\} + \frac{2\pi}{\hbar} \sum_{\ell'=1}^{2}{}' \sum_{j,j'=1}^{2}{}' \left|V_{\ell',j;j',\ell}^{\mathrm{eh}}(t)\right|^2 \times [1 - n_{\ell'}^{\mathrm{e}}(t)]\, [1 - n_j^{\mathrm{h}}(t)]\, n_{j'}^{\mathrm{h}}(t)\, \mathcal{L}_0(\overline{E}_{\ell'}^{\mathrm{e}}(t) + \overline{E}_{j}^{\mathrm{h}}(t) - \overline{E}_{\ell}^{\mathrm{e}}(t) - \overline{E}_{j'}^{\mathrm{h}}(t), \hbar\gamma_0)\ . \tag{13b}$$

Here, the first term on the right-hand-side corresponds to the phonon-assisted intraband relaxation, whereas the second term results from the Coulomb-facilitated intraband relaxation.[38–40] In Eqs. (13a) and (13b), the primed summations exclude the terms satisfying either $j = j'$ or $\ell' = \ell$, $N_0(\Omega_0) = [\exp(\hbar\Omega_0/k_{\mathrm{B}}T) - 1]^{-1}$ is the Bose function for thermal-equilibrium phonons, $\hbar\gamma_0$ is the quasi-particle lifetime broadening, Ω_0 and Γ_0 are the frequency and decay rate of longitudinal-optical phonons in host semiconductor, and $\mathcal{L}_0(a,b) = (b/\pi)/(a^2+b^2)$ is a Lorentz-shape function.

In a similar way, the Boltzmann-type scattering term for hole non-radiative energy relaxation in Eq. (2) take the form

$$\left.\frac{\partial n_j^{\mathrm{h}}}{\partial t}\right|_{\mathrm{rel}} = \overline{\mathcal{W}}_j^{(\mathrm{in})}(t)\, [1 - n_j^{\mathrm{h}}(t)] - \overline{\mathcal{W}}_j^{(\mathrm{out})}(t)\, n_j^{\mathrm{h}}(t)\ , \tag{14}$$

where the microscopic scattering-in and scattering-out rates are given by

$$\overline{\mathcal{W}}_{j}^{(\mathrm{in})}(t) = \frac{2\pi}{\hbar} \sum_{j'=1}^{2}{}' \left|V_{j,j'}^{\mathrm{hp}}(t)\right|^2 n_{j'}^{\mathrm{h}}(t) \Big\{ N_0(\Omega_0)\, \mathcal{L}_0(\overline{E}_{j}^{\mathrm{h}}(t) - \overline{E}_{j'}^{\mathrm{h}}(t) - \hbar\Omega_0, \hbar\Gamma_0) + [N_0(\Omega_0)+1]\, \mathcal{L}_0(\overline{E}_{j}^{\mathrm{h}}(t) - \overline{E}_{j'}^{\mathrm{h}}(t) + \hbar\Omega_0, \hbar\Gamma_0) \Big\} + \frac{2\pi}{\hbar} \sum_{\ell,\ell'=1}^{2}{}' \sum_{j'=1}^{2}{}' \left|V_{\ell,j;j',\ell'}^{\mathrm{eh}}(t)\right|^2 \times [1 - n_{\ell}^{\mathrm{e}}(t)]\, n_{j'}^{\mathrm{h}}(t)\, n_{\ell'}^{\mathrm{e}}(t)\, \mathcal{L}_0(\overline{E}_{\ell}^{\mathrm{e}}(t) + \overline{E}_{j}^{\mathrm{h}}(t) - \overline{E}_{\ell'}^{\mathrm{e}}(t) - \overline{E}_{j'}^{\mathrm{h}}(t), \hbar\gamma_0)\ , \tag{15a}$$

$$\overline{\mathcal{W}}_{j}^{(\mathrm{out})}(t) = \frac{2\pi}{\hbar} \sum_{j'=1}^{2}{}' \left|V_{j,j'}^{\mathrm{hp}}(t)\right|^2 [1 - n_{j'}^{\mathrm{h}}(t)] \Big\{ N_0(\Omega_0)\, \mathcal{L}_0(\overline{E}_{j'}^{\mathrm{h}}(t) - \overline{E}_{j}^{\mathrm{h}}(t) - \hbar\Omega_0, \hbar\Gamma_0) + [N_0(\Omega_0)+1]\, \mathcal{L}_0(\overline{E}_{j'}^{\mathrm{h}}(t) - \overline{E}_{j}^{\mathrm{h}}(t) + \hbar\Omega_0, \hbar\Gamma_0) \Big\} + \frac{2\pi}{\hbar} \sum_{\ell,\ell'=1}^{2}{}' \sum_{j'=1}^{2}{}' \left|V_{\ell,j';j,\ell'}^{\mathrm{eh}}(t)\right|^2 \times [1 - n_{\ell}^{\mathrm{e}}(t)]\, [1 - n_{j'}^{\mathrm{h}}(t)]\, n_{\ell'}^{\mathrm{e}}(t)\, \mathcal{L}_0(\overline{E}_{\ell}^{\mathrm{e}}(t) + \overline{E}_{j'}^{\mathrm{h}}(t) - \overline{E}_{\ell'}^{\mathrm{e}}(t) - \overline{E}_{j}^{\mathrm{h}}(t), \hbar\gamma_0)\ , \tag{15b}$$

and again the primed summations in Eqs. (15a) and (15b) exclude the terms satisfying either $j' = j$ or $\ell = \ell'$. In Eqs. (13a)-(13b), as well as in Eqs. (15a)-(15b), the interactions between longitudinal-optical phonons and electrons or holes in a QD are found to be [55]

$$\left|V_{\ell,\ell'}^{\mathrm{ep}}(t)\right|^2 = \frac{e^2\hbar\Omega_0}{8\pi^3\epsilon_0} \left(\frac{1}{\epsilon_\infty} - \frac{1}{\epsilon_s}\right) \int d^3\boldsymbol{q}\ \left|\mathcal{F}_{\ell,\ell'}^{\mathrm{e}}(\boldsymbol{q})\right|^2 \left[\frac{1}{q^2 + Q_s^2(t)}\right]\ , \tag{16a}$$

$$\left|V_{j,j'}^{\mathrm{hp}}(t)\right|^2 = \frac{e^2\hbar\Omega_0}{8\pi^3\epsilon_0} \left(\frac{1}{\epsilon_\infty} - \frac{1}{\epsilon_s}\right) \int d^3\boldsymbol{q}\ \left|\mathcal{F}_{j,j'}^{\mathrm{h}}(\boldsymbol{q})\right|^2 \left[\frac{1}{q^2 + Q_s^2(t)}\right]\ , \tag{16b}$$

ACCEPTED MANUSCRIPT
Journal of Applied Physics
This is the author's peer reviewed, accepted manuscript. However, the online version of record will be different from this version once it has been copyedited and typeset.
PLEASE CITE THIS ARTICLE AS DOI: 10.1063/5.0081067
AIP Publishing

where ϵ_∞ and ϵ_s refer to the high-frequency and static dielectric constants of the host polar semiconductor.

By generalizing the Kubo-Martin-Schwinger relation [55], the relatively-slow transient spontaneous emission rate $\mathcal{R}_j^{\rm sp}(t)$, introduced in Eqs. (1) and (2), can be expressed as

$$\mathcal{R}_j^{\rm sp}(t) \;=\; \frac{3\left|(\boldsymbol{d}'_{cv}(t)\right|^2}{\epsilon_0\sqrt{\epsilon_b}}\left|\int d^3\boldsymbol{r}\,\psi_j^{\rm e}(\boldsymbol{r})\,\psi_j^{\rm h}(\boldsymbol{r})\right|^2\int_0^\infty d\omega'\,\mathcal{B}_0\left[\hbar\omega'-E_{\rm G}(T)-\Delta\mathcal{E}_{\rm G}(t)-E_j^{\rm e}-E_j^{\rm h}\right]$$
$$\times\;\hbar\omega'\rho_0(\omega')\left\{\frac{\hbar\gamma_0}{[\hbar\omega'-E_{\rm G}(T)-\Delta\mathcal{E}_{\rm G}(t)-E_j^{\rm e}-E_j^{\rm h}]^2+\hbar^2\gamma_0^2}\right\}\,, \tag{17}$$

where small exciton effect is neglected at room temperature, $\mathcal{B}_0(x)=1/2+(1/\pi)\,\tan^{-1}(x/\gamma_0)$ is a broadened unity-step function, the Coulomb-renormalized interband dipole-moment $\boldsymbol{d}'_{cv}(t)$ is

$$\left|\boldsymbol{d}'_{cv}(t)\right|^2=\frac{e^2\hbar^2}{2m_0\,E_{\rm G}(T)}\left[1+\frac{\Delta\mathcal{E}_{\rm G}(t)}{E_{\rm G}(T)}\right]\left(\frac{m_0}{m_{\rm e}^*}-1\right)\,, \tag{18}$$

$\rho_0(\omega')=(\omega')^2/c^3\pi^2\hbar$ represents the density-of-states for spontaneously-emitted photons in vacuum, m_0 is the free electron mass, $m_{\rm e}^*$ is the effective mass of electrons in the host semiconductor, and the Coulomb correction $\Delta\mathcal{E}_{\rm G}(t)$ to the bandgap $E_{\rm G}(T)$ is [7,8]

$$\Delta\mathcal{E}_{\rm G}(t) \;=\; \sum_{\ell_1=1}^{2}n_{\ell_1}^{\rm e}(t)\left[V_{1,\ell_1;\ell_1,1}^{\rm ee}(t)-V_{1,\ell_1;1,\ell_1}^{\rm ee}(t)\right]+\sum_{j_1=1}^{2}n_{j_1}^{\rm h}(t)\left[V_{1,j_1;j_1,1}^{\rm hh}(t)-V_{1,j_1;1,j_1}^{\rm hh}(t)\right]$$
$$-\;\sum_{\ell_1=1}^{2}n_{\ell_1}^{\rm e}(t)\,V_{\ell_1,1;1,\ell_1}^{\rm eh}(t)-\sum_{j_1=1}^{2}n_{j_1}^{\rm h}(t)\,V_{1,j_1;j_1,1}^{\rm eh}(t)-\left[1-n_1^{\rm e}(t)-n_1^{\rm h}(t)\right]\,V_{1,1;1,1}^{\rm eh}(t)\,. \tag{19}$$

In Eq. (19), the first two terms come from Hartree-exchange energies of e-h pairs, while the combination of remaining terms e-h pair Hartree energy. Moreover, from Eq. (17) we are able to get the transient photoluminescence spectrum $\mathcal{S}_{\rm sp}(\omega'|\,t)$, given by

$$\mathcal{S}_{\rm sp}(\omega'|\,t) \;=\; \sum_{j=1}^{2}\left[\frac{\partial\mathcal{R}_j^{\rm sp}(t)}{\partial\omega'}\right]n_j^{\rm e}(t)\,n_j^{\rm h}(t)=\frac{3\left|(\boldsymbol{d}'_{cv}(t)\right|^2}{\epsilon_0\sqrt{\epsilon_b}}\sum_{j=1}^{2}n_j^{\rm e}(t)\,n_j^{\rm h}(t)\left|\int d^3\boldsymbol{r}\,\psi_j^{\rm e}(\boldsymbol{r})\,\psi_j^{\rm h}(\boldsymbol{r})\right|^2$$
$$\times\;\mathcal{B}_0\left[\hbar\omega'-E_{\rm G}(T)-\Delta\mathcal{E}_{\rm G}(t)-E_j^{\rm e}-E_j^{\rm h}\right]\hbar\omega'\rho_0(\omega')\left\{\frac{\hbar\gamma_0}{[\hbar\omega'-E_{\rm G}(T)-\Delta\mathcal{E}_{\rm G}-E_j^{\rm e}-E_j^{\rm h}]^2+\hbar^2\gamma_0^2}\right\}\,, \tag{20}$$

which includes contributions from both ground state ($j=1$) and excited state ($j=2$).

Physically, by making use of the interband quantum coherence $Y_\ell^j(t)$, we are able to define an interband optical-polarization field $\boldsymbol{\mathcal{P}}_{QD}(\boldsymbol{r},\,t\,|\,\omega_0)$ for photo-excited e-h pairs in a QD [56], yielding

$$\boldsymbol{\mathcal{P}}_{QD}(\boldsymbol{r},\,t\,|\,\omega_0)=-\left|\xi_0(\boldsymbol{r})\right|^2\boldsymbol{\mathcal{D}}_{QD}(t\,|\,\omega_0)\,, \tag{21}$$

which is in opposite direction of $\boldsymbol{\mathcal{E}}_{\rm ext}^{(0)}(t)$, where $\boldsymbol{\mathcal{D}}_{QD}(t\,|\,\omega_0)$ is the laser-induced QD interband dynamical dipole-moment, $|\xi_0(\boldsymbol{r})|^2\sim\delta(\boldsymbol{r})$ is a normalized Gaussian-type probability function describing spatial confinement of a QD centered at $\boldsymbol{r}=0$, and $\boldsymbol{\mathcal{D}}_{QD}(t\,|\,\omega_0)$ is given by [8]

$$\boldsymbol{\mathcal{D}}_{QD}(t\,|\,\omega_0)=6\,\boldsymbol{d}_{cv}(T)\left\{\int d^3\boldsymbol{r}'\,[\psi_1^{\rm e}(\boldsymbol{r}')]^*\,[\psi_1^{\rm h}(\boldsymbol{r}')]^*\right\}\,Y_1^1(t\,|\,\omega_0)\equiv 6\,\boldsymbol{d}_{cv}(T)\,\mathcal{G}_{cv}\,Y_1^1(t\,|\,\omega_0)\,. \tag{22}$$

In Eq. (22), the spin-orbit degeneracy is taken into account, and $\mathcal{G}_{cv}\sim 1$ represents an overlap factor between ground-state wave functions of e-h pairs. From Maxwell's electrodynamics theory [3], the result in Eq. (21) can be

ACCEPTED MANUSCRIPT
Journal of Applied Physics
AIP Publishing
This is the author's peer reviewed, accepted manuscript. However, the online version of record will be different from this version once it has been copyedited and typeset.
PLEASE CITE THIS ARTICLE AS DOI: 10.1063/5.0081067

further incorporated for constructing a self-consistent electric field $\boldsymbol{\mathcal{E}}_{\rm intra}(\boldsymbol{r},\, t\,|\,\omega_0)$ in a perturbative way, resulting from photo-excited e-h pairs in a QD. This yields [23]

$$\boldsymbol{\mathcal{E}}_{\rm intra}(\boldsymbol{r},\, t\,|\,\omega_0) \equiv \frac{1}{\epsilon_0\epsilon_b}\,\boldsymbol{\mathcal{P}}_{QD}(\boldsymbol{r},\, t\,|\,\omega_0) = -\frac{6\,|\xi_0(\boldsymbol{r})|^2\,\boldsymbol{d}_{cv}(T)}{\epsilon_0\epsilon_b}\,\mathcal{G}_{cv}\,Y_1^1(t\,|\,\omega_0)\ , \tag{23}$$

which exerts a back action to e-h pairs in a QD self-consistently, as seen in Eq. (11). Under the steady-state condition $dY_1^1(t) = 0$, from Eqs. (4), (11) and (23) we find the transient local-plasmon energy $\hbar\Omega_{pl}^{(\rm s)}(t)$, given by [28]

$$\hbar\Omega_{pl}^{(\rm s)}(t) = \left[E_{\rm G}(T) + E_1^{\rm e} + E_1^{\rm h} - V_{1,1;1,1}^{\rm eh}\right] + \Delta E_{\rm HF}^{\rm e}(t) + \Delta E_{\rm HF}^{\rm h}(t) + \frac{6\,d_{cv}^2(T)}{\epsilon_0\epsilon_b\mathcal{V}_0}\left[1 - n_1^{\rm e}(t) - n_1^{\rm h}(t)\right]\ , \tag{24}$$

which is higher than the Coulomb-renormalized bandgap energy due to many-body effects from the induced depolarization field (last term), where the Hartree-exchange correction to kinetic energies of e-h pairs are given by

$$\Delta E_{\rm HF}^{\rm e}(t) = \sum_{\ell_1=1}^{2} n_{\ell_1}^{\rm e}(t)[V_{1,\ell_1;\ell_1,1}^{\rm ee}(t) - V_{1,\ell_1;1,\ell_1}^{\rm ee}(t)]\ , \tag{25a}$$

$$\Delta E_{\rm HF}^{\rm h}(t) = \sum_{j_1=1}^{2} n_{j_1}^{\rm h}(t)[V_{1,j_1;j_1,1}^{\rm hh}(t) - V_{1,j_1;1,j_1}^{\rm hh}(t)]\ , \tag{25b}$$

and $n_{\ell_1}^{\rm e}(t)$ and $n_{j_1}^{\rm h}(t)$ are computed by Eqs. (1), (2) and (4). Under the steady-state condition $dY_\ell^j(t)/dt = 0$, we obtain from Eq. (4) the induced interband quantum coherence $Y_\ell^j(t)$ in terms of the renormalized interaction $\widetilde{\mathcal{M}}_{\ell,j}^{\rm eh}(t)$ between e-h pairs and the total optical field $\boldsymbol{\mathcal{E}}_{\ell,j}^{\rm tot}(t)$ as given by Eq. (11). Moreover, this effective optical field $\boldsymbol{\mathcal{E}}_{\ell,j}^{\rm tot}(t)$ is a sum of the incident laser field $\boldsymbol{\mathcal{E}}_{\rm ext}^{(0)}(t)$ and the self-sustained intradot depolarization field $\boldsymbol{\mathcal{E}}_{\rm intra}(\boldsymbol{r},t)$, which is proportional to $Y_\ell^j(t)$, as seen in Eq. (23). In this way, an inhomogeneous linear equation for $Y_\ell^j(t)$ can be established with a source term containing $\boldsymbol{\mathcal{E}}_{\rm ext}^{(0)}(t)$. Consequently, for a single QD, by taking a zero coefficient in the corresponding linear equation of $Y_\ell^j(t)$ under the condition of $\boldsymbol{\mathcal{E}}_{\rm ext}^{(0)}(t) = 0$, we acquire a self-sustained intradot-plasmon mode as shown in Eq. (24).

By considering resonant excitation between two ground states of electrons and holes and neglecting non-radiative energy relaxation and spontaneous emission, from Eqs. (1), (2) and (4) for $\ell = j = 1$, we find constants for the equation of motion, [57–62] i.e.,

$$\frac{d}{dt}\left\{\left[1 - 2n_1^{\rm e}(t)\right]^2 + 4\left|Y_1^1(t)\right|^2\right\} = 0\ , \tag{26a}$$

$$\frac{d}{dt}\left[n_1^{\rm e}(t) - n_1^{\rm h}(t)\right] = 0\ , \tag{26b}$$

as well as the dynamical equation for interband quantum coherence

$$\begin{aligned}\frac{d^2Y_1^1(t)}{dt^2} &\approx \frac{1}{i\hbar}\left[E_{\rm G}(T) + \overline{E}_1^{\rm e}(t) + \overline{E}_1^{\rm h}(t) - \hbar(\omega_0 + i\gamma_1)\right]\frac{dY_1^1(t)}{dt} - \frac{1}{i\hbar}\left[\frac{dn_1^{\rm e}(t)}{dt} + \frac{dn_1^{\rm h}(t)}{dt}\right]\mathcal{M}_{1,1}^{\rm eh}(t)\\ &\approx -\left\{\gamma_1 - i\left[\delta_1 - \Delta_1(t)\right]\right\}\frac{dY_1^1(t)}{dt} - 4i\,\omega_R^2\,{\rm Im}\left[Y_1^1(t)\right]\ ,\end{aligned} \tag{27}$$

where $\omega_R = d_{cv}(T)\,\mathcal{E}_{\rm ext}^{(0)}/\hbar$ is the Rabi frequency, γ_1 is a damping parameter, $\delta_1 = \omega_0 - [E_{\rm G}(T) + E_1^{\rm e} + E_1^{\rm h}]/\hbar$ is the frequency detuning, and $\Delta_1(t) = [\overline{E}_1^{\rm e}(t) + \overline{E}_1^{\rm h}(t) - \left(E_1^{\rm e} + E_1^{\rm h}\right)]/\hbar$ is the Coulomb correction to frequency detuning. If one considers ${\rm Im}\left[Y_1^1(t)\right]$ in Eq. (27), it formally resembles a damped harmonic oscillator with a complex time-dependent damping parameter $\gamma_1 + i\,[\Delta_1(t) - \delta_1]$. As a special case with $\omega_R = 0$ and $\gamma_1 = 0$, we find $dY_1^1(t)/dt \sim \exp[-i\Delta_1(t)t]\,\exp(+i\delta_1 t)$, appearing as frequency-modulated oscillations (since $\Delta_1(t) \propto n_1^{\rm e,h}(t) \propto {\rm Im}[Y_1^1(t)]$) with respect to the central detunnig-frequency δ_1. On the other hand, if $\gamma_1 = 0$ and $\Delta_1(t) = 0$, we obtain $d^2{\rm Im}[Y_1^1(t)]/dt^2 = -(\delta_1^2 + 4\omega_R^2)\,{\rm Im}[Y_1^1(t)]$, and then, ${\rm Im}[Y_1^1(t)] \sim \sin(t\sqrt{\delta_1^2 + 4\omega_R^2})$ displaying Rabi oscillations [1] with a frequency $\sqrt{\delta_1^2 + 4\omega_R^2}$ and a time period $2\pi/\sqrt{\delta_1^2 + 4\omega_R^2}$.

ACCEPTED MANUSCRIPT
Journal of Applied Physics
AIP Publishing
This is the author's peer reviewed, accepted manuscript. However, the online version of record will be different from this version once it has been copyedited and typeset.
PLEASE CITE THIS ARTICLE AS DOI: 10.1063/5.0081067

B. Multiple-Quantum-Dot Radiation-Dipole Coupling

In Section II A, we have established a GDME theory for accurately describing ultrafast dynamics of interacting photo-excited e-h pairs within a single QD under a pulsed-laser field. For situation with multiple QDs sitting at $\boldsymbol{r} = \boldsymbol{r}_1, \boldsymbol{r}_2, \cdots, \boldsymbol{r}_N$, Eqs. (1), (2) and (4) presented in Sec. II A can still be applied to each individual QD. However, the intradot self-consistent electric field $\boldsymbol{\mathcal{E}}_{\rm intra}(\boldsymbol{r}, t\,|\,\omega_0)$ in Eq. (11) for a single QD must be generalized to include contributions from multiple laser-coupled QDs.

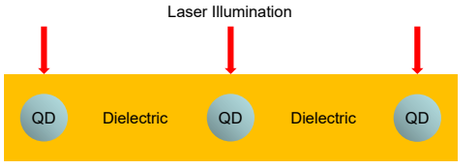

FIG. 2: Illustration for dielectric-embedded array of GaAs quantum dots (QDs) in the presence of pulsed-laser illumination.

Mathematically, we can approximately view N photo-excited QDs as N dynamical point dipoles. Using an approximation as illustrated in Fig. 2, we consider a linear array of multiple QDs embedded in a dielectric medium under laser illumination. For this effective one-dimensional system, the interdot self-consistent electric field $\boldsymbol{\mathcal{E}}_{\rm inter}(\boldsymbol{r}_n, t\,|\,\omega_0)$ at $\boldsymbol{r} = \boldsymbol{r}_n = \{x_n, 0, 0\}$ for the nth QD is calculated as [3,63,64]

$$\boldsymbol{\mathcal{E}}_{\rm inter}(\boldsymbol{r}_n, t\,|\,\omega_0) = -6\,\mathcal{G}_{cv}\,\boldsymbol{d}_{cv}(T)\sum_{s=1}^{N}{}'\left[\frac{\mathsf{e}^{iq_x(x_n-x_s)}}{2\pi\epsilon_0\epsilon_b|x_n-x_s|^3}\right]Y_1^1(t\,|\,s,\omega_0)\;, \tag{28}$$

where $x_n = nd$, d is the separation between two nearest-neighbouring dots, $q_x \geq 0$ takes values around $q_0 = \omega_0\sqrt{\epsilon_b}/c$ for a transient pulse, and $\boldsymbol{\mathcal{D}}_{QD}(t\,|\,\omega_0)$ in Eq. (22) has been utilized. In Eq. (28), the primed s-summation excludes the term satisfying $s = n$, and we have neglected the insignificant retardation effect [3] on electric-dipole-radiation fields. Moreover, $Y_1^1(t\,|\,s,\omega_0)$ in Eq. (28) can still be determined by solving coupled Eqs. (1), (2) and (4) for the sth QD. However, the *effective* total optical field for the nth QD, i.e.,

$$\begin{aligned}\boldsymbol{\mathcal{E}}^{\rm tot}_{\ell,j}(\boldsymbol{q}, t\,|\,n,\omega_0)\cdot\boldsymbol{d}_{cv}(T) &= \delta_{\ell,1}\delta_{j,1}\left\{\Theta_0(t-t_0)\,\left[\boldsymbol{\mathcal{E}}^{(0)}_{\rm ext}(t)\cdot\boldsymbol{d}_{cv}(T)\right]\int d^3\boldsymbol{r}\,[\psi_1^{\rm e}(\boldsymbol{r}\,|\,n)]^*\,\exp\left(i\boldsymbol{q}\cdot\boldsymbol{r}\right)\,\left[\psi_1^{\rm h}(\boldsymbol{r}\,|\,n)\right]^*\right\}\\
&- \frac{6\,d_{cv}^2(T)}{\epsilon_0\epsilon_b}\,\mathcal{G}_{cv}\,Y_1^1(t\,|\,n,\omega_0)\int d^3\boldsymbol{r}\,[\psi_\ell^{\rm e}(\boldsymbol{r}\,|\,n)]^*\,|\xi_0(\boldsymbol{r}\,|\,n)|^2\,\left[\psi_j^{\rm h}(\boldsymbol{r}\,|\,n)\right]^*\\
&- \frac{3\,d_{cv}^2(T)}{\pi\epsilon_0\epsilon_b}\,\mathcal{G}_{cv}\sum_{s=1}^{N}{}'\,Y_1^1(t\,|\,s,\omega_0)\,V_{\rm c}(q\,|\,n,s)\end{aligned} \tag{29}$$

must be employed to replace $\boldsymbol{\mathcal{E}}^{\rm tot}_{\ell,j}(\boldsymbol{q}, t)$ for a single-QD in Eq. (11), where the primed s-summation excludes the term satisfying $s = n$ and

$$V_{\rm c}(q\,|\,n,s) = \exp(-i\boldsymbol{q}\cdot\boldsymbol{r}_s)\int d^3\boldsymbol{r}\,[\psi_1^{\rm e}(\boldsymbol{r}-\boldsymbol{r}_n)]^*\,\frac{\exp(i\boldsymbol{q}\cdot\boldsymbol{r})}{|\boldsymbol{r}-\boldsymbol{r}_s|^3}\,\left[\psi_1^{\rm h}(\boldsymbol{r}-\boldsymbol{r}_n)\right]^* \approx \frac{\exp[i\boldsymbol{q}\cdot(\boldsymbol{r}_n-\boldsymbol{r}_s)]}{|\boldsymbol{r}_n-\boldsymbol{r}_s|^3}\,\mathcal{F}_{1,1}^{\rm eh}(\boldsymbol{q}\,|\,n)\;, \tag{30}$$

$$\mathcal{F}_{1,1}^{\rm eh}(\boldsymbol{q}\,|\,n) = \int d^3\boldsymbol{r}\,[\psi_1^{\rm e}(\boldsymbol{r}\,|\,n)]^*\,\exp(i\boldsymbol{q}\cdot\boldsymbol{r})\,\left[\psi_1^{\rm h}(\boldsymbol{r}\,|\,n)\right]^* = \left[\mathcal{F}_{1,1}^{\rm eh}(\boldsymbol{q}\,|\,n)\right]^*\;. \tag{31}$$

In Eq. (29), three terms on its right-hand-side are associated with contributions from the external laser field, intradot and interdot self-consistent depolarization fields, respectively. Both the intradot and interdot self-consistent depolarization fields in Eq. (29) will lead to optical nonlinearity [1] ($2\omega_R$, $4\omega_R$, $\cdots$ for oscillation frequencies of $Y_1^1(t)$) for interband quantum coherence. Similarly in obtaining Eq. (24), Eq. (29) constitutes a set of inhomogeneous linear equations with a source term $\boldsymbol{\mathcal{E}}^{(0)}_{\rm ext}(t)$ for $\boldsymbol{\mathcal{E}}^{\rm tot}_{\ell,j}(\boldsymbol{q}, t\,|\,n,\omega_0)$ having different site index n and level indexes $\{\ell, j\}$, and

ACCEPTED MANUSCRIPT
Journal of Applied Physics
This is the author's peer reviewed, accepted manuscript. However, the online version of record will be different from this version once it has been copyedited and typeset.
PLEASE CITE THIS ARTICLE AS DOI: 10.1063/5.0081067
AIP Publishing

the zero determinant of the coefficient matrix determines multiple plasmon blanches for coupled QDs in the system. Similar to Eq. (24), in this case we get N-coupled plasmon branches $\hbar\Omega_{pl}^{(j)}(q\,|\,t)$ for $j = 1, 2, \cdots, N$, determined by N roots of the following determinant equation

$$\mathcal{D}et\left\{\delta_{n,s} - \delta_{n,s}\left(\frac{6\,d_{cv}^2(T)}{\epsilon_0\epsilon_b\mathcal{V}_0}\right)\left[\frac{1 - n_1^{\rm e}(t\,|\,n) - n_1^{\rm h}(t\,|\,n)}{\hbar\Omega - E_{\rm G}(T) - E_1^{\rm e}(n) - E_1^{\rm h}(n) + V_{1,1;1,1}^{\rm eh}(n) - \Delta E_{\rm HF}^{\rm e}(t\,|\,n) - \Delta E_{\rm HF}^{\rm h}(t\,|\,n)}\right] - (1-\delta_{n,s})\right.$$
$$\left.\times\left(\frac{3\,d_{cv}^2(T)}{\pi\epsilon_0\epsilon_b}\right)V_{\rm c}(q\,|\,n,s)\left[\frac{1 - n_1^{\rm e}(t\,|\,s) - n_1^{\rm h}(t\,|\,s)}{\hbar\Omega - E_{\rm G}(T) - E_1^{\rm e}(s) - E_1^{\rm h}(s) + V_{1,1;1,1}^{\rm eh}(s) - \Delta E_{\rm HF}^{\rm e}(t\,|\,s) - \Delta E_{\rm HF}^{\rm h}(t\,|\,s)}\right]\right\} = 0\ , \quad (32)$$

where s, $n = 1, 2, \cdots, N$ are site indexes, and s, and $n_1^{\rm e,h}(t\,|\,s)$ and $\Delta E_{\rm HF}^{\rm e,h}(t\,|\,s)$ are calculated from Eqs. (1), (2) and (4) and from Eqs. (25a) and (25b), respectively.

As a special case, for double QDs with s, $n = 1, 2$ we find two nonlocal-plasmon modes $\hbar\Omega_{pl}^{\pm}(q\,|\,t)$ from Eq. (32), given by

$$\hbar\Omega_{pl}^{\pm}(q\,|\,t) = \frac{1}{2}\left\{\Delta_1(t) + \Delta_2(t) + R_1[Z_1(t) + Z_2(t)]\right.$$
$$\left. \pm \sqrt{\{\Delta_1(t) - \Delta_2(t) + R_1[Z_1(t) - Z_2(t)]\}^2 + 4R_2^2\,V_{\rm c}(q\,|\,2,1)V_{\rm c}(q\,|\,1,2)Z_1(t)Z_2(t)}\right\}\ , \quad (33)$$

where $R_1 = 6\,d_{cv}^2(T)/\epsilon_0\epsilon_b\mathcal{V}_0$, $R_2 = 3\,d_{cv}^2(T)/\pi\epsilon_0\epsilon_b$, $Z_1(t) = 1 - n_1^{\rm e}(t\,|\,1) - n_1^{\rm h}(t\,|\,1)$, $Z_2(t) = 1 - n_1^{\rm e}(t\,|\,2) - n_1^{\rm h}(t\,|\,2)$, $\Delta_1(t) = [E_{\rm G}(T) + E_1^{\rm e}(1) + E_1^{\rm h}(1) - V_{1,1;1,1}^{\rm eh}(1)] + \Delta E_{\rm HF}^{\rm e}(t\,|\,1) + \Delta E_{\rm HF}^{\rm h}(t\,|\,1)$, and $\Delta_2(t) = [E_{\rm G}(T) + E_1^{\rm e}(2) + E_1^{\rm h}(2) - V_{1,1;1,1}^{\rm eh}(2)] + \Delta E_{\rm HF}^{\rm e}(t\,|\,2) + \Delta E_{\rm HF}^{\rm h}(t\,|\,2)$. The signs $\pm$ in Eq. (33) define the split in-phase (+) and out-of-phase (−) plasmon modes, separately. [22–24]

From Eq. (33) we expect that two Coulomb-split plasmon modes will show up in this double-quantum-dot system with quite different dispersion features. Specifically, as the incident laser field approaches its peak value, the Coulomb coupling $V_c(q\,|\,n,s)$ introduced in Eq. (30) gives rise to both an upper in-phase and a lower out-of-phase plasmon modes due to very high level populations in two QDs and an enhanced suppression of the off-resonance contribution in Eq. (30) at the same time. When the laser field approaches its tail value, on the other hand, the Coulomb coupling between these two split-plasmon modes becomes insignificant due to enhanced off-resonance effect in Eq. (30). Therefore, we acquire quite distinctive but constant populations in two QDs, and expect a nearly flat in-phase plasmon mode as well as a monotonically decreasing out-of-phase plasmon mode as a function of wave number q. Physically, quantum-dot sizes $L_{x,y,z}$ can be used for varying energy levels of electrons in a QD, while laser frequency $\hbar\omega_0$, peak-field strength $\mathcal{E}_0$ and pulse width σ_0 for modifying ultrafast dynamics of photo-generated e-h pairs. Additionally, laser-frequency detuning δ_0 and interband dephasing rate $\hbar\gamma_{\rm dp}$ can further be employed for controlling magnitude and decay of induced quantum coherence, and finally separation d between two QDs for altering interdot dipole coupling.

III. NUMERICAL RESULTS AND DISCUSSIONS

In our numerical calculations, we have taken: $L_x = L_y = L_z = 220\,\text{Å}$, $m_{\rm e}^* = 0.067\,m_0$, $m_{\rm h}^* = 0.62\,m_0$, $\epsilon_b = 12$, $\epsilon_s = 11$, $\epsilon_\infty = 13$, $T = 300\,\text{K}$, $\hbar\Omega_0 = 36\,\text{meV}$, $\hbar\gamma_0 = 0.1\,\text{meV}$, $\hbar\Gamma_0 = 0.1\,\text{meV}$, $\hbar\gamma_{\rm dp} = 0.1\,\text{meV}$, $\mathcal{E}_0 = 6\,\text{MV/m}$, $2\sigma_0 = 1\,\text{ps}$, and $\delta_0 = -2\,\text{meV}$. The bandgap $E_{\rm G}(T)$ of the quantum-dot host material is evaluated as $1.83\,\text{eV}$ at $T = 300\,\text{K}$.

A. Results for Single Quantum Dot

In Sec. III A, we will present our calculated results for occupation factor, quantum coherence, stimulated-transition rate, induced intradot depolarization field, radiative decay, energy-relaxation rate and transient plasmon energy in a single-QD system, including their dependence on time t, frequency detuning $\delta_0 = [E_{\rm G}(T) + E_1^{\rm e} + E_1^{\rm h} - V_{1,1;1,1}^{\rm eh}] - \hbar\omega_0$, emitted-photon energy $\hbar\omega'$ and different pulse profiles.

The calculated t dependence of two level-occupation factors $n_1^{\rm e}(t)$ and $n_1^{\rm h}(t)$ from Eqs. (1) and (2) for electrons and holes, respectively, are presented in Fig. 3, where the relation $n_1^{\rm e}(t) = n_1^{\rm h}(t)$ is maintained and only one cycle

ACCEPTED MANUSCRIPT
Journal of Applied Physics
AIP Publishing
This is the author's peer reviewed, accepted manuscript. However, the online version of record will be different from this version once it has been copyedited and typeset.
PLEASE CITE THIS ARTICLE AS DOI: 10.1063/5.0081067

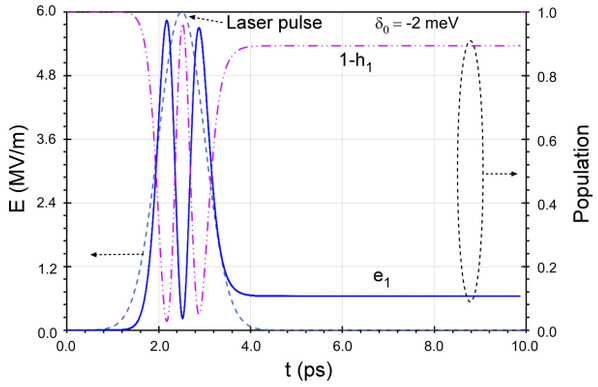

FIG. 3: Calculated level-occupation factors $n_1^{\rm e}(t)$ for electrons (solid curve & right scale) and $1-n_1^{\rm h}(t)$ for holes (double-dot-dashed curve & right scale) as functions of time t, where the pulsed-laser profile (dashed curve & left scale) is also displayed for convenience.

of Rabi oscillation with split peaks is observed due to moderate strength for peak laser field $\mathcal{E}_0$ and narrow pulse width $2\sigma_0$, corresponding to a relatively large Rabi oscillation time period ($\sim \pi/\omega_R$) compared to $2\sigma_0$, which agrees with the prediction made by Eq. (27) as well as its discussions afterward. Meanwhile, the maximum values of $n_1^{\rm e}(t)$ and $n_1^{\rm h}(t)$ are found slightly below unity, which mainly results from a finite frequency detuning $\delta_0 = -2\,$meV in the system. From Eqs. (1) and (2), we know that the e-h stimulated transitions stop after the incident laser pulse, and then, $n_1^{\rm e}(t)$ and $n_1^{\rm h}(t)$ reach constants as observed in Fig. 3. Furthermore, the time-independent part of $n_1^{\rm e}(t)$ and $n_1^{\rm h}(t)$ after $t = 4\,$ps indicates that the energy-relaxation processes for e-h pairs are slow compared to the 10 ps time scale. At the same time, the radiative-decay (photoluminescence) process between two ground states of e-h pairs is also insignificant on the 10 ps time scale.

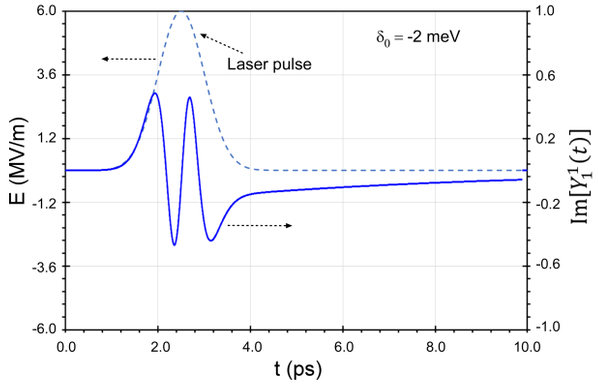

FIG. 4: Calculated imaginary part of induced quantum coherence $\mathrm{Im}[Y_1^1(t)]$ for e-h pairs (solid curve & right scale) as a function of t, where the pulsed-laser profile (dashed curve) is also presented for convenience.

Known from the description and explanation given for Fig. 3, the Rabi oscillations appearing in transient occupation factors $n_1^{\rm e,h}(t)$ originate from stimulated transitions for generation of e-h pairs, i.e., the first term $(2/\hbar)\,\mathrm{Im}\{\big[Y_1^1(t)\big]^*\,\widetilde{\mathcal{M}}_{1,1}^{\rm eh}(t)\}$ on the right-hand sides of Eqs. (1) and (2). As shown in Fig. 4, under a laser pulse or $\mathcal{M}_{1,1}^{\rm eh}(t) \neq 0$, the oscillations in induced quantum coherence $Y_1^1(t)$ are initiated as predicted by Eq. (4). Although the Rabi oscillations in $n_1^{\rm e,h}(t)$ are suppressed as $\omega_R = 0$, nonzero $Y_1^1(t)$ is maintained in the system even after the laser pulse and supported by $\boldsymbol{\mathcal{E}}_{\rm intra}(t\,|\,\omega_0)$ given in Eq. (23) but with an exponential decay after the laser pulse due to finite diagonal-dephasing rate $\hbar\gamma_{\rm dp} = 0.1\,$meV.

To further explore transient coupling dynamics between a pulsed laser and photo-generated e-h pairs in a QD, we plot in Fig. 5 the calculated stimulated-transition rate $(2/\hbar)\,\mathrm{Im}\{\big[Y_1^1(t)\big]^*\,\widetilde{\mathcal{M}}_{1,1}^{\rm eh}(t)\}$ as a function of time, where

ACCEPTED MANUSCRIPT
Journal of Applied Physics
AIP Publishing
This is the author's peer reviewed, accepted manuscript. However, the online version of record will be different from this version once it has been copyedited and typeset.
PLEASE CITE THIS ARTICLE AS DOI: 10.1063/5.0081067

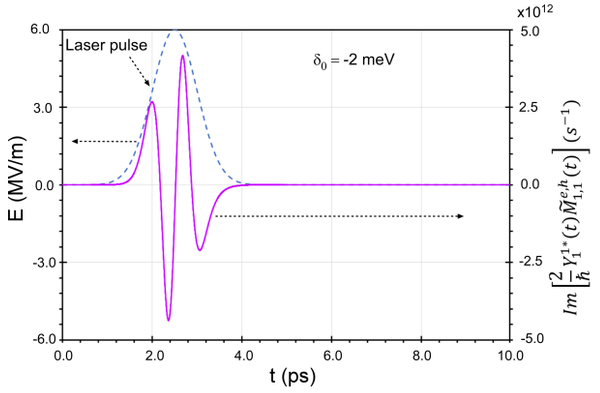

FIG. 5: Calculated stimulated-transition rate $(2/\hbar)\,\mathrm{Im}\{[Y_1^1(t)]^*\,\widetilde{\mathcal{M}}_{1,1}^{\mathrm{eh}}(t)\}$ for e-h pairs (solid curve) as a function of t, where the pulsed-laser profile (dashed curve) is also shown.

positive and negative signs of this rate correspond to upward and downward transitions between two ground states of electrons and holes in a QD. Physically, Rabi oscillations are responsible for transferring electrons back and forth between conduction and valence bands across a bandgap in the system. This carrier transferring process stops beyond the pulse time although induced quantum coherence $Y_1^1(t)$ may still alive. Here, the peaks and valleys in Figs. 3, 4 and 5 are found fully correlated to each other, and electrons start with an upward transition but end with a downward transition by combining Figs. 3 and 5.

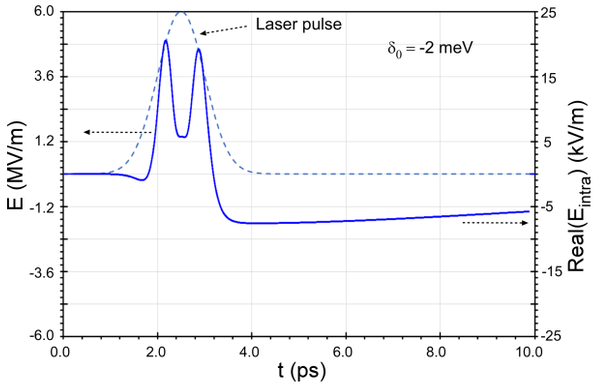

FIG. 6: Calculated real part of the self-consistent intradot depolarization field $\mathrm{Re}[\mathcal{E}_{\mathrm{intra}}(t)]$ in Eq. (23) as a function of t, where the pulsed-laser profile (dashed curve) is also presented.

From Eq. (23) we find that the self-consistent intradot depolarization field $\mathrm{Re}[\mathcal{E}_{\mathrm{intra}}(t\,|\,\omega_0)]$ is proportional to $\mathrm{Re}[Y_1^1(t\,|\,\omega_0)]$ which is determined by Eq. (4). Although a decayed $\mathrm{Im}[Y_1^1(t\,|\,\omega_0)]$ occurs after laser pulse, as displayed in Fig. 4, we still see a strong but slowly decreasing $\mathrm{Re}[\mathcal{E}_{\mathrm{intra}}(t\,|\,\omega_0)]$ in Fig. 6, which, in turn, enables a finite $Y_1^1(t\,|\,\omega_0)$ as a function of time. Here, it is very interesting to notice the occurrence of a split peak for $\mathrm{Re}[\mathcal{E}_{\mathrm{intra}}(t\,|\,\omega_0)]$ in Fig. 6 during the laser-pulse time. Such an doublet feature can be associated with optical nonlinearity in the system due to the presence of a term $n_1^{\mathrm{e,h}}(t)\,\mathcal{E}_{\mathrm{intra}}(t) \sim d_{cv}^2(T)\,n_1^{\mathrm{e,h}}(t)\,Y_1^1(t\,|\,\omega_0)$ in Eq. (4). Importantly, the peak of $\mathrm{Re}[\mathcal{E}_{\mathrm{intra}}(t\,|\,\omega_0)]$ acquires a positive sign for $\delta_0 = -2\,\mathrm{meV}$, which greatly enhances the quantum coherence $Y_1^1(t)$ and demonstrates the laser-frequency control of $Y_1^1(t)$. From a physics perspective, the existence of a finite $\mathrm{Re}[\mathcal{E}_{\mathrm{intra}}(t\,|\,\omega_0)]$ can be viewed as a plasmon mode for interacting e-h pairs with its energy given by Eq. (24). We further notice from Fig. 6 that a peak $\mathrm{Re}[\mathcal{E}_{\mathrm{intra}}(t\,|\,\omega_0)]$ that is two orders of magnitude down from the peak pump field, which is consistent with the result in Ref. [8] for a nanowire.

The self-sustained intradot depolarization field $\boldsymbol{\mathcal{E}}_{\mathrm{intra}}(t\,|\,\omega_0)$, presented in Fig. 6 for its real part, has been defined by Eq. (23) and is proportional to interband quantum coherence $Y_1^1(t\,|\,\omega_0)$. After the laser pulse has passed a QD, $\boldsymbol{\mathcal{E}}_{\mathrm{intra}}(t\,|\,\omega_0)$ starts decaying with time due to dephasing but still remains to be finite due to supported by induced

ACCEPTED MANUSCRIPT
Journal of Applied Physics
This is the author's peer reviewed, accepted manuscript. However, the online version of record will be different from this version once it has been copyedited and typeset.
PLEASE CITE THIS ARTICLE AS DOI: 10.1063/5.0081067
AIP Publishing

self-sustained plasmon oscillations within the QD, as can be verified from Fig. 4 for $\mathrm{Im}[Y_1^1(t\,|\,\omega_0)]$. For the same reason, we obtain a finite $\mathrm{Re}[Y_1^1(t\,|\,\omega_0)]$ or $\mathrm{Re}[\boldsymbol{\mathcal{E}}_{\rm intra}(t\,|\,\omega_0)]$ even after the laser pulse but with a relatively slower decaying rate in comparison with that of $\mathrm{Im}[\boldsymbol{\mathcal{E}}_{\rm intra}(t\,|\,\omega_0)]$. On the other hand, the simple fact that $\boldsymbol{\mathcal{E}}^{\rm tot}_{\ell,j}(t)$ relies on $\boldsymbol{\mathcal{E}}^{(0)}_{\rm ext}(t)$ in Eq. (11) produces so-called bandedge nonlinearity ($\propto |\boldsymbol{\mathcal{E}}^{(0)}_{\rm ext}(t)|^2$, $|\boldsymbol{\mathcal{E}}^{(0)}_{\rm ext}(t)|^4$, $\cdots$ for level populations) through stimulated transitions. Moreover, the dependence of $\boldsymbol{\mathcal{E}}^{\rm tot}_{\ell,j}(t)$ on $\boldsymbol{\mathcal{E}}_{\rm intra}(t\,|\,\omega_0)$ leads to transient optical nonlinearity (with oscillating frequencies $2\omega_R$, $4\omega_R$, $\cdots$ for quantum coherence). Furthermore, the asymmetry in double peaks for $\mathrm{Re}[\boldsymbol{\mathcal{E}}_{\rm intra}(t\,|\,\omega_0)]$ in Fig. 6 is a reminiscent of two Rabi oscillations in populations $n_1^{\rm e,h}(t)$ within the pulse width as found in Fig. 3. Here, we would like to emphasize that the transient optical nonlinearity discussed in this paper is completely different from the usual optical nonlinearity in crystals, such as second- and third-harmonic generations.

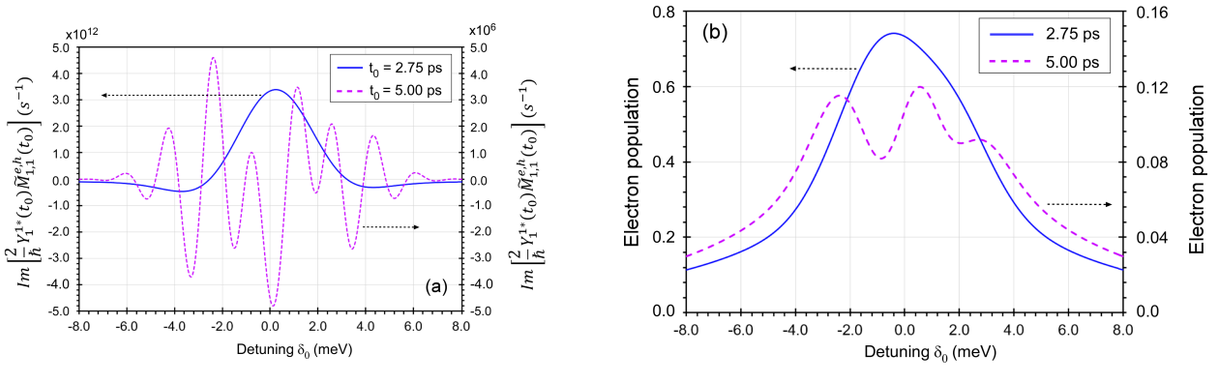

FIG. 7: (a) Calculated stimulated-transition rates $(2/\hbar)\,\mathrm{Im}\{\big[Y_1^1(\delta_0\,|\,t)\big]^*\,\mathcal{M}^{\rm eh}_{1,1}\}$ for e-h pairs at time $t = 2.75$ ps (solid curve & left scale) and 5.0 ps (dashed curve & right scale) as functions of frequency detuning δ_0. (b) Obtained effective optical spectra $n_1^{\rm e}(\delta_0\,|\,t)$ at moments $t = 2.75$ ps (solid curve) and 5.0 ps (dashed curve).

The calculated stimulated-transition rates are presented in Fig. 7(a) while the effective optical spectra are exhibited in Fig. 7(b), where two moments at $t = 2.75$ and 5.0 ps are considered in each panel for comparison. As indicated in the explanation to Fig. 5, the positive and negative signs for $(2/\hbar)\,\mathrm{Im}\{\big[Y_1^1(t)\big]^*\,\widetilde{\mathcal{M}}^{\rm eh}_{1,1}(t)\}$ as a function of frequency detuning δ_0 correspond, respectively, to upward and downward stimulated transitions. For fixed time, the change of occupation factors can also be fulfilled by varying δ_0. At $t = 2.75$ ps close to the second peak time of $n_1^{\rm e}(t)$ in Fig. 3, the stimulated-transition rate indeed switches its sign around $\delta_0 = -2$ meV in Fig. 7(a) and approaches zero for $|\delta_0| \gg 1$. For $t = 5.0$ ps at the tail of a Gaussian laser pulse, we know $dY_1^1(t)/dt \sim \exp[-i\Delta(\delta_0)t]\,\exp(-i\delta_0 t)$ from the discussion right after Eq. (27), which leads to $(2/\hbar)\,\mathrm{Im}\{\big[Y_1^1(\delta_0)\big]^*\,\mathcal{M}^{\rm eh}_{1,1}\} \propto \cos\{[\delta_0+\Delta(\delta_0)]t\}/[\delta_0+\Delta(\delta_0)]$ as well as complex oscillating features as a function of δ_0. On the other hand, in order to quantify the number of absorbed laser photons by electrons, we display an "effective" optical spectrum $n_1^{\rm e}(\delta_0\,|\,t)$ as a function of δ_0 in Fig. 7(b). For $n_1^{\rm e}(\delta_0\,|\,t)$ around the tail time, its value $n_1^{\rm e}(\delta_0\,|\,t) \propto \sin\{[\delta_0+\Delta(\delta_0)]t\}/[\delta_0+\Delta(\delta_0)]^2$ becomes very sensitive to the phase δ_0 of a Rabi oscillation before exiting to a constant. Around the peak time, however, $n_1^{\rm e}(\delta_0\,|\,t)$ is expected to remain close to its maximum for small values of δ_0.

Physically, whenever a constant time t_0 is given, the leading-order of laser interaction $\widetilde{\mathcal{M}}^{\rm eh}_{1,1}(t) \propto \mathcal{E}^{(0)}_{\rm ext}(t)$ with e-h pairs becomes fixed. However, the induced quantum coherence $Y_1^1(t)$ in a QD can still change with detuning δ_0 in an oscillating way through its phase factor $t_0\sqrt{\delta_0^2+4\omega_R^2}$. If t_0 takes the peak time 2.75 ps of a laser pulse, we expect a resonant electronic transition in e-h pairs as an appearance of a single peak in Figs. 7(a) and 7(b) at $\delta_0 = 0$ and approaching zero for very large $|\delta_0|$, i.e., similar to a regular optical-absorption spectrum. As t_0 switches to the tail time 5.0 ps of a laser pulse, on the other hand, we observe oscillating $n_1^{\rm e,h}(t)$ in Fig. 7(b) as a function of δ_0, which results from the varying phase factor $[\delta_0+\Delta(\delta_0)]t_0$ with changing δ_0.

We display obtained energy-relaxation rates $\partial n^{\rm e}_{1,2}(t)/\partial t|_{\rm rel}$ from Eq. (12), i.e., the second term on the right-hand side of Eq. (1), as functions of time t for electrons in Fig. 8(a) as well as for holes from Eq. (14) in Fig. 8(b), respectively. From Figs. 8(a) and 8(b) we find that $\partial n^{\rm e,h}_2(t)/\partial t|_{\rm rel} = -\partial n^{\rm e,h}_1(t)/\partial t|_{\rm rel} > 0$, which indicates the process for a net transferring process of electrons or holes from the lower occupied level-1 to the higher unoccupied level-2. After the pulse time ($t > 4$ ps), all energy-relaxation rates reduce to a constant as a consequence of time-independent level-occupation factors $n^{\rm e,h}_{1,2}(t)$ in Fig. 3. Moreover, the appearance of a dip in $|\partial n^{\rm e,h}_{1,2}(t)/\partial t|_{\rm rel}|$ close to the pulse-peak time is attributed to the presence of a valley between two split peaks for $n_1^{\rm e,h}(t)$ in Fig. 3 due to optical nonlinearity.

ACCEPTED MANUSCRIPT
Journal of Applied Physics
AIP Publishing
This is the author's peer reviewed, accepted manuscript. However, the online version of record will be different from this version once it has been copyedited and typeset.
PLEASE CITE THIS ARTICLE AS DOI: 10.1063/5.0081067

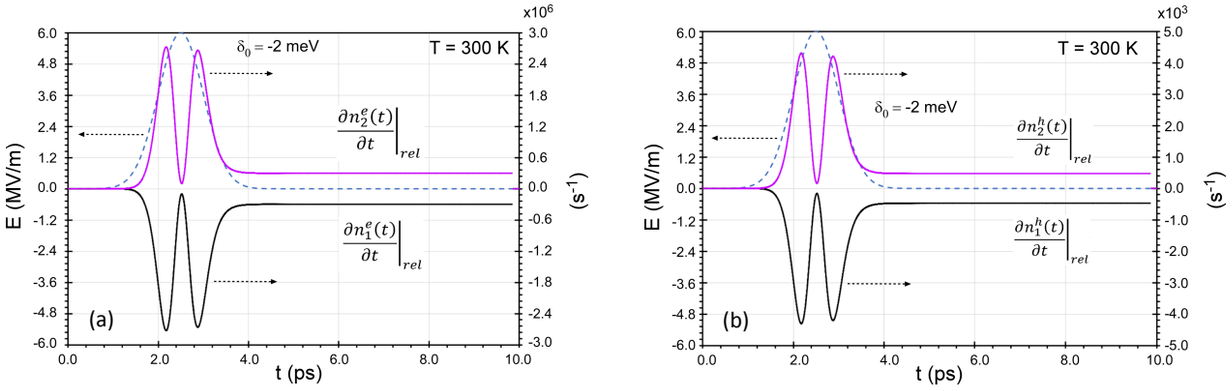

FIG. 8: (a) Calculated energy-relaxation rates $\partial n^{\rm e}_{1,2}(t)/\partial t|_{\rm rel}$ from Eq. (12) for electrons, as well as (b) energy-relaxation rates $\partial n^{\rm h}_{1,2}(t)/\partial t|_{\rm rel}$ from Eq. (14) for holes, as functions of t. Here, $\partial n^{\rm e}_{1,2}(t)/\partial t|_{\rm rel}$ for the first and second QD energy levels correspond to lower and upper solid curves in Fig. 8. For convenience, we also include the profile (dashed curve & left scale) of incident laser pulse in both panels.

Quantitatively, $\partial n^{\rm e}_{1,2}(t)/\partial t|_{\rm rel}$ becomes much faster than $\partial n^{\rm h}_{1,2}(t)/\partial t|_{\rm rel}$ by three orders of magnitude due to very large difference in their effective masses. Particularly, we must emphasize that phonon-scattering processes become quite different for electrons and holes, where the phonon scattering of electrons remains resonant but phonon scattering for the holes is out of resonance, leading to three-order difference between them. On the other hand, the Coulomb scatterings for electrons and holes are expected to behave similarly. This implies that the phonon scattering of electrons and holes dominates their energy-relaxation rates.

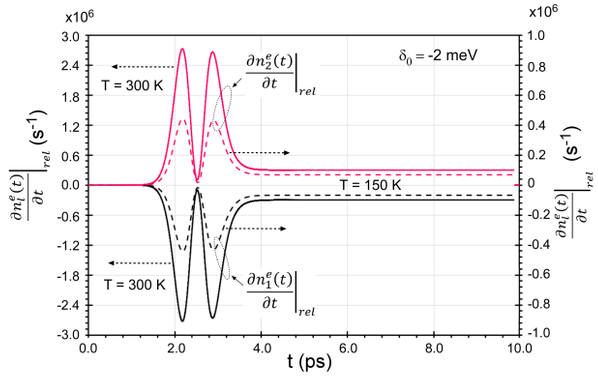

FIG. 9: Calculated energy-relaxation rates $\partial n^{\rm e}_{1,2}(t)/\partial t|_{\rm rel}$ from Eq. (12) for electrons as functions of t at two temperatures $T = 150$ and 300 K. Here, $\partial n^{\rm e}_{1,2}(t)/\partial t|_{\rm rel}$ for the first and second QD energy levels of electrons are represented by solid curves for $T = 300$ K but dashed curves for $T = 150$ K.

Figure 9 presents thermal effect on energy-relaxation rates $\partial n^{\rm e}_{1,2}(t)/\partial t|_{\rm rel}$ of electrons for two energy levels at different temperatures $T = 300$ K and 150 K. The thermal effects are reflected in three aspects, i.e., the static inverse screening length $Q_0 \sim 1/\sqrt{T}$ in Eq. (7), the optical-phonon occupation $N_0(\Omega_0) \sim \exp(-\hbar\Omega_0/k_BT)$ in Eqs. (13a) and (13b), and the electric-dipole-moment $d_{cv}(T)$ in Eq. (A8). Indeed, with decreasing T from 300 K to 150 K, the peaks of both $\partial n^{\rm e}_{1,2}(t)/\partial t|_{\rm rel}$ are reduced by about six times as seen in Fig. 9, which mainly results from the decreased phonon-scattering contribution in Eqs. (13a) and (13b) due to a larger static-screening wave number Q_0 and a smaller optical-phonon population $N_0(\Omega_0)$ at $T = 150$ K compared to corresponding ones at $T = 300$ K.

In Fig. 10, we present numerically calculated transient photoluminescence spectra $\mathcal{S}_{\rm sp}(\omega'\,|t)$ at three selected times $t = 1.9$, 2.9, 7.5 ps, corresponding to before, after and away from the peak time as indicated in Fig. 10(a), where $\mathcal{S}_{\rm sp}(\omega'\,|t)$ in Eq. (20) is related to third terms $\mathcal{R}^{\rm sp}_1(t)$ on the right-hand sides of Eqs. (1) and (2) and a peak in $\mathcal{S}_{\rm sp}(\omega'\,|t)$ occurs at the Coulomb-renormalized bandedge. As seen in Eq. (20), the peak strength of $\mathcal{S}_{\rm sp}(\omega'\,|t)$ is mainly

ACCEPTED MANUSCRIPT
Journal of Applied Physics
AIP Publishing
This is the author's peer reviewed, accepted manuscript. However, the online version of record will be different from this version once it has been copyedited and typeset.
PLEASE CITE THIS ARTICLE AS DOI: 10.1063/5.0081067

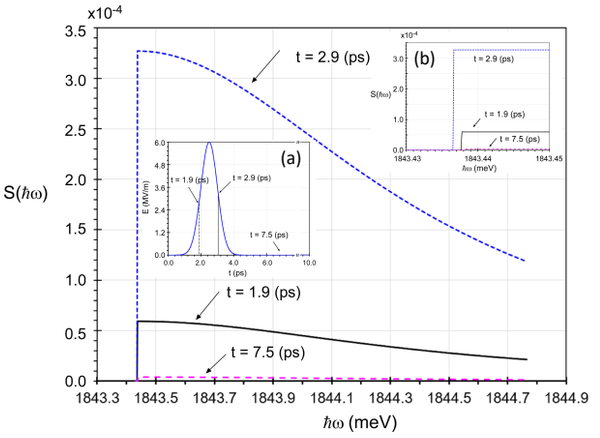

FIG. 10: Calculated transient photoluminescence spectra $\mathcal{S}_{\rm sp}(\omega'|t)$ from Eq. (20) for three moments $t = 1.9$, 2.9, 7.5 ps, where the pulsed-laser profile is displayed in (a) with arrow indications for selected time while the blow-up view of $\mathcal{S}_{\rm sp}(\omega'|t)$ near the bandedge is presented in (b).

proportional to the product $n_1^{\rm e}(t)n_1^{\rm h}(t)/\hbar\gamma_0$ which, in turn, is determined by the first term at the right-hand sides of Eqs. (1) and (2) for stimulated interband transitions of electrons and holes, whereas the contribution from $n_2^{\rm e}(t)n_2^{\rm h}(t)$ is negligible. Clearly, both the energy relaxations and radiative decays of occupation factors $n_1^{\rm e,h}(t)$ are found still insignificant at the 10 ps time scale, as verified by Fig. 3. On the other hand, a very sharp rise of $\mathcal{S}_{\rm sp}(\omega'|t)$ occurs at the bandgap frequency in Fig. 10, which is followed by a half-Lorentz-type tail above the bandgap as a function of emitted-photon frequency. As found from Fig. 3, $n_1^{\rm e,h}(t)$ is enhanced in a time sequence $t = 7.5$, 1.9, 2.9 ps. Furthermore, from Eq. (4), Eqs. (5a) and (5b) we know that the bandgap will be Coulomb-renormalized by transient Hartree-exchange energies. As a whole, this leads to a reduced bandgap with increasing $n_1^{\rm e}(t)$ and $n_1^{\rm h}(t)$ as demonstrated by the downshift of bandedge in Fig. 10(b) for $t = 7.5$, 1.9, 2.9 ps. In fact, both enhanced peak strength and downshift of peak frequency follow the increased $n_1^{\rm e,h}(t)$ in a time sequence $t = 7.5$, 1.9, 2.9 ps.

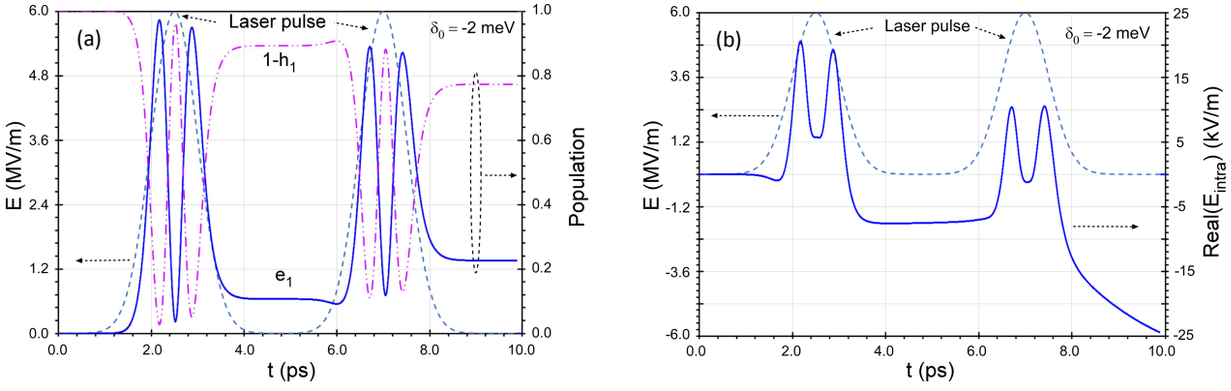

FIG. 11: (Left) Calculated level-occupation factors $n_1^{\rm e}(t)$ for electrons (solid curve) and $1 - n_1^{\rm h}(t)$ for holes (double-dot-dashed curve) as functions of t. (Right) Obtained real part of intradot depolarization field $\mathrm{Re}[\mathcal{E}_{\rm intra}(t)]$ as a function of time. For convenience, we also include the profile (dashed curve) for double pulses of incident laser in both panels.

In Figs. 3 and 4, the initial conditions $n_{1,2}^{\rm e,h}(0) = Y_\ell^j(0) = 0$ with ℓ, $j = 1, 2$ have been set at $t = 0$ for Eqs. (1), (2) and (4). In order to understand the physical implication of these initial conditions, we introduce a consecutive double-pulse sequence for incident laser field, as displayed by dashed curves in both left and right panels of Figs. 11. Under a double-pulse sequence, the first pulse-ending constant occupations $n_{1,2}^{\rm e,h}$ in the left panel acquire a new excitation from the following second laser pulse by repeating a similar splitting-peak feature with a slightly reduced amplitude. After ending time of the second laser pulse, we are again left with constant occupations $n_{1,2}^{\rm e,h}$ but with twice the respective

ACCEPTED MANUSCRIPT
Journal of Applied Physics
AIP Publishing
This is the author's peer reviewed, accepted manuscript. However, the online version of record will be different from this version once it has been copyedited and typeset.
PLEASE CITE THIS ARTICLE AS DOI: 10.1063/5.0081067

magnitudes, approximately. For the real part of the intradot depolarization field $\mathcal{E}_{\rm intra}(t) \propto {\rm Re}[Y_1^1(t)]$ in the right panel, however, after ending time of the second laser pulse, its amplitude increases greatly from the first pulse-ending constant value although the splitting-peak feature remains. These unique features in Fig. 11 show the presence of optical memory for an applied sequence of laser pulses, and also, provide laser controlling of ultrafast electron dynamics and coherence in a QD. Although the laser-pulse amplitude drops to zero, the strength of depolarization field remains strong and is even more intense after the second pulse with the π-phase shift. However, such an optical memory only survives within the coherence time and will vanish if the relaxation time is very short.

The interband coherence time is given by $1/\gamma_{\rm dp}$. Since $\hbar\gamma_{\rm dp} = 0.1\,{\rm meV}$ is chosen in current work, this gives a coherence time of 6.6 ps. Here, two subsequent pulse peaks in Fig. 11(a) are separated by about 5 ps, slightly shorter than the coherence time. Meanwhile, in our study, only interband optical transitions are studied, and no intraband optical transitions and intraband decoherence are considered. However, we do include a much longer intraband phonon-scattering or relaxation time (on the order of μs) as revealed by Figs. 8 and 9.

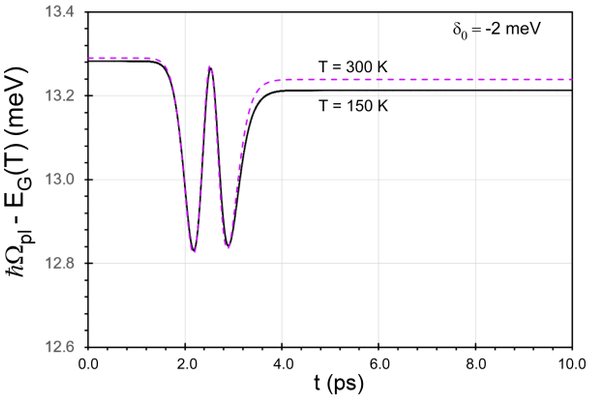

FIG. 12: Calculated local-plasmon-mode energy $\hbar\Omega_{pl}^{(\rm s)}(t) - E_{\rm G}(T)$ from Eq. (24) as a function of t at two temperatures $T = 150$ (solid curve) and 300 K (dashed curve)

In the presence of a laser field, it couples not only to single-particle motion but also to the collective motion of electrons in QD system.[27] After a pulsed-laser field is applied to a QD system, the single-particle excitation, such as Rabi oscillations in $n_{1,2}^{\rm e,h}(t)$ in Fig. 3, occurs. Since there exists Coulomb interaction among these photo-generated electrons and holes, the single-particle excitation in the system will be modified by Coulomb interaction or many-body effects, leading to a plasmon mode based on charge-density-fluctuation in this QD system. In Fig. 12, we compare calculated time dependence for the change of induced local-plasmon-mode energy $\hbar\Omega_{pl}^{(\rm s)}(t) - E_{\rm G}(T)$ from Eq. (24) at two different temperatures $T = 300$ and 150 K in order to highlight thermal dependence of this many-body effect. At $T = 300\,K$, $\hbar\Omega_{pl}^{(\rm s)}(t) - E_{\rm G}(T)$ has first experienced double dips due to the factor $1 - n_1^{\rm e}(t) - n_1^{\rm h}(t)$ in the last intradot-depolarization term of Eq. (24), and then, reaches a constant after the laser pulse. As T decreases from 300 K to 150 K, the electric-dipole-moment $d_{cv} \propto 1/\sqrt{E_{\rm G}(T)}$ decreases due to increased $E_{\rm G}(T)$, giving rise to a smaller many-body interaction in the last term of Eq. (24) and a downshift of the constant plasmon energy after laser pulse.

Using double Gaussian laser pulses in Fig. 11, we have revealed optical-memory effect in $n_1^{\rm e,h}(t)$ after the first laser pulse. In order to explore laser controlling of ultrafast electron dynamics in a QD, we present corresponding results of $n_1^{\rm e,h}(t)$ for a step laser pulse in the left panel of Fig. 13. As seen from the comparison of left panel in Fig. 13 with Fig. 3 after a laser pulse, instead of a constant we find continuous Rabi oscillations but with a slowly decaying amplitude due to finite dephasing rate $\hbar\gamma_{\rm dp} = 0.1\,{\rm meV}$. Additionally, a direct comparison of two right panels in Figs. 11 and 13, new continuous Rabi oscillations with a decaying amplitude show up in real part of the induced intradot depolarization field $\mathcal{E}_{\rm intra}(t)$. Therefore, we can view dephasing time $1/\gamma_{\rm dp}$ as a coherence time for the QD system, and the formalism for exact computation of the diagonal part of $\gamma_{\rm dp}$ can be found from Ref. [8].

B. Results for Double Quantum Dots

In Sec. III B, we will present our numerically obtained results, including transient dynamics for occupation factors, quantum coherence, interdot depolarization field, and coupled plasmon modes in a double-QD system, as well as

ACCEPTED MANUSCRIPT
Journal of Applied Physics
AIP Publishing
This is the author's peer reviewed, accepted manuscript. However, the online version of record will be different from this version once it has been copyedited and typeset.
PLEASE CITE THIS ARTICLE AS DOI: 10.1063/5.0081067

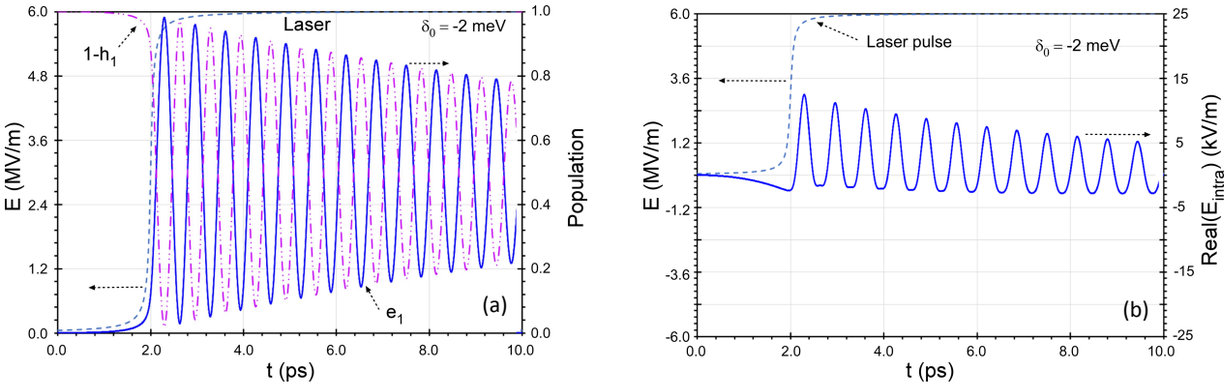

FIG. 13: (Left) Calculated level-occupation factors $n_1^{\rm e}(t)$ for electrons (solid curve) and $1-n_1^{\rm h}(t)$ for holes (double-dot-dashed curve) as functions of t for a step laser pulse. (Right) Obtained real part of intradot depolarization field $\mathrm{Re}[\mathcal{E}_{\rm intra}(t)]$ as a function of time for the step laser pulse. For convenience, we also include the transient profile (dashed curve) for step pulse of incident laser in both panels.

their dependence on static detuning δ_0 and different pulse profiles. In our numerical calculations, we take $L_x(1) = L_y(1) = L_z(1) = 60\,\text{Å}$ for QD-1 but $L_x(2) = L_y(2) = L_z(2) = 59.5\,\text{Å}$ for QD-2 to count for small dot-size fluctuations, and $|x_2 - x_1| = 100\,\text{Å}$ for center-to-center separation. For average-frequency detuning δ_0, we choose: $\delta_0(\omega_0) = E_{\rm G}(T) - \hbar\omega_0 + [E_1^{\rm e}(1) + E_1^{\rm h}(1) - V_{1,1;1,1}^{\rm eh}(1)]/2 + [E_1^{\rm e}(2) + E_1^{\rm h}(2) - V_{1,1;1,1}^{\rm eh}(2)]/2$, and then $\delta_1 = \delta_0(\omega_0) - \Delta\delta/2$, $\delta_2 = \delta_0(\omega_0) + \Delta\delta/2$, where $\Delta\delta = [E_1^{\rm e}(2) + E_1^{\rm h}(2) - V_{1,1;1,1}^{\rm eh}(2)] - [E_1^{\rm e}(1) + E_1^{\rm h}(1) - V_{1,1;1,1}^{\rm eh}(1)]$ is the difference of level offsets in two QDs. Other parameters are kept the same as those in Sec. III A. Here, we would like to emphasize that resonant Rabi oscillations can only be active in one of two QDs if the difference in QD sizes becomes large. In addition, the small dot size, compared to 22 nm for a single-QD system, gives rise to a very high polarization-charge density, and then a much large intradot depolarization field. Furthermore, the Rabi oscillations in QDs will be greatly enhanced if the signs for peaks of both intradot and interdot depolarization fields can match the sign of laser-pulse peak with a proper choice of $\delta_0(\omega)$ value. Otherwise, the interdot electromagnetic coupling will be very weak.

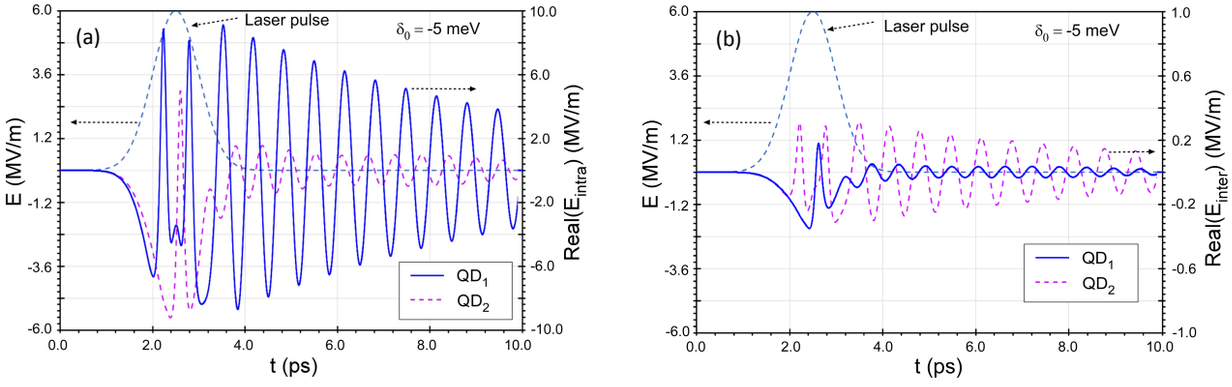

FIG. 14: (a) Calculated real part of intradot depolarization fields $\mathrm{Re}[\mathcal{E}_{\rm intra}(t)]$ from Eq. (23) for QD-1 (solid curve) and QD-2 (dashed curve) as functions of t. (b) Obtained real part of interdot depolarization fields $\mathrm{Re}[\mathcal{E}_{\rm inter}(t)]$ from Eq. (28) for QD-1 (solid curve) and QD-2 (dashed curve) as functions of time. Here, $\delta_0(\omega_0) = -5\,\text{meV}$ is chosen in computations. For convenience, we also include the transient profile (dashed curve & left scale) for Gaussian pulse of incident laser in both panels.

To understand the laser-frequency (ω_0) controlling [63] of self-consistently induced intradot and interdot depolarization fields for electromagnetically-coupled double quantum dots, we compare in Fig. 14 the calculated intradot and interdot depolarization fields in (a) and (b), separately, for QD-1 and QD-2. Known from Eq. (4), we find the phases of $Y_1^1(t\,|\,n,\omega_0)$ can be tuned by average-frequency detuning $\delta_0(\omega_0)$ through laser frequency ω_0 for QD-1 ($n = 1$) and QD-2 ($n = 2$) simultaneously. Indeed, as $\delta_0(\omega_0) = -5\,\text{meV}$ is chosen, both $\mathrm{Re}[\mathcal{E}_{\rm intra}(\boldsymbol{r},\, t\,|\,n,\omega_0)]$ in Fig. 14(a) and $\mathrm{Re}[\mathcal{E}_{\rm inter}(\boldsymbol{r}_n,\, t\,|\,n,\omega_0)]$ in Fig. 14(b) appear significant, which is attributed to matching the signs for

ACCEPTED MANUSCRIPT
Journal of Applied Physics
AIP Publishing
This is the author's peer reviewed, accepted manuscript. However, the online version of record will be different from this version once it has been copyedited and typeset.
PLEASE CITE THIS ARTICLE AS DOI: 10.1063/5.0081067

peaks of $\mathrm{Re}[\mathcal{E}_{\rm intra}(\boldsymbol{r},\, t\,|\,\omega_0)]$ and $\mathrm{Re}[\mathcal{E}_{\rm inter}(\boldsymbol{r}_n,\, t\,|\,\omega_0)]$ with the sign of laser-pulse peak so as to maximize the stimulated-transition rates simultaneously in both QDs around the peak time $t = 2.7\,$ps. Meanwhile, since the sizes of two QDs are unequal, we see from Fig. 14(a) that Rabi-oscillation profiles for $\mathrm{Re}[\mathcal{E}_{\rm intra}(\boldsymbol{r},\, t\,|\,n,\omega_0)]$ display different transient dependence with greatly enhanced Rabi oscillations in QD-1 and reach the same order as the peak of incident laser pulse. Instead, much stronger $\mathrm{Re}[\mathcal{E}_{\rm inter}(\boldsymbol{r}_n,\, t\,|\,\omega_0)]$ is found in QD-2 ($n = 2$) in comparison with that in QD-1 since the dipole-radiation source in QD-1 acquires a higher quantum coherence $Y_1^1(t\,|\,n = 1, \omega_0)$. Moreover, $\mathrm{Re}[\mathcal{E}_{\rm inter}(\boldsymbol{r}_n,\, t\,|\,\omega_0)]$ is about one order of magnitude smaller than $\mathrm{Re}[\mathcal{E}_{\rm intra}(\boldsymbol{r},\, t\,|\,n,\omega_0)]$ because of large reduction from inverse-cubic law [3] with respect to the separation between two QDs.

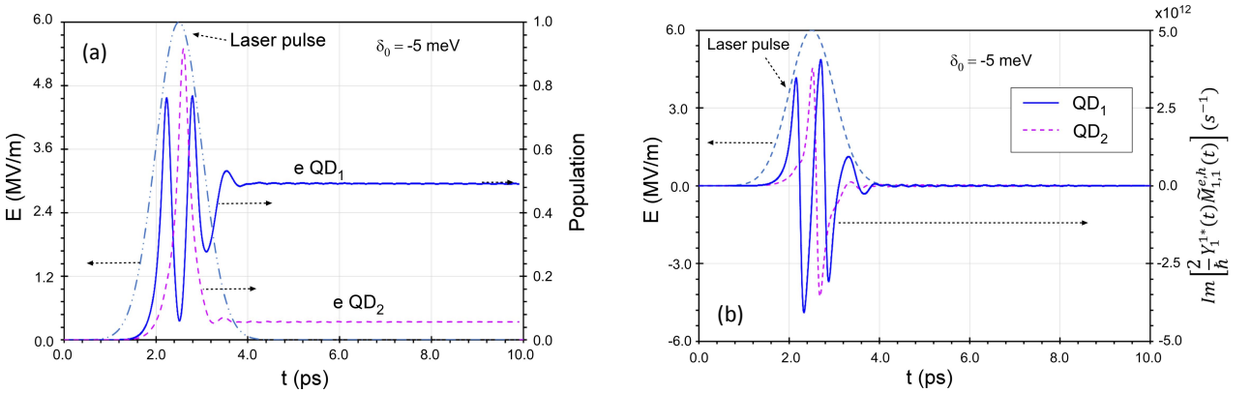

FIG. 15: (a) Calculated level-occupation factors $n_1^{\rm e}(t)$ for QD-1 (solid curve) and QD-2 (dashed curve) as functions of t. (b) Obtained stimulated-transition rates $(2/\hbar)\,\mathrm{Im}\{\big[Y_1^1(t\,|\,n,\delta_0)\big]^*\,\widetilde{\mathcal{M}}_{1,1}^{\rm eh}(t)\}$ for QD-1 (solid curve) and QD-2 (dashed curve) as functions of time. Here, $\delta_0(\omega_0) = -5\,$meV is chosen in computations. For convenience, we also include the transient profile (dashed curve & left scale) for Gaussian pulse of incident laser in both panels.

To reveal the mechanism behind ω_0-dependent controlling [63] of ultrafast nonlinear optical responses from e-h pairs in a dipole-radiation coupled double-quantum-dot system, we compare in Fig. 15 the calculated level-occupation factors $n_1^{\rm e}(t\,|\,n)$, as well as stimulated-transition rates $(2/\hbar)\,\mathrm{Im}\{\big[Y_1^1(t\,|\,n,\delta_0)\big]^*\,\widetilde{\mathcal{M}}_{1,1}^{\rm eh}(t)\}$, of both QD-1 ($n = 1$) and QD-2 ($n = 2$) in ($a$) and ($b$), respectively. As explained in Fig. 14, the selection of average-frequency detuning $\delta_0(\omega_0) = -5\,$meV maximizes the stimulated-transition rates $(2/\hbar)\,\mathrm{Im}\{\big[Y_1^1(t\,|\,n,\delta_0)\big]^*\,\widetilde{\mathcal{M}}_{1,1}^{\rm eh}(t)\}$ for both QDs, as verified in Fig. 15(b). This outcome directly leads to enhanced Rabi oscillations, as demonstrated in Fig. 15(a) for QD-1. For QD-2, on the other hand, the Rabi-oscillating feature is largely smeared out due to a smaller intradot depolarization field $\mathrm{Re}[\mathcal{E}_{\rm intra}(\boldsymbol{r},\, t\,|\,n = 2, \omega_0)]$ and then a longer oscillation period. Interestingly, we also notice that the magnitudes of stimulated-transition rates in two QDs become comparable to each other although less oscillations are found in QD-2. Such a unique feature results from a balance between a larger $\mathrm{Re}[\mathcal{E}_{\rm intra}(\boldsymbol{r},\, t\,|\,n,\omega_0)]$ accompanied by a smaller $\mathrm{Re}[\mathcal{E}_{\rm inter}(\boldsymbol{r}_n,\, t\,|\,\omega_0)]$ in QD-1 ($n = 1$) and a lower $\mathrm{Re}[\mathcal{E}_{\rm intra}(\boldsymbol{r},\, t\,|\,n,\omega_0)]$ along with a higher $\mathrm{Re}[\mathcal{E}_{\rm inter}(\boldsymbol{r}_n,\, t\,|\,\omega_0)]$ for QD-2 ($n = 2$). Here, the drop of depolarization-field strength from $\mathrm{Re}[\mathcal{E}_{\rm intra}(\boldsymbol{r},\, t\,|\,n,\omega_0)]$ to $\mathrm{Re}[\mathcal{E}_{\rm inter}(\boldsymbol{r},\, t\,|\,n,\omega_0)]$ is larger in QD-1 ($n = 1$) compared to that of QD-2 ($n = 2$).

We know from Eq. (33) that two split plasmon modes (with respect to $\pm$ signs) in the dipole-radiation coupled double-quantum-dot system will display distinctive dispersion as a function of the wave number q for photo-generated e-h pairs. As shown in Fig. 16(a) at the peak time $t = 2.75\,$ps, an indirect gap appears with the minima and maxima at different q values, resulting from slightly varied energy levels in QDs-1, 2. For $t = 2.75\,$ps, Coulomb coupling $V_c(q\,|\,n,s)$ in Eq. (30) between the upper in-phase ($+$) and lower out-of-phase ($-$) plasmon modes is expected to be very strong due to similar high occupations for electrons and holes in both QDs, as seen in Fig. 15(a), and a suppression of the off-resonance term (first one inside the square root) in Eq. (33) as well. At the tail time $t = 5.0\,$ps for Fig. 16(b), instead, the coupling between two split plasmon modes becomes very weak due to the large off-resonance term in Eq. (33). For this case, quite different but constant occupations with time occur in QD-1, 2, and therefore we observe a nearly dispersion-less in-phase plasmon mode plus a strongly dispersive out-of-phase plasmon mode with a negative phase velocity, i.e., $d\Omega_{\rm pl}^-(q\,|\,t)/dq < 0$. In Figs. 16($a$) and 16($b$), we only plot q dependence in $\hbar\Omega_{\rm pl}^{\pm}(q\,|\,t)$ within the range of $0 \le q/q_0 \le 1$. Since $V_{\rm c}(q\,|\,n,s) \sim 1/q$ in Eq. (33) as long as $q_jL_j \gg 1$ for $j = x,\, y,\, z$, we expect $d\Omega_{\rm pl}^{\pm}(q\,|\,t)/dq \to 0$ eventually as $q/q_0 \gg 1$ for fixed L_j.

To demonstrate the quenching of Rabi oscillations in two QDs, we present calculated level populations $n_1^{\rm e}(t)$ for electrons in Fig. 17(a) as functions of time t with a different frequency detuning $\delta_0 = -2\,$meV. Compared to Figs. 15(a)

ACCEPTED MANUSCRIPT
Journal of Applied Physics
This is the author's peer reviewed, accepted manuscript. However, the online version of record will be different from this version once it has been copyedited and typeset.
PLEASE CITE THIS ARTICLE AS DOI: 10.1063/5.0081067
AIP Publishing

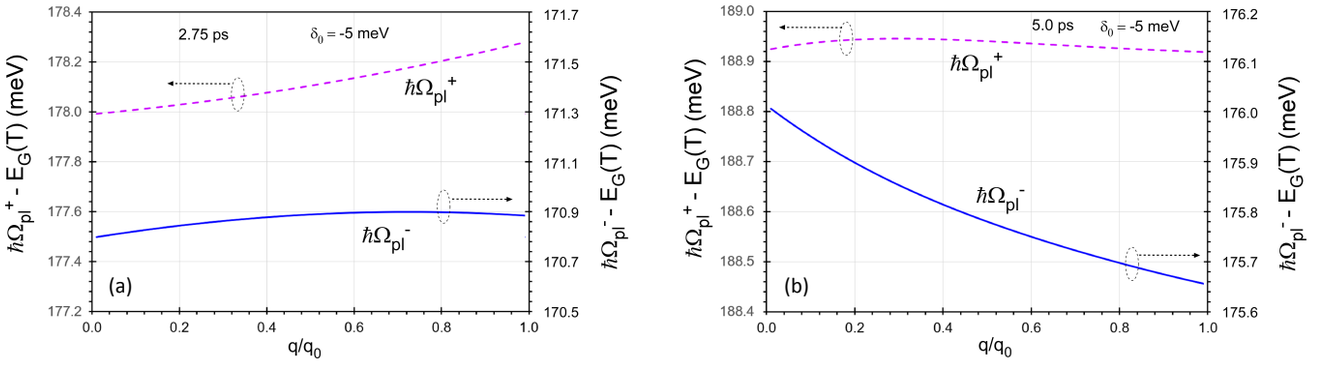

FIG. 16: Calculated split plasmon-mode energies $\hbar\Omega_{pl}^{\pm}(q\,|\,t) - E_{\rm G}(T)$ from Eq. (33) for the dipole-radiation coupled double-quantum-dot system as functions of scaled wave number q/q_0 at the peak time $t = 2.75\,$ps in (a) and at the tail time $t = 5.0\,$ps in (b), where $q_0 = \sqrt{\epsilon_b}\,\omega_0\,/c$ is the wave number of incident laser field. Here, $\delta_0(\omega_0) = -5\,$meV is selected for computations.

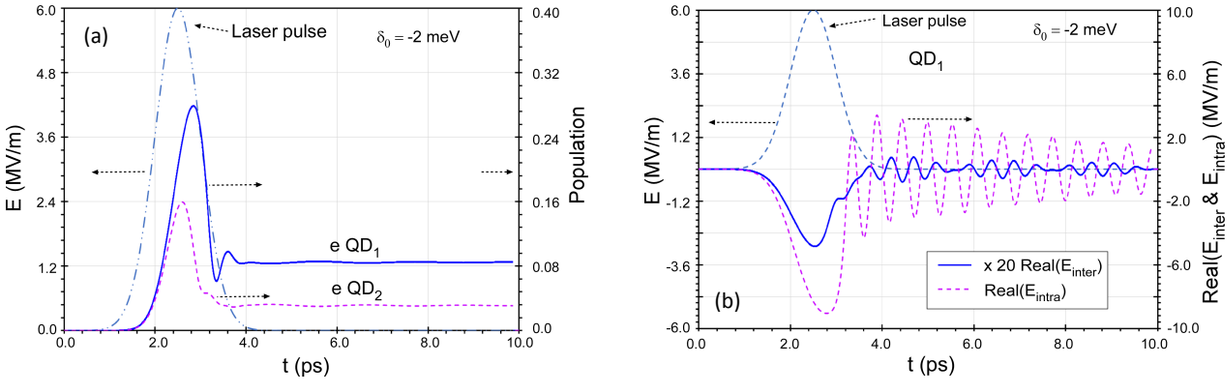

FIG. 17: (a) Calculated level-occupation factors $n_1^{\rm e}(t)$ for QD-1 (solid curve) and QD-2 (dashed curve) as functions of t. (b) Obtained real parts of intradot depolarization field $\mathrm{Re}[\mathcal{E}_{\rm intra}(t)]$ (solid curve) and interdot depolarization field $\mathrm{Re}[\mathcal{E}_{\rm inter}(t)]$ (dashed curve & amplified by a factor of $\times 20$) for QD-1 as functions of time. Here, $\delta_0(\omega_0) = -2\,$meV is chosen in computations. For convenience, we also include the transient profile (dash-dotted and dashed curves & left scale) for Gaussian pulse of incident laser in panels (a) and (b), respectively.

and 15(b), the induced interband quantum coherence $Y_1^1(t)$ in this case is reduced greatly, leading to much smaller peak values 0.28 and 0.16 for $n_1^{\rm e}(t)$ in QDs-1,2, respectively. From this phenomenon, we know that the induced quantum coherence of a photo-excited QD can be changed by altering laser-frequency ω_0 for the same peak-field strength $\mathcal{E}_0$. Furthermore, to reveal the physical mechanism behind the unique features in Fig. 17(a), we compare in Fig. 17(b) the intradot $\mathrm{Re}[\mathcal{E}_{\rm intra}(t)]$ and interdot $\mathrm{Re}[\mathcal{E}_{\rm inter}(t)]$ depolarization fields within QD-1 as function of t, where it is easy to find that the signs of these two depolarizarion fields are the same but opposite to the applied laser field $\mathcal{E}_{\rm ext}^{(0)}(t)$. This is quite different from the cases shown in Fig. 6 for $\mathrm{Re}[\mathcal{E}_{\rm intra}(t)]$ and in Fig. 15(b) for $\mathrm{Re}[\mathcal{E}_{\rm inter}(t)]$ although $\mathrm{Re}[\mathcal{E}_{\rm inter}(t)]$ is a factor of 1/20 smaller than $\mathrm{Re}[\mathcal{E}_{\rm intra}(t)]$ in Fig. 17(b).

IV. SUMMARY AND REMARKS

In summary, by employing the generalized density-matrix equations, we have studied extensively the ultrafast dynamics of resonantly photo-generated electron-hole pairs and revealed the physics mechanism behind the laser-controlled transient nonlinear-optical response of electron-hole pairs in the system of electromagnetically-coupled double quantum dots. In particular, the carrier-phonon and carrier-carrier scatterings have been incorporated into this theory for describing microscopic ultrafast energy-relaxation process of photo-carriers beyond the simple energy-relaxation-time approximation. Meanwhile, radiative recombination of excited electron-hole pairs are also taken

ACCEPTED MANUSCRIPT
Journal of Applied Physics
This is the author's peer reviewed, accepted manuscript. However, the online version of record will be different from this version once it has been copyedited and typeset.
PLEASE CITE THIS ARTICLE AS DOI: 10.1063/5.0081067
AIP Publishing

into consideration quantum-mechanically. Furthermore, the contributions from self-consistently induced intradot and interdot depolarization fields are included in stimulated interband transitions of interacting photo-carriers for higher-order correlation effects of electron-hole pairs.

First, for a single-dot system, we have presented numerical results to display transient dependence of carrier occupation factors and induced quantum coherence of electron-hole pairs for both single- and double-pulse profiles, as well as for a step profile, of incident laser fields. The effect of phase controlling on the transient profile of self-consistently induced intradot depolarization field has been demonstrated by comparing it with given transient profiles of an incident laser field. In addition, we have also shown the thermal effect on scattering rates of carriers in their energy-relaxation process. Meanwhile, the time-resolved photo-luminescence spectra are compared at peak, mid-height and tail times of an incident laser pulse, and the change of spectral peaks and the shift of spectral onset are found due to reduction of bandgap resulting from many-body effects. Particularly, for the fixed peak and tail time of an incident laser pulse, we have compared the calculated frequency-detuning spectra for both stimulated-transition rates and occupation factors of photo-carriers at different time moments.

Next, for a dipole-radiation coupled double-dot system, by introducing a small fluctuation to dot sizes, we have numerically computed the time dependence of both intradot and interdot self-consistent depolarization fields, and meantime, have further indicated the importance for matching their phases (or the sign of peaks) with a given incident-laser pulse so as to achieve non-quenched Rabi oscillations in both quantum dots simultaneously. Interestingly, the self-compensation of a smaller interdot depolarization field by a larger intradot one is automatically maintained in this system, leading to similar stimulated-transition rates for both quantum dots. Moreover, the calculated dispersion for two split plasmon modes at the peak time are presented to reveal the appearance of a plasmon indirect gap between the upper in-phase and lower out-of-phase modes. From obtained plasmon spectra at tail time, on the other hand, we find the coupling between two plasmon modes becomes very weak due to existence of a large off-resonance contribution.

Finally, from the perspective of application, our proposed theoretical model, the analysis method, and the obtained results for ultrafast study of nonlinear, non-adiabatic and quantum interactions can greatly assist the design and realization of artificial quantum molecules composed of a finite number of arbitrarily located quantum dots interacting mutually with nonlocal quantum interactions and entanglement, accompanied by laser manipulation of electron states within artificial quantum molecules. Such a theoretical study reveals physics mechanism, which dominates ultrafast and strong interactions of matter and electromagnetic fields, are of great interests in practical applications such as, high-speed optically-controlled electron states, energy-level shift and modulation due to strong light-matter interaction, as well as electromagnetic field-induced spatial quantum coherence and entanglement.

Acknowledgments

X.L. and J.G. acknowledge the support from the Air Force Research Lab Summer Faculty Fellowship Program sponsored by AFOSR and AFSOR DURI program (Grant No. FA9550-18-1-0444). D.H. would like to acknowledge the financial support from the Air Force Office of Scientific Research (AFOSR). The contribution of J.G. in this material is based upon work supported by the National Science Foundation under Grant No. 1903462.

Appendix A: Electronic States of a Quantum Dot

We have assumed a box-type potential with hard walls for a quantum dot, given by

$$V(\boldsymbol{r}) = \begin{cases} 0\ , & |x_i| \le L_i/2 \text{ for } i = 1,\, 2,\, 3 \\ \infty\ , & \text{otherwise} \end{cases} \quad , \tag{A1}$$

where the position vector $\boldsymbol{r} = \{x_1, x_2, x_3\}$, and L_1, L_2 and L_3 stand for the widths of potential along the $\hat{\boldsymbol{e}}_1$, $\hat{\boldsymbol{e}}_2$ and $\hat{\boldsymbol{e}}_3$ directions, respectively. As a result, the static Schrödinger equation for a single electron or hole in this quantum dot is written as

$$-\frac{\hbar^2}{2m^*}\left[\frac{\partial^2}{\partial x_1^2} + \frac{\partial^2}{\partial x_2^2} + \frac{\partial^2}{\partial x_3^2} + V(\boldsymbol{r})\right]\psi(\boldsymbol{r}) = E\,\psi(\boldsymbol{r})\ , \tag{A2}$$

ACCEPTED MANUSCRIPT
Journal of Applied Physics
This is the author's peer reviewed, accepted manuscript. However, the online version of record will be different from this version once it has been copyedited and typeset.
PLEASE CITE THIS ARTICLE AS DOI: 10.1063/5.0081067
AIP Publishing

where the effective mass m^* is $m_{\rm e}^*$ for electrons or $m_{\rm h}^*$ for holes. The wave function for eigenstate of Eq. (A2) is calculated as

$$\psi_{n_1,n_2,n_3}(\boldsymbol{r}) = \frac{2\sqrt{2}}{\sqrt{L_1 L_2 L_3}} \sin\left[\frac{n_1\pi}{L_1}\left(x_1+\frac{L_1}{2}\right)\right] \sin\left[\frac{n_2\pi}{L_2}\left(x_2+\frac{L_2}{2}\right)\right] \sin\left[\frac{n_3\pi}{L_3}\left(x_3+\frac{L_3}{2}\right)\right] , \tag{A3}$$

which is fomally identical for both electrons and holes. The eigenstate-energy levels associated with the wave function in Eq. (A3) are

$$E_{n_1,n_2,n_3} = \frac{\hbar^2}{2m^*}\left[\left(\frac{n_1\pi}{L_1}\right)^2 + \left(\frac{n_2\pi}{L_2}\right)^2 + \left(\frac{n_3\pi}{L_3}\right)^2\right] , \tag{A4}$$

where the quantum numbers n_1, n_2, $n_3 = 1, 2, \cdots$.

Based on the calculated wave functions in Eq. (A3), the form factors introduced in Eqs. (8a) and (8b) can be obtained from

$$\mathcal{F}^{\rm e}_{n_1,n_2,n_3;\,n_1',n_2',n_3'}(\boldsymbol{q}) = \mathcal{F}^{\rm h}_{n_1,n_2,n_3;\,n_1',n_2',n_3'}(\boldsymbol{q}) = \mathcal{Q}^{(1)}_{n_1,n_1'}(q_1)\,\mathcal{Q}^{(2)}_{n_2,n_2'}(q_2)\,\mathcal{Q}^{(3)}_{n_3,n_3'}(q_3) , \tag{A5}$$

where the wave vector $\boldsymbol{q} = \{q_1, q_2, q_3\}$. In Eq. (A5), we have utilized the following notation for $j = 1, 2, 3$, i.e.,

$$\begin{aligned}\mathcal{Q}^{(j)}_{n_j,n_j'}(q_j) \;&\equiv\; \left(\frac{2}{L_j}\right)\int_{-L_j/2}^{L_j/2} dx_j\, \sin\left[\frac{n_j\pi}{L_j}\left(x_j+\frac{L_j}{2}\right)\right] \exp(iq_jx_j) \sin\left[\frac{n_j'\pi}{L_j}\left(x_j+\frac{L_j}{2}\right)\right] \\ &=\; [\mathcal{A}_0(x_1) - \mathcal{A}_0(x_2) - \mathcal{A}_0(x_3) + \mathcal{A}_0(x_4)]\exp(-iq_jL_j/2) ,\end{aligned} \tag{A6}$$

where the function $\mathcal{A}_0(x) = -\exp(ix/2)\sin(x/2)/x$, while $x_1 = q_jL_j + n_j\pi + n_j'\pi$, $x_2 = q_jL_j + n_j\pi - n_j'\pi$, $x_3 = q_jL_j - n_j\pi + n_j'\pi$ and $x_4 = q_jL_j - n_j\pi - n_j'\pi$. Moreover, the overlap of electron and hole wave-functions in this model can be easily calculated as

$$\int d^3\boldsymbol{r}\, \psi^{\rm e}_{n_1,n_2,n_3}(\boldsymbol{r})\, \psi^{\rm h}_{n_1',n_2',n_3'}(\boldsymbol{r}) = \delta_{n_1,n_1'}\,\delta_{n_2,n_2'}\,\delta_{n_3,n_3'} , \tag{A7}$$

which gives $\mathcal{G}_{cv} = 1$. The interband electric-dipole-moment $\boldsymbol{d}_{cv}(T) = d_{cv}(T)\,\hat{\boldsymbol{e}}_d$ at the isotropic $\boldsymbol{\Gamma}$-point, which is defined in Eq. (10), can be calculated according to the Kane approximation [65,66], yielding

$$d_{cv}(T) = \sqrt{\frac{e^2\hbar^2}{2m_0\,E_{\rm G}(T)}\left(\frac{m_0}{m_{\rm e}^*} - 1\right)} , \tag{A8}$$

which is temperature dependent, where m_0 represents the free-electron mass and $E_{\rm G}(T)$ is the temperature-dependent bandgap energy of host semiconductor.

The data that supports the findings of this study are available within the article.

[1] X. Lu, D. H. Huang and S. Fan, Phys. Rev. A **103**, 043504 (2021).
[2] D. J. Griffiths, *Introduction to Quantum Mechanics* (3dd ed., Cambridge University Press & Assessment, Pearson, 1995).
[3] J. D. Jackson, *Classical Electrodynamics* (John Wiley & Sons, 1975).
[4] M. Lindberg and S. W. Koch, Phys. Rev. B **38**, 3342 (1988).
[5] H. Haug and S. W. Koch, *Quantum Theory of the Optical and Electronic Properties of Semiconductors* (5th ed., World Scientific Publishing Co. Pte. Ltd., 2009).
[6] J. R. Kuklinski and S. Mukamel, Phys. Rev. B **44**, 11253 (1991).

ACCEPTED MANUSCRIPT
Journal of Applied Physics
AIP Publishing
This is the author's peer reviewed, accepted manuscript. However, the online version of record will be different from this version once it has been copyedited and typeset.
PLEASE CITE THIS ARTICLE AS DOI: 10.1063/5.0081067

[7] D. H. Huang, M. M. Easter, G. Gumbs, A. A. Maradudin, S.-Y. Lin, D. A. Cardimona, and X. Zhang, Optics Express **22**, 27576 (2014).
[8] J. R. Gulley and D. H. Huang, Optics Express **27**, 17154 (2019).
[9] H. Haug and A.-P. Jauho, *Quantum Kinetics in Transport and Optics of Semiconductors* (2nd ed., Springer-Verlag, Berlin, 2008).
[10] S. W. Koch, *Microscopic Theory of Semiconductors: Quantum Kinetics, Confinement and Lasers* (World Scientific, Singapore, 1995).
[11] V. M. Axt and T. Kuhn, Rep. Prog. Phys. **67**, 433 (2004).
[12] M. Kira and S. W. Koch, Prog. Quantum Electron. **30**, 155 (2006).
[13] Y. R. Shen, *The Principles of Nonlinear Optics* (John Wiley & Sons, 1984).
[14] D. H. Huang, Phys. Rev. B **53**, 13645 (1996).
[15] R. P. Smith, J. K. Wahlstrand, A. C. Funk, R. P. Mirin, S. T. Cundiff, J. T. Steiner, M. Schafer, M. Kira, and S. W. Koch, Phys. Rev. Lett. **104**, 247401 (2010).
[16] G. Khitrova, H. M. Gibbs, M. Kira, S. W. Koch, and A. Scherer, Nature Phys. **2**, 81 (2006).
[17] G. Khitrova, H. M. Gibbs, F. Jahnke, M. Kira, and S. W. Koch, Rev. Mod. Phys. **71**, 1591 (1999).
[18] Y. Z. Hu, M. Lindberg, and S. W. Koch, Phys. Rev. B **42**, 1713 (1990).
[19] G. Gumbs and D. H. Huang, Phys. Rev. B **50**, 15148 (1994).
[20] D. H. Huang and G. Gumbs, Phys. Rev. B **47**, 9597 (1993).
[21] D. H. Huang and P. R. Antoniewicz, Phys. Rev. B **43**, 2168 (1991).
[22] D. H. Huang and S.-X. Zhou, Phys. Rev. B **38**, 13061 (1988).
[23] A. C. Tselis and J. J. Quinn, Phys. Rev. B **29**, 3318 (1984).
[24] S. Das Sharma and J. J. Quinn, Phys. Rev. B **25**, 7603 (1982).
[25] D. H. Huang and D. A. Cardimona, Phys. Rev. A **64**, 013822 (2001).
[26] M. S. Kushwaha, Surf. Sci. Rep. **41**, 1 (2001).
[27] G. Gumbs and D. H. Huang, *Properties of Interacting Low-Dimensional Systems* (John Wiley & Sons, 2011).
[28] A. Iurov, D. H. Huang, G. Gumbs, W. Pan and A. A. Maradudin, Phys. Rev. B **96**, 081408(R) (2017).
[29] A. L. Fetter and J. D. Walecka, *Quantum Theory of Many-Particle Systems* (McGraw-Hii Book Company, New York, 1971).
[30] G. D. Mahan, *Many-Particle Physics* (1st ed., Plenum Press, New York, 1990).
[31] C. S. Ting, S. C. Ying, and J. J. Quinn, Phys. Rev. B **14**, 4439 (1976).
[32] X. L. Lei and C. S. Ting, Phys. Rev. B **32**, 1112 (1985).
[33] D. H. Huang and G. Gumbs, Phys. Rev. B **80**, 033411 (2009).
[34] D. H. Huang, A. Iurov, H.-Y. Xu, Y.-C. Lai, and G. Gumbs, Phys. Rev. B **99**, 245412 (2019).
[35] D. H. Huang, P. M. Alsing, T. Apostolova, and D. A. Cardimona, Phys. Rev. B **71**, 195205 (2005).
[36] D. H. Huang, T. Apostolova, P. M. Alsing, and D. A. Cardimona, Phys. Rev. B **69**, 075214 (2004).
[37] J. M. Ziman, *Principles of the Theory of Solids* (2nd ed., Cambridge University Press, Cambridge, 1972).
[38] S. K. Lyo and D. H. Huang, Phys. Rev. B **64**, 115320 (2001).
[39] S. K. Lyo and D. H. Huang, Phys. Rev. B **68**, 115317 (2003).
[40] S. K. Lyo and D. H. Huang, Phys. Rev. B **73**, 205336 (2006).
[41] T. Holstein, Ann. Phys. **29**, 410 (1964).
[42] Y. Zhu, D. H. Huang, and S. Feng, Phys. Rev. B **40** 3170 (1989).
[43] W. Que, G. Kirczenow, and E. Castao, Phys. Rev. B **43** 14079 (1991).
[44] G. Gumbs, D. H. Huang, H. Qiang, F. H. Pollak, P. D. Wang,, C. M. Sotomayor Torres, and M. C. Holland, Phys. Rev. B **50** 10962 (1994).
[45] D. H. Huang, G. Gumbs, and N. J. M. Horing, Phys. Rev. B **49** 11463 (1994).
[46] M. S. Kushwaha, J. Chem. Phys. **135**, 124704 (2011).
[47] X. Zhu, X. Xia, J. J. Quinn, and P. Hawrylak, Phys. Rev. B **38** 5617 (1988).
[48] D. H. Huang, G. Gumbs, and M. O. Manasreh, Phys. Rev. B **52** 14126 (1995).
[49] G. Gumbs, D. H. Huang, and D. N. Talwar, Phys. Rev. B **53** 15436 (1996).
[50] D. H. Huang and G. Gumbs, Phys. Rev. B **47**, 9597 (1993).
[51] D. H. Huang, G. Gumbs, M. Lanius, A. R. Jalil, P. Schuffelgen, G. Mussler, D. Grutzmacher, and V. Narayan, Phys. Lett. A **411**, 127550 (2021).
[52] K. M. Indlekofer, A. Föster, and H. Lüth, Physica B: Condens. Metter **314**, 499 (2002).
[53] R. W. Meulenberg, J. R. I. Lee, A. Wolcott, J. Z. Zhang, L. J. Terminello, and T. van Buuren, ACS Nano **3**, 325 (2009).
[54] Z. Xiao, J. Appl. Phys. **86**, 4509 (1999).
[55] D. H. Huang and P. M. Alsing, Phys. Rev. B **78**, 035206 (2008).
[56] S. Schmitt-Rink, D. S. Chemla, and H. Haug, Phys. Rev. B **37**, 941 (1988).
[57] S. Schmitt-Rink, D. S. Chemla, and D. A. B. Miller, Phys. Rev. B **32**, 6601 (1985).
[58] D. A. B. Miller, D. S. Chemla, and S. Schmitt-Rink, Phys. Rev. B **33**, 6976 (1986).
[59] S. Schmitt-Rink, D. A. B. Miller, and D. S. Chemla, Phys. Rev. B **35**, 8113 (1987-II).
[60] S. Schmitt-Rink, D. S. Chemla, and H. Haug, Phys. Rev. B **37**, 941 (1988).
[61] S.-L. Chuang, S. Schmitt-Rink, D. A. B. Miller, and D. S. Chemla, Phys. Rev. B **43**, 1500 (1991).
[62] D. S. Chemla, D. A. B. Miller, and S. Schmitt-Rink, Phys. Rev. Lett. **59**, 1018 (1987).
[63] N. Mojaverian, G. Gu, and X. Lu, J. Phys D: Appl. Phys. **48**, 475102 (2015).
[64] S. Ravets, H. Labuhn, D. Barredo, T. Lahaye, and A. Browaeys, Phys. Rev. A **92**, 020701(R) (2015).

[65] E. O. Kane, J. Physi. Chem. Solids **1**, 249 (1957).
[66] U. Bockelmann and G. Bastard, Phys. Rev. B **45**, 1688 (1992).

ACCEPTED MANUSCRIPT
Journal of Applied Physics
AIP Publishing
This is the author's peer reviewed, accepted manuscript. However, the online version of record will be different from this version once it has been copyedited and typeset.
PLEASE CITE THIS ARTICLE AS DOI: 10.1063/5.0081067

ACCEPTED MANUSCRIPT

Journal of Applied Physics

This is the author's peer reviewed, accepted manuscript. However, the online version of record will be different from this version once it has been copyedited and typeset.
PLEASE CITE THIS ARTICLE AS DOI: 10.1063/5.0081067

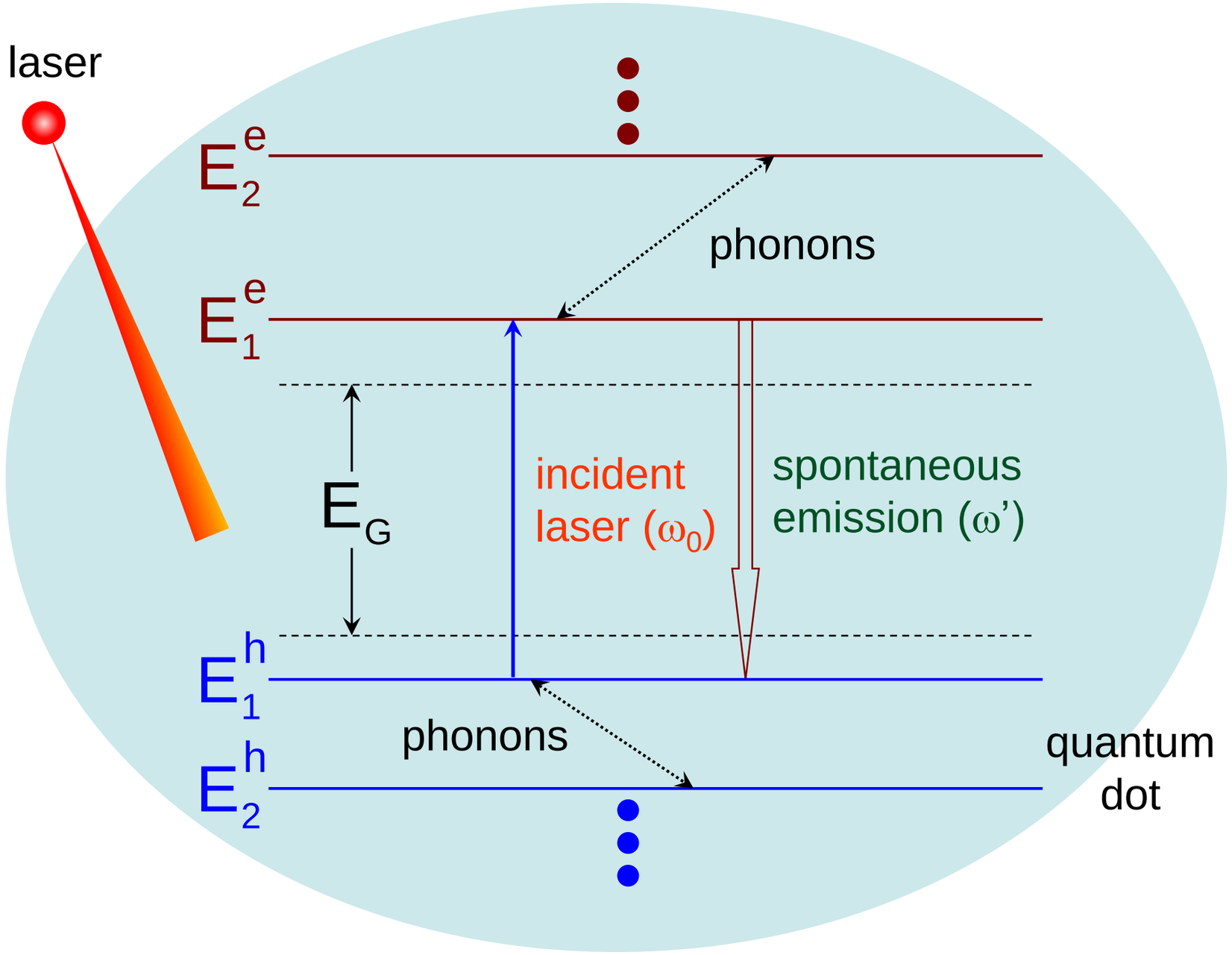

AIP Publishing

Journal of Applied Physics

ACCEPTED MANUSCRIPT

This is the author's peer reviewed, accepted manuscript. However, the online version of record will be different from this version once it has been copyedited and typeset.

PLEASE CITE THIS ARTICLE AS DOI: 10.1063/5.0081067

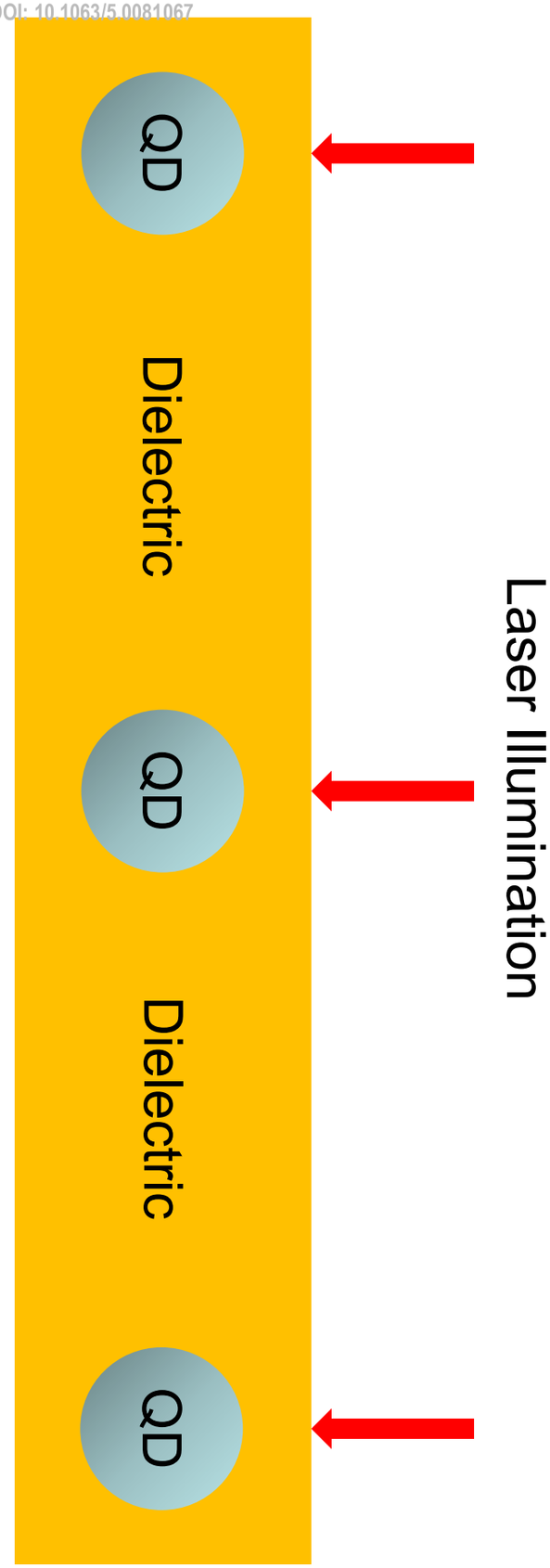

Journal of Applied Physics

ACCEPTED MANUSCRIPT

This is the author's peer reviewed, accepted manuscript. However, the online version of record will be different from this version once it has been copyedited and typeset.

PLEASE CITE THIS ARTICLE AS DOI: 10.1063/5.0081067

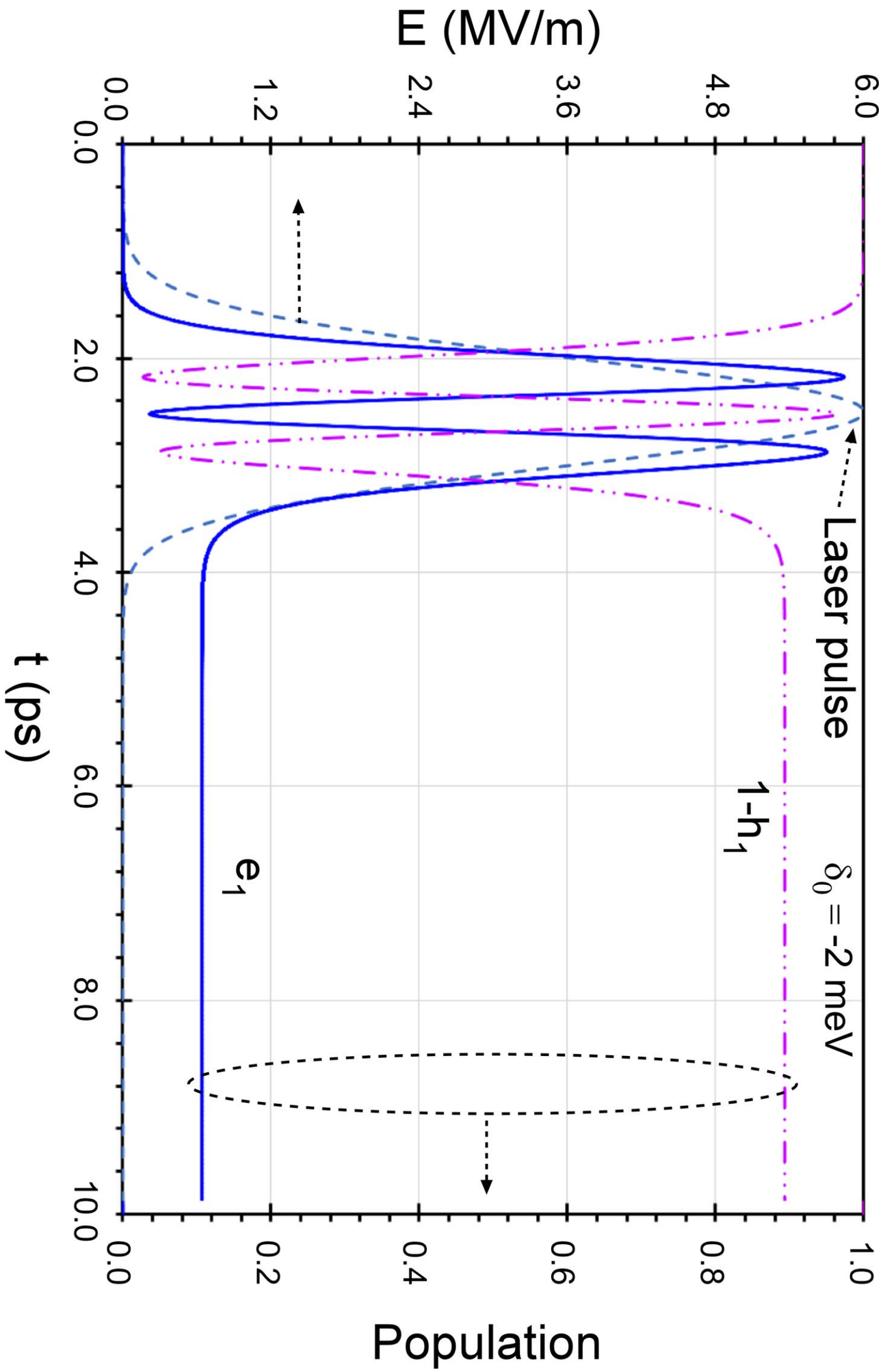

AIP Publishing

Journal of Applied Physics

ACCEPTED MANUSCRIPT

This is the author's peer reviewed, accepted manuscript. However, the online version of record will be different from this version once it has been copyedited and typeset.
PLEASE CITE THIS ARTICLE AS DOI: 10.1063/5.0081067

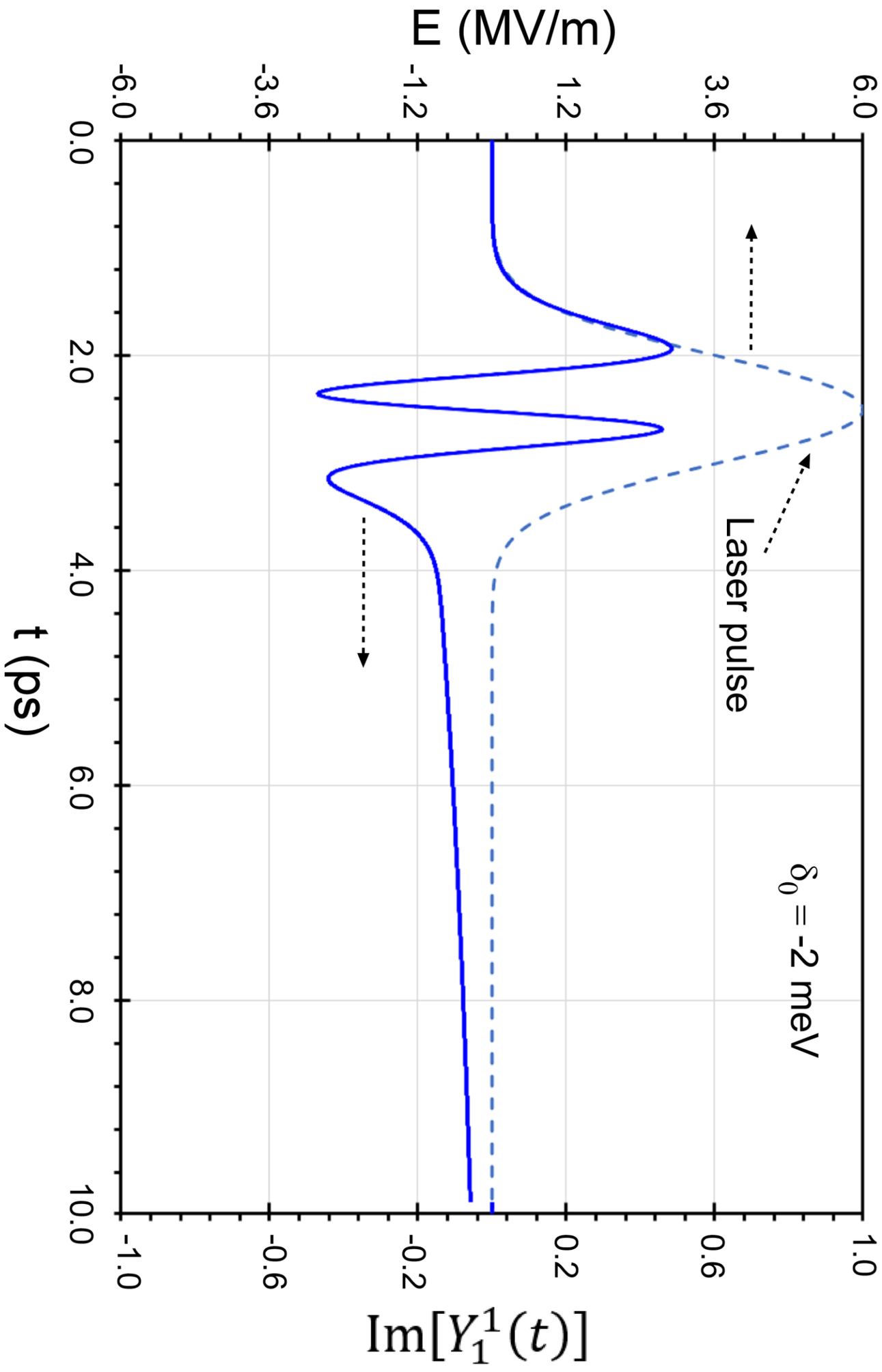

AIP Publishing

Journal of Applied Physics

ACCEPTED MANUSCRIPT

This is the author's peer reviewed, accepted manuscript. However, the online version of record will be different from this version once it has been copyedited and typeset.
PLEASE CITE THIS ARTICLE AS DOI: 10.1063/5.0081067

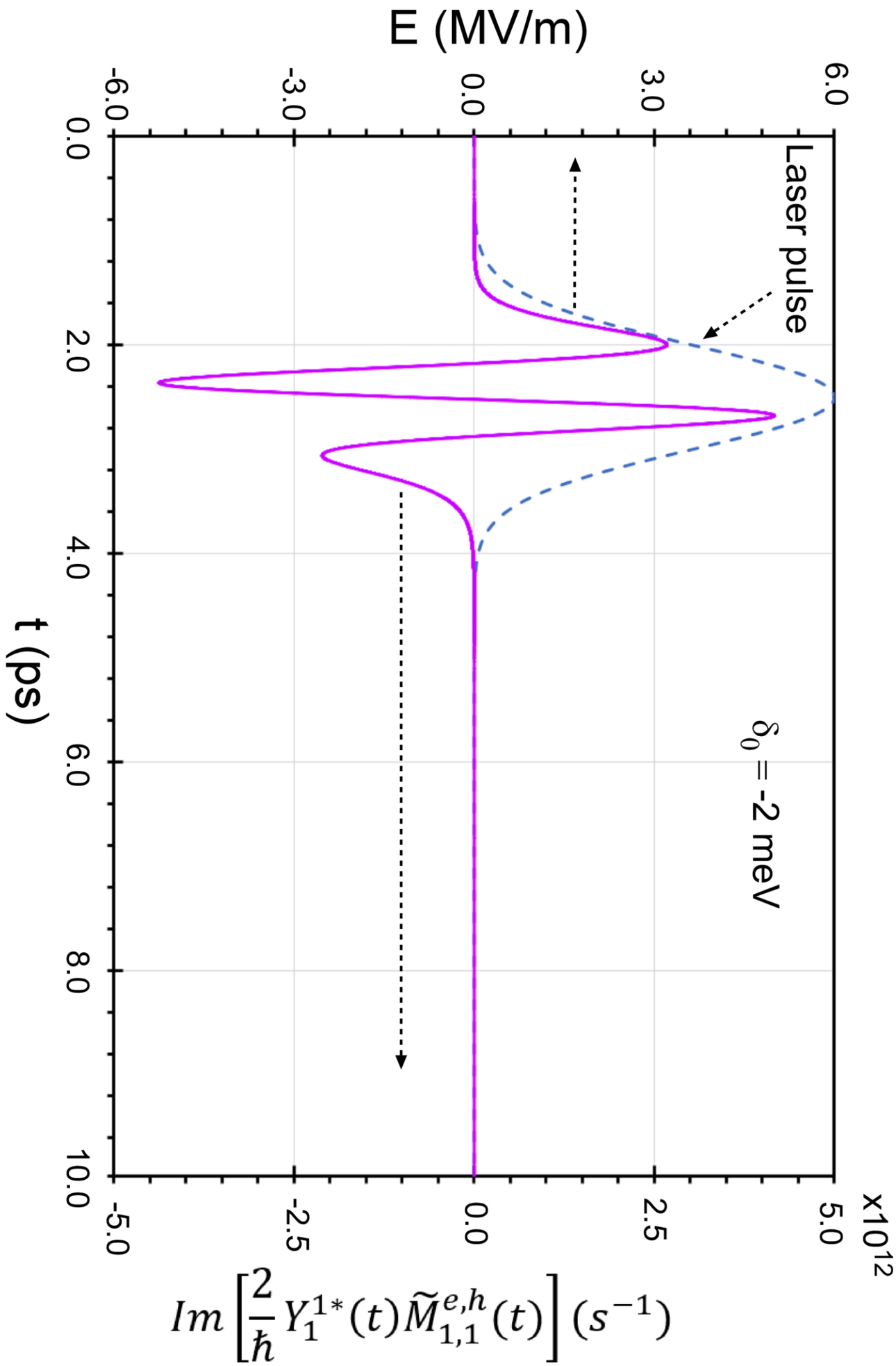

Journal of Applied Physics

ACCEPTED MANUSCRIPT

This is the author's peer reviewed, accepted manuscript. However, the online version of record will be different from this version once it has been copyedited and typeset.

PLEASE CITE THIS ARTICLE AS DOI: 10.1063/5.0081067

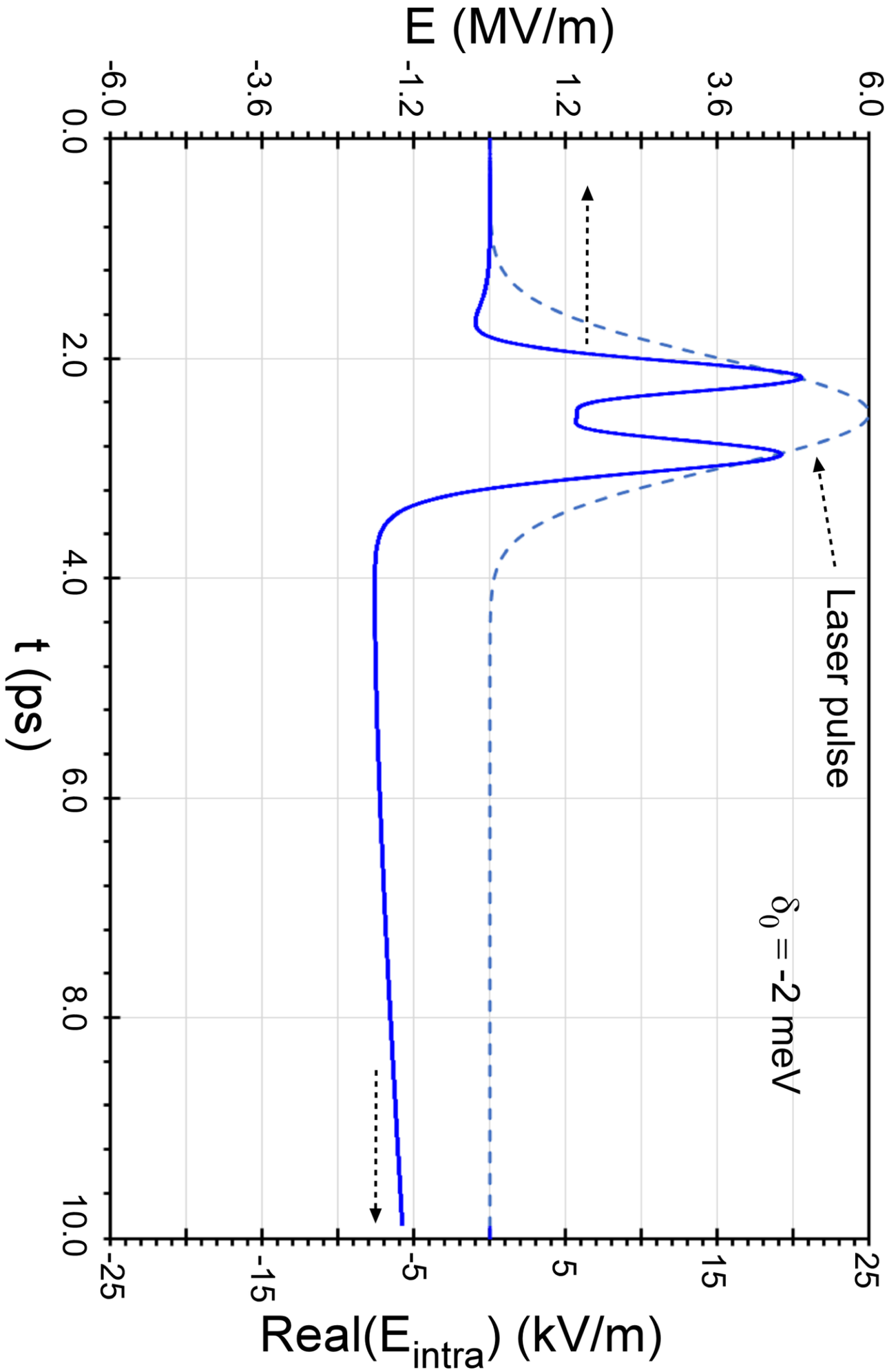

AIP Publishing

Journal of Applied Physics

ACCEPTED MANUSCRIPT

This is the author's peer reviewed, accepted manuscript. However, the online version of record will be different from this version once it has been copyedited and typeset.
PLEASE CITE THIS ARTICLE AS DOI: 10.1063/5.0081067

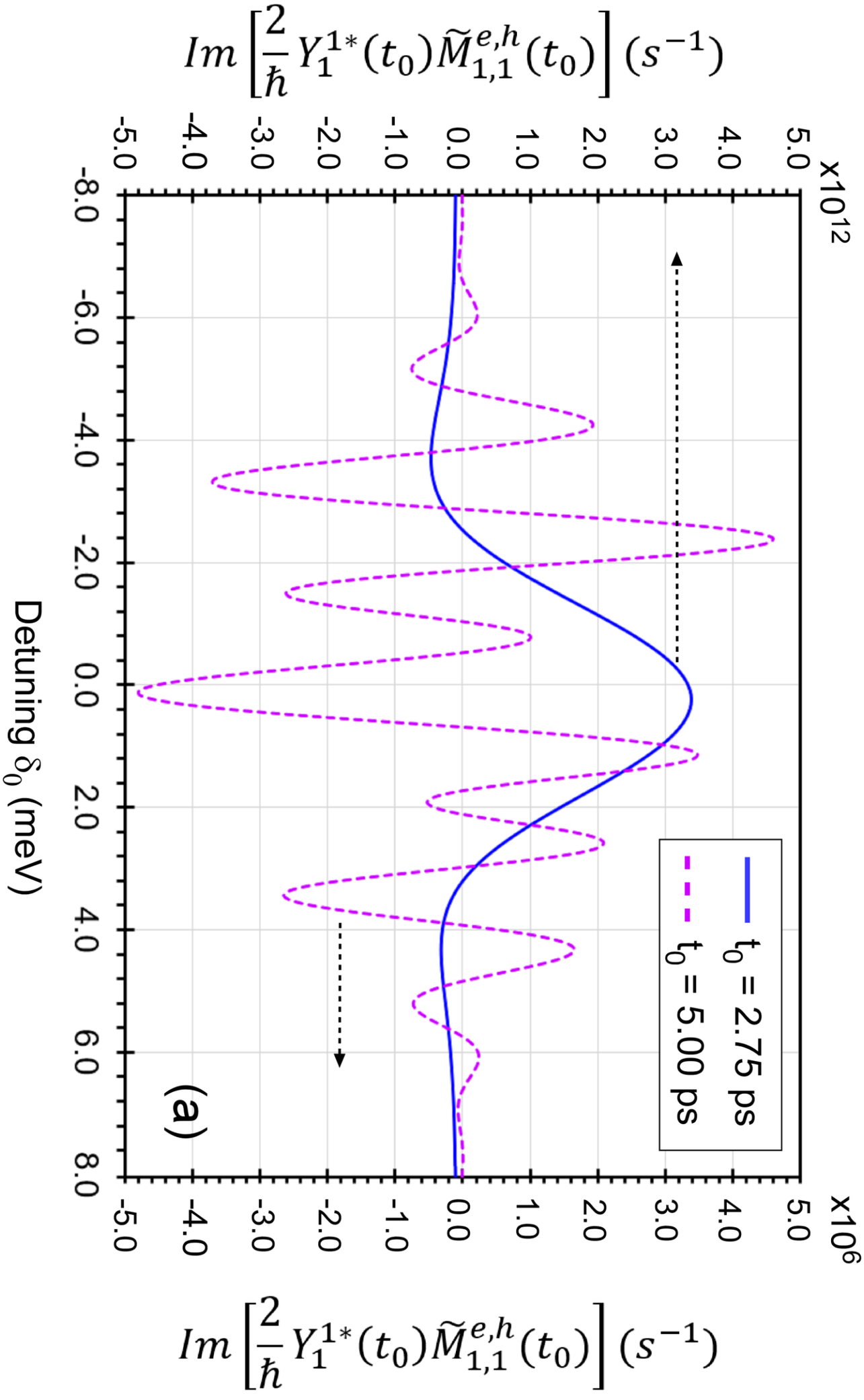

AIP Publishing
Journal of Applied Physics
ACCEPTED MANUSCRIPT

This is the author's peer reviewed, accepted manuscript. However, the online version of record will be different from this version once it has been copyedited and typeset.
PLEASE CITE THIS ARTICLE AS DOI: 10.1063/5.0081067

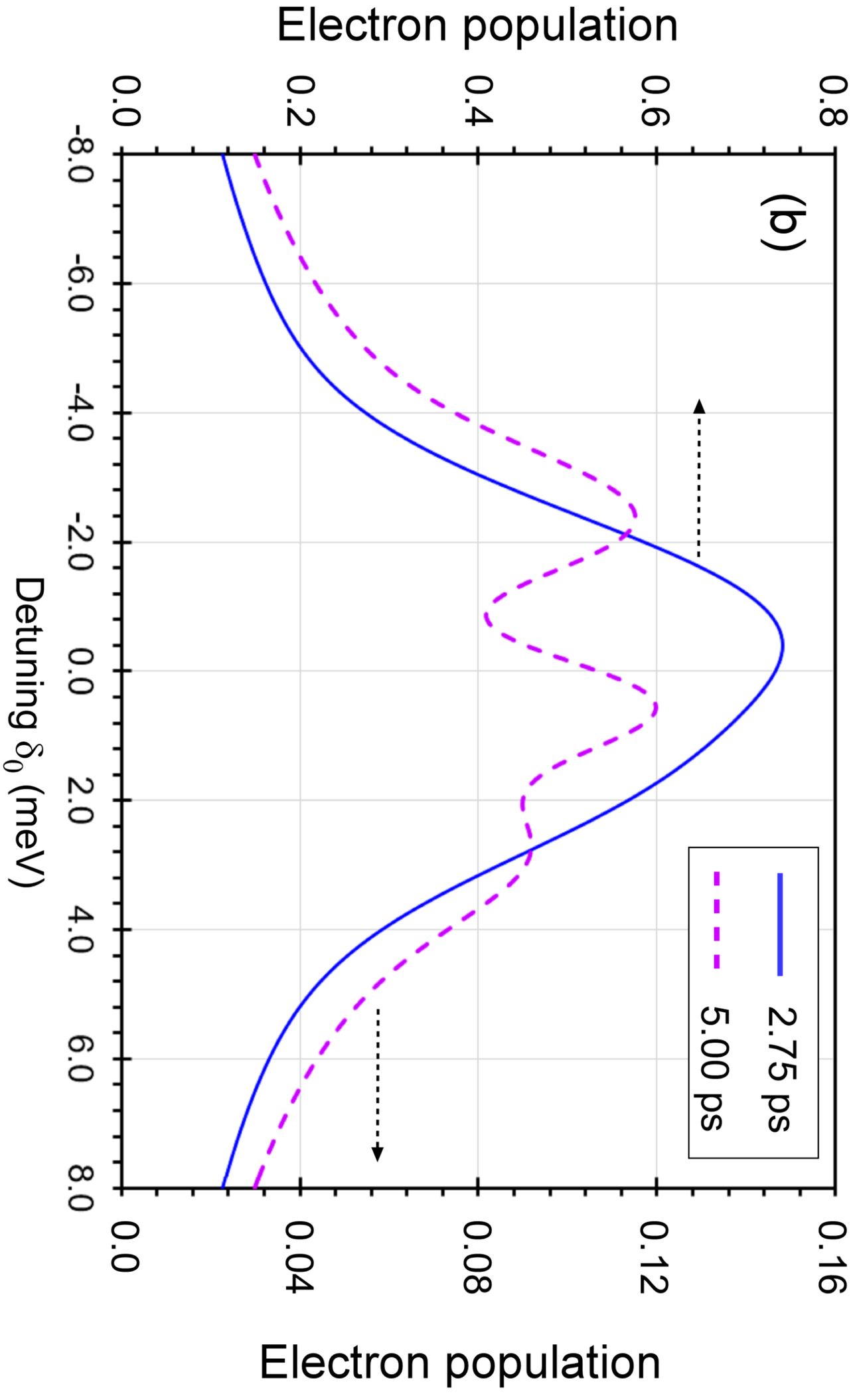

AIP Publishing

Journal of Applied Physics

ACCEPTED MANUSCRIPT

This is the author's peer reviewed, accepted manuscript. However, the online version of record will be different from this version once it has been copyedited and typeset.
PLEASE CITE THIS ARTICLE AS DOI: 10.1063/5.0081067

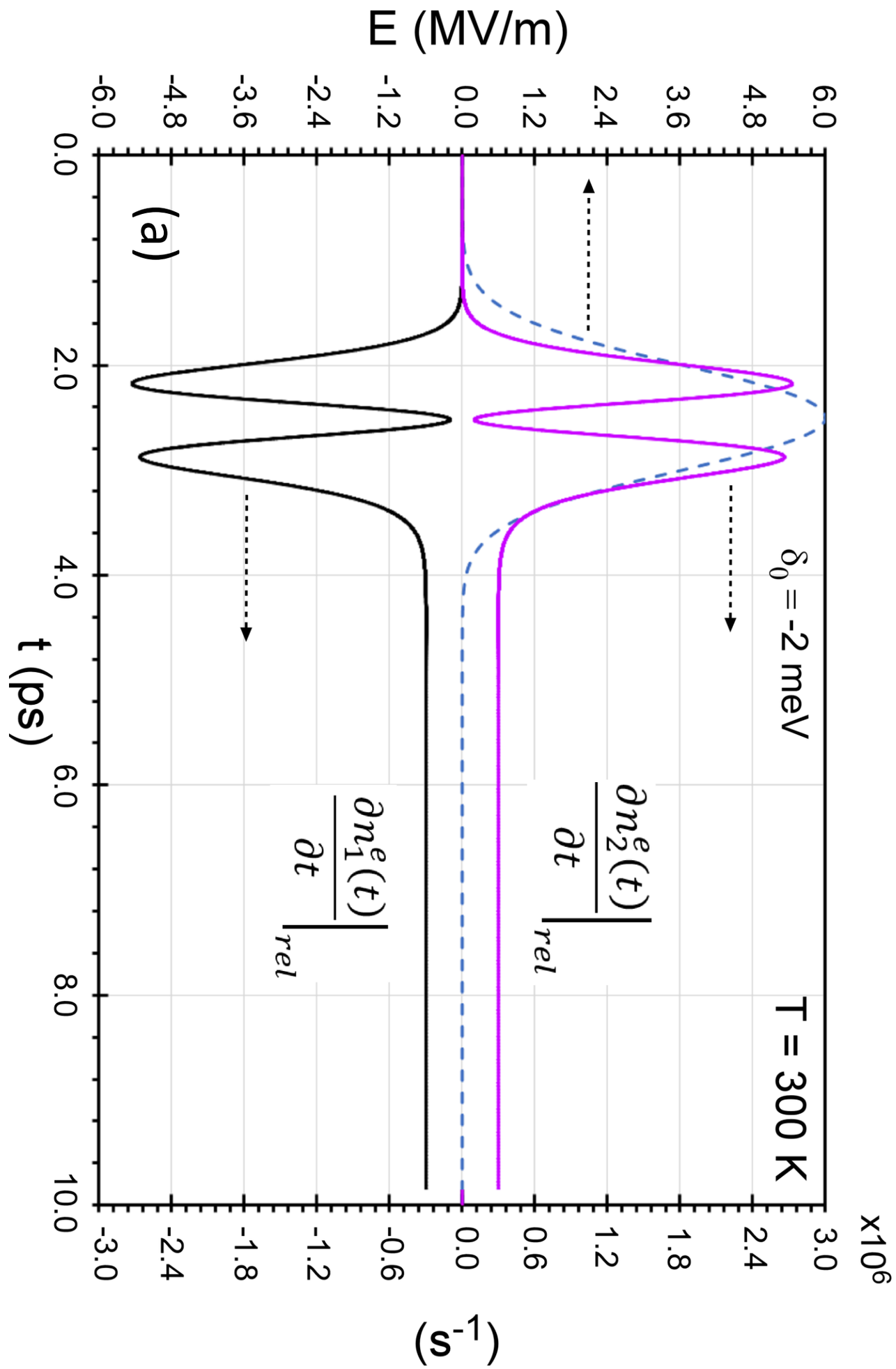

AIP Publishing

Journal of Applied Physics

ACCEPTED MANUSCRIPT

This is the author's peer reviewed, accepted manuscript. However, the online version of record will be different from this version once it has been copyedited and typeset.
PLEASE CITE THIS ARTICLE AS DOI: 10.1063/5.0081067

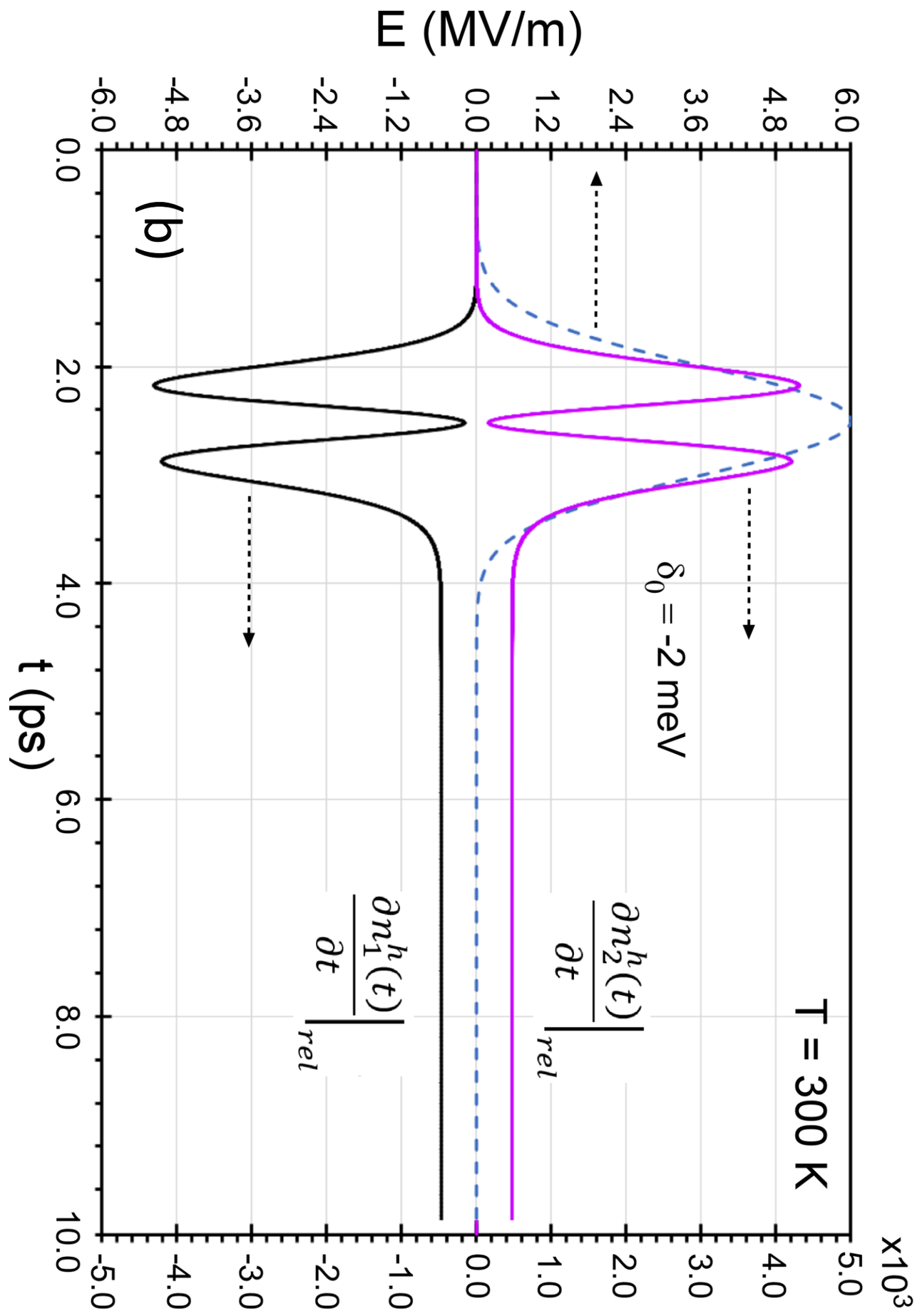

AIP Publishing

Journal of Applied Physics

ACCEPTED MANUSCRIPT

This is the author's peer reviewed, accepted manuscript. However, the online version of record will be different from this version once it has been copyedited and typeset.
PLEASE CITE THIS ARTICLE AS DOI: 10.1063/5.0081067

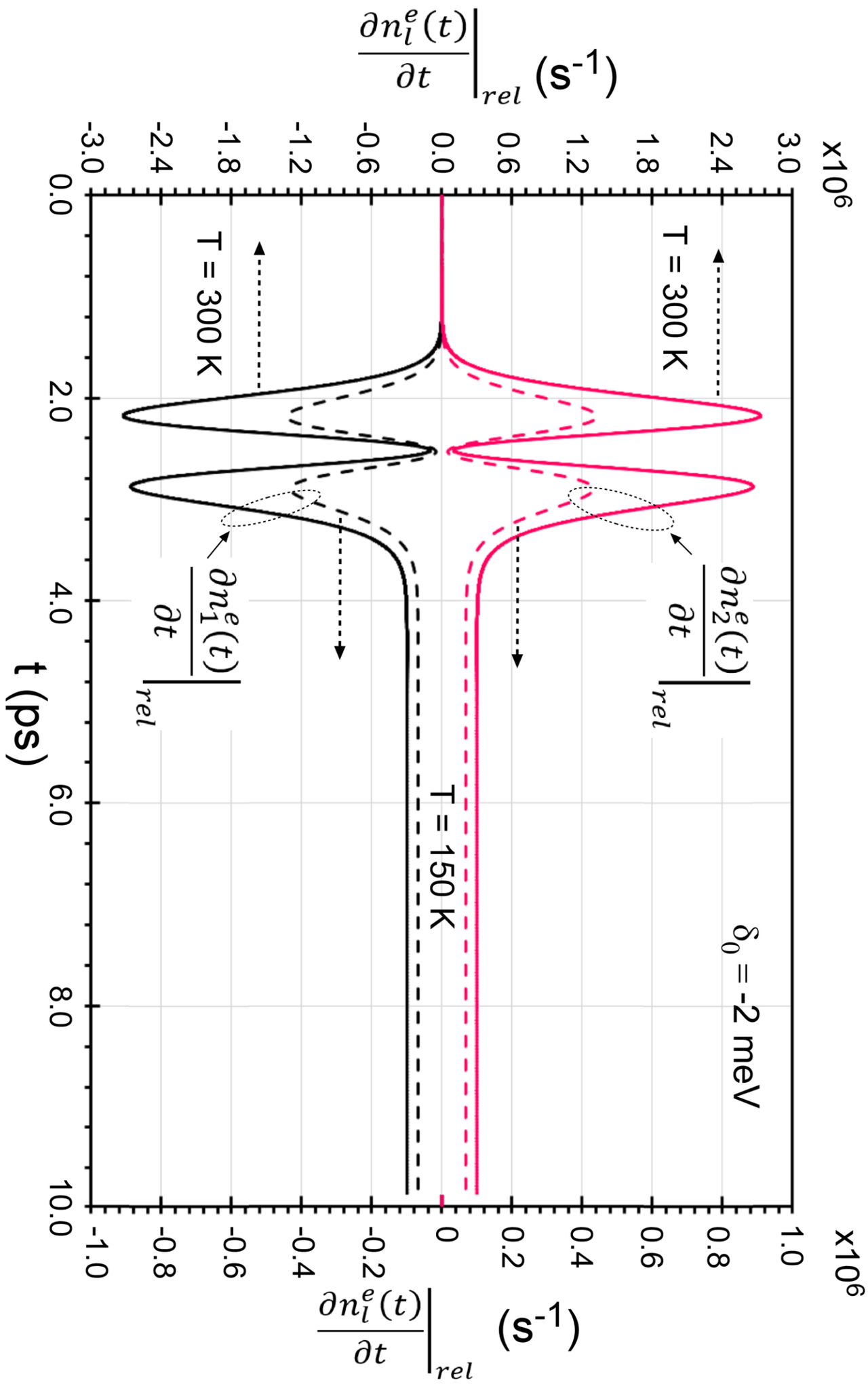

ACCEPTED MANUSCRIPT

Journal of Applied Physics

AIP Publishing

This is the author's peer reviewed, accepted manuscript. However, the online version of record will be different from this version once it has been copyedited and typeset.
PLEASE CITE THIS ARTICLE AS DOI: 10.1063/5.0081067

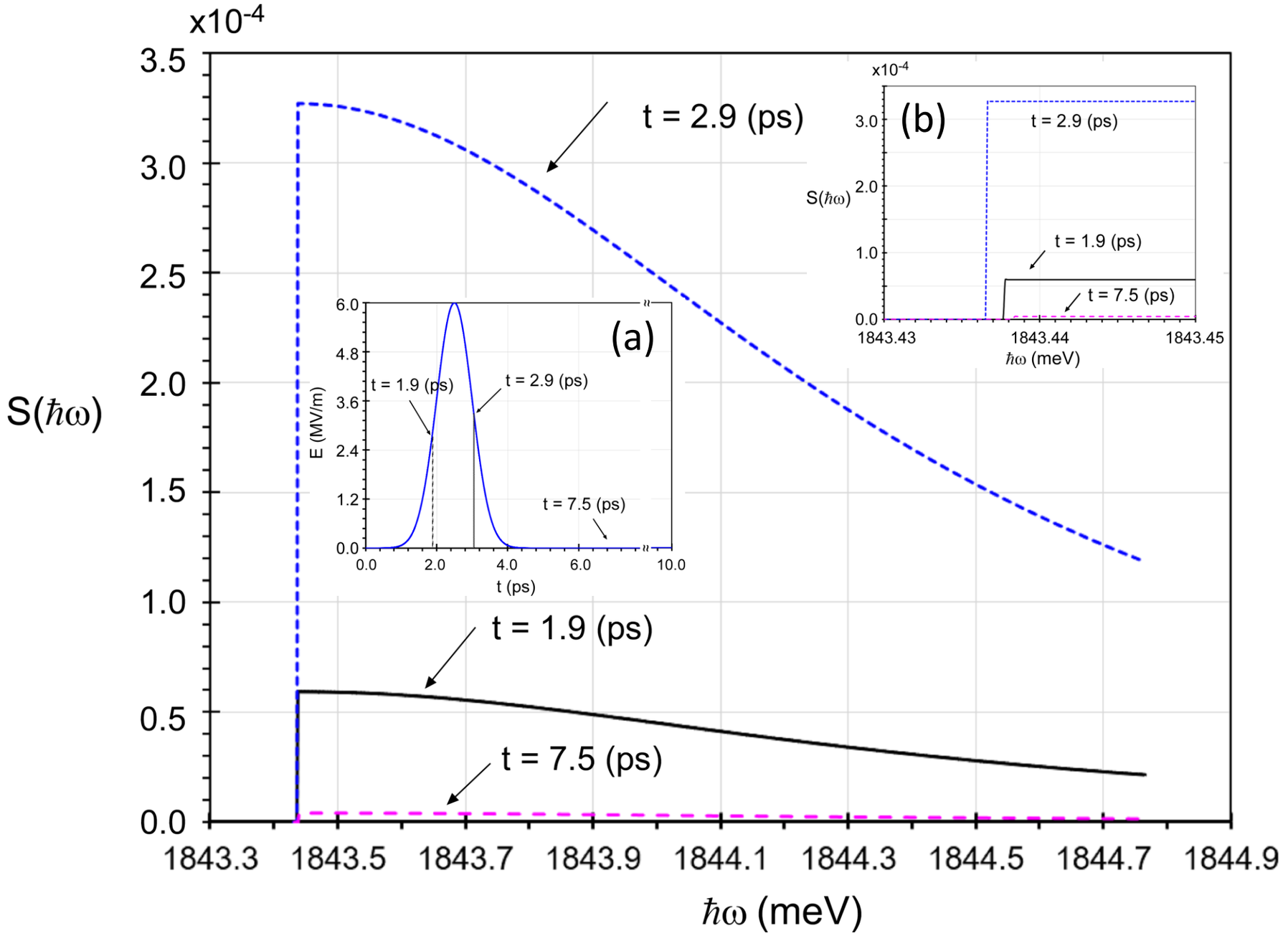

AIP Publishing
Journal of Applied Physics
ACCEPTED MANUSCRIPT

This is the author's peer reviewed, accepted manuscript. However, the online version of record will be different from this version once it has been copyedited and typeset.
PLEASE CITE THIS ARTICLE AS DOI: 10.1063/5.0081067

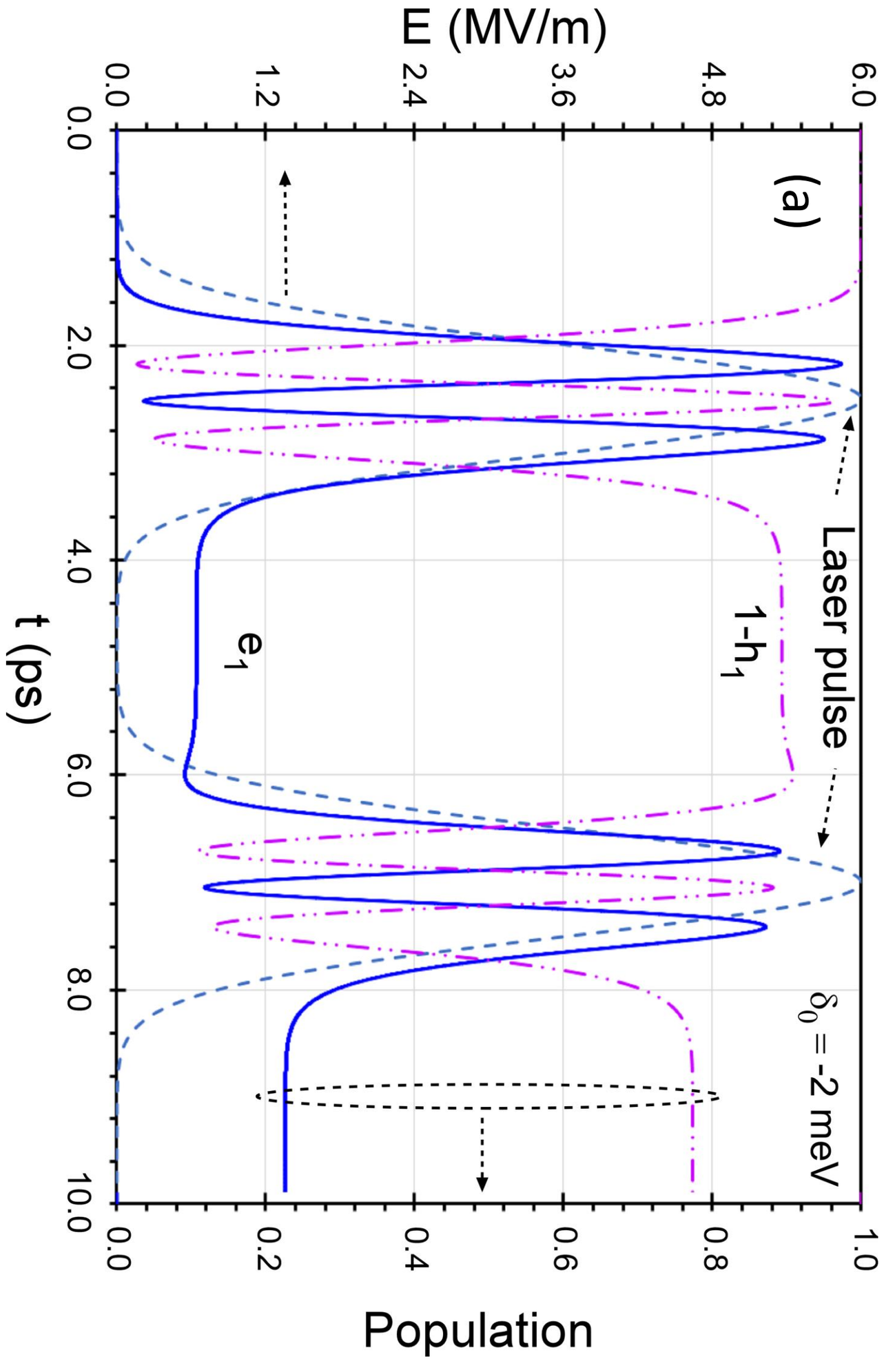

AIP Publishing

Journal of Applied Physics

ACCEPTED MANUSCRIPT

This is the author's peer reviewed, accepted manuscript. However, the online version of record will be different from this version once it has been copyedited and typeset.
PLEASE CITE THIS ARTICLE AS DOI: 10.1063/5.0081067

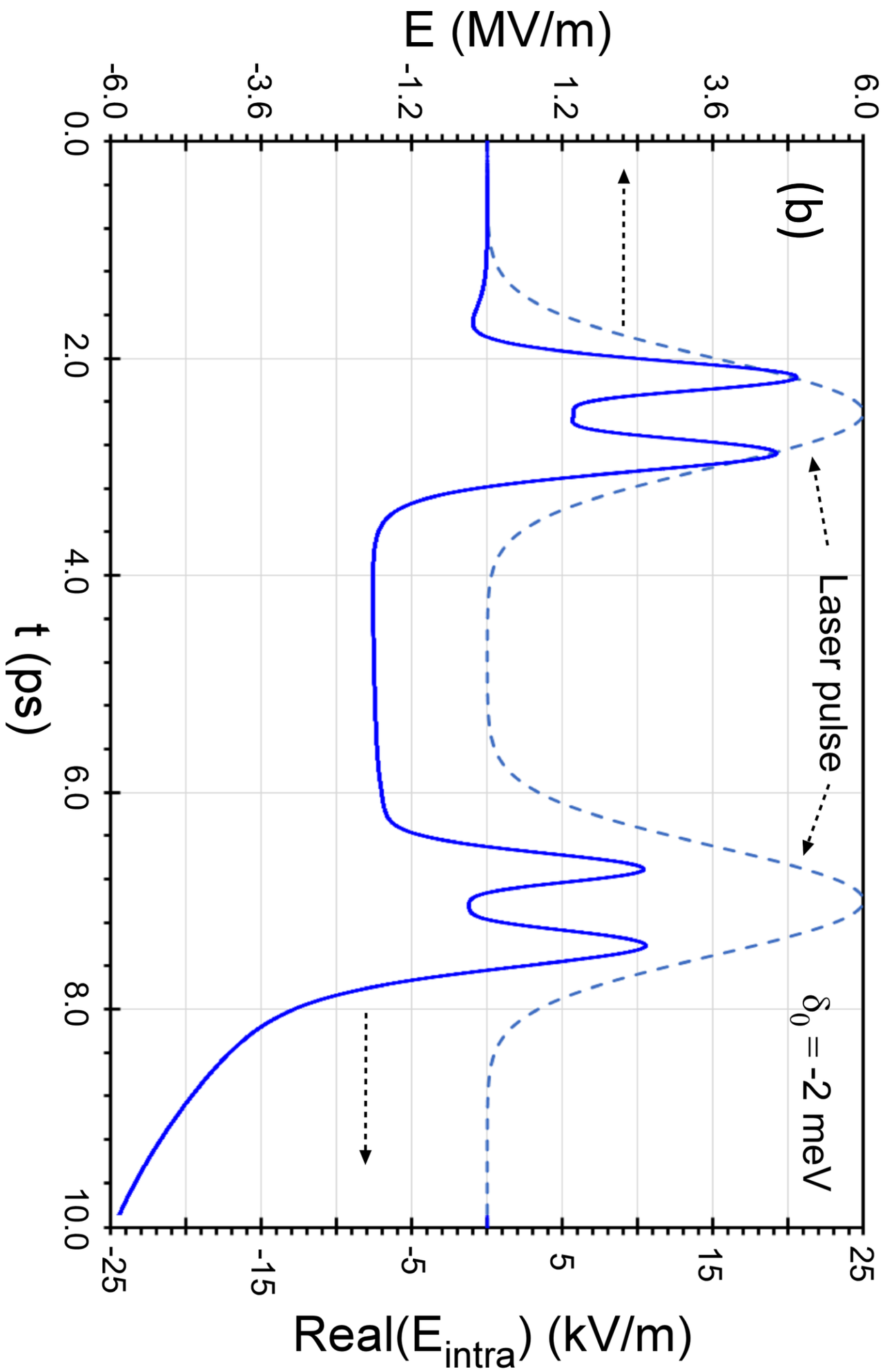

AIP Publishing
Journal of Applied Physics
ACCEPTED MANUSCRIPT

This is the author's peer reviewed, accepted manuscript. However, the online version of record will be different from this version once it has been copyedited and typeset.
PLEASE CITE THIS ARTICLE AS DOI: 10.1063/5.0081067

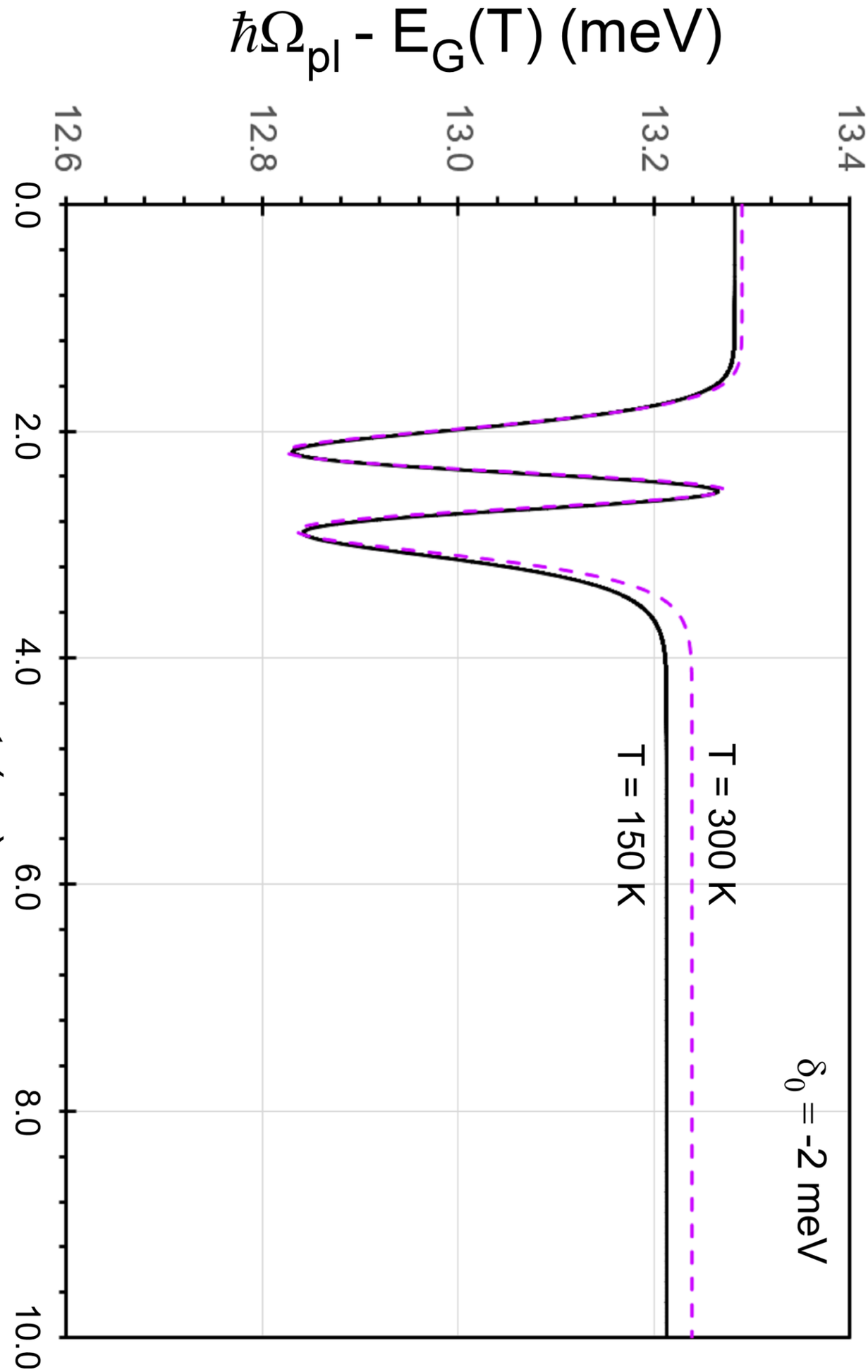

AIP Publishing

Journal of Applied Physics

ACCEPTED MANUSCRIPT

This is the author's peer reviewed, accepted manuscript. However, the online version of record will be different from this version once it has been copyedited and typeset.
PLEASE CITE THIS ARTICLE AS DOI: 10.1063/5.0081067

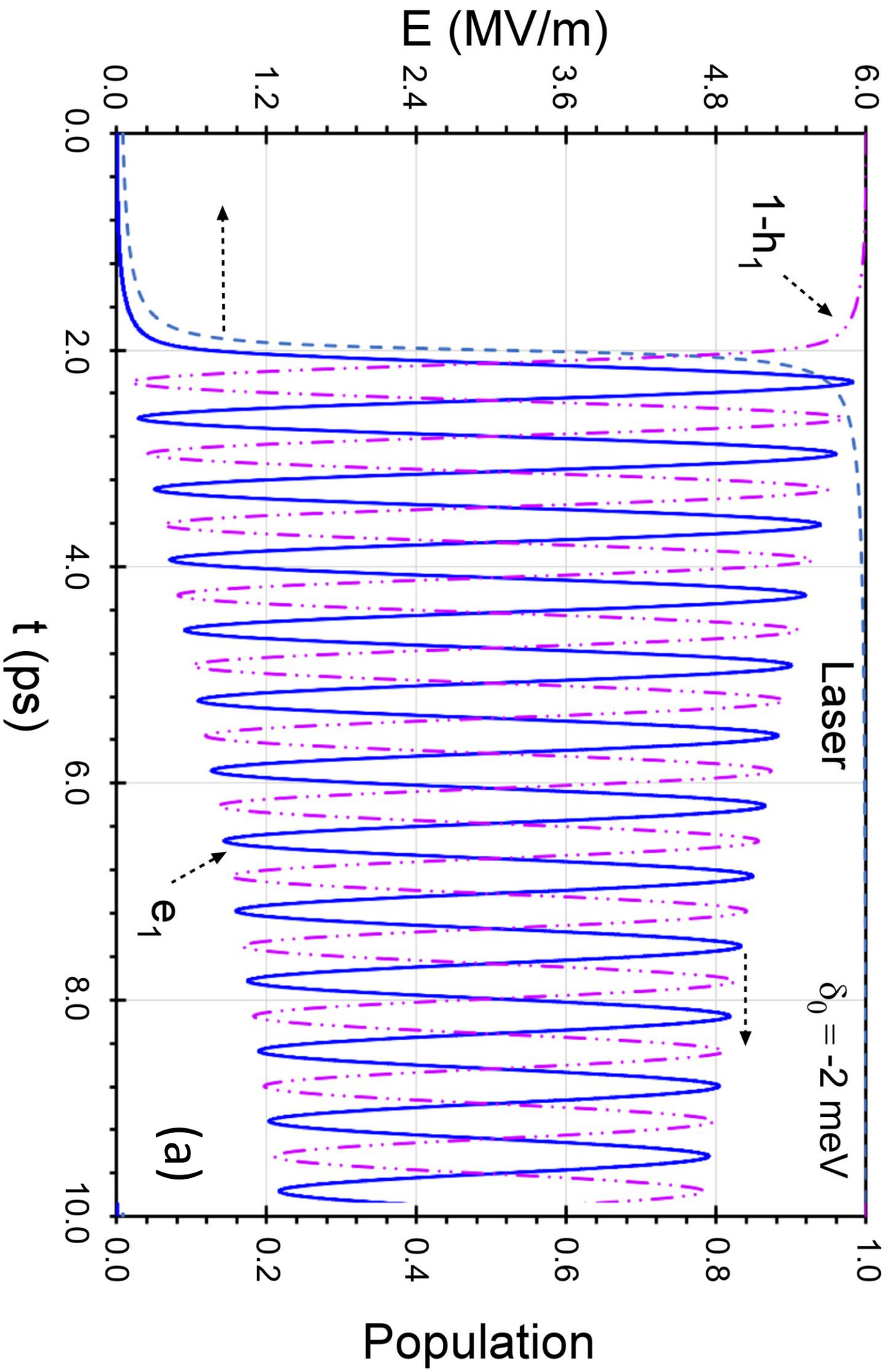

AIP Publishing
Journal of Applied Physics
ACCEPTED MANUSCRIPT

This is the author's peer reviewed, accepted manuscript. However, the online version of record will be different from this version once it has been copyedited and typeset.
PLEASE CITE THIS ARTICLE AS DOI: 10.1063/5.0081067

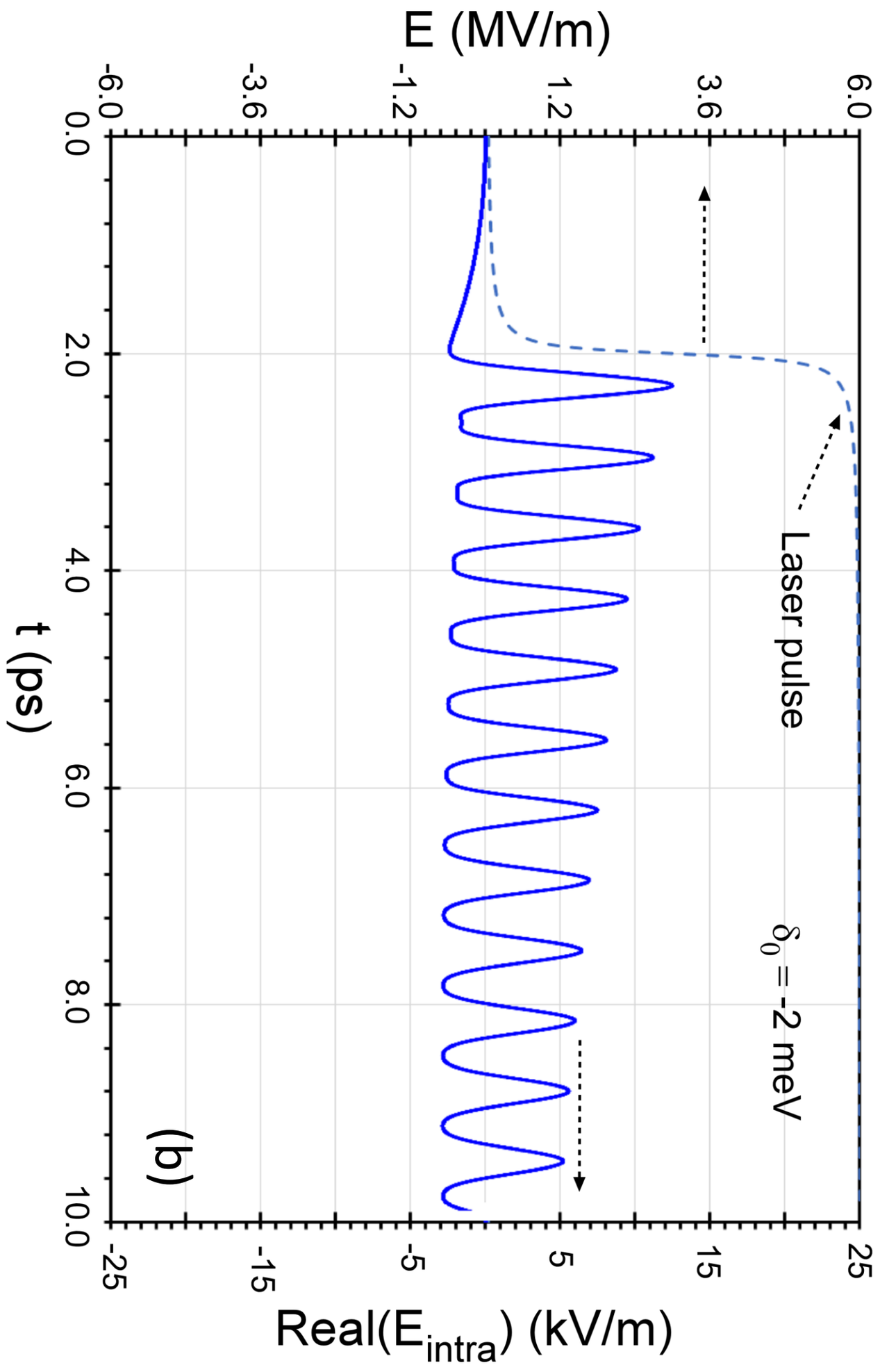

Journal of Applied Physics

ACCEPTED MANUSCRIPT

This is the author's peer reviewed, accepted manuscript. However, the online version of record will be different from this version once it has been copyedited and typeset.

PLEASE CITE THIS ARTICLE AS DOI: 10.1063/5.0081067

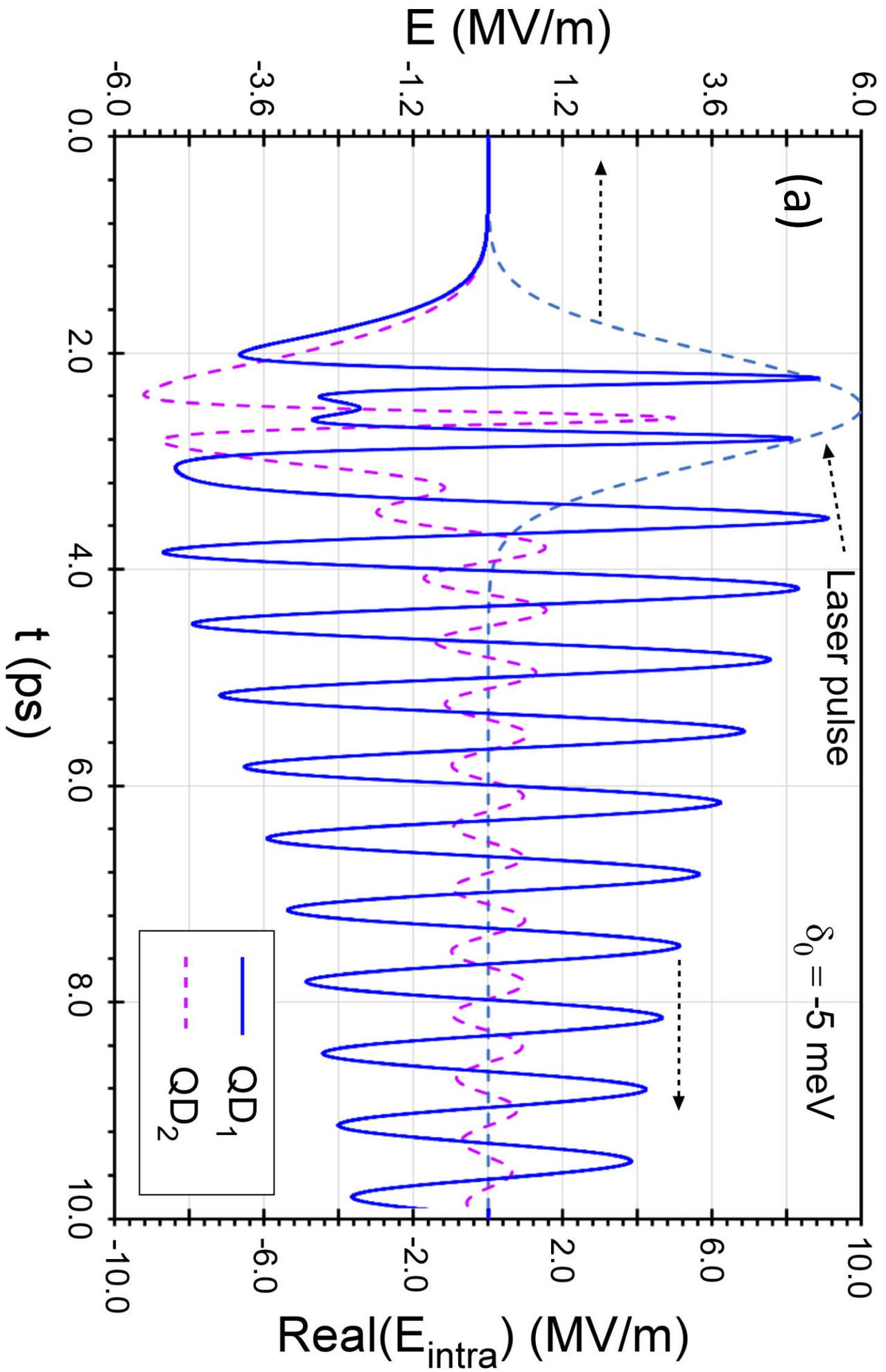

AIP Publishing
Journal of Applied Physics
ACCEPTED MANUSCRIPT

This is the author's peer reviewed, accepted manuscript. However, the online version of record will be different from this version once it has been copyedited and typeset.
PLEASE CITE THIS ARTICLE AS DOI: 10.1063/5.0081067

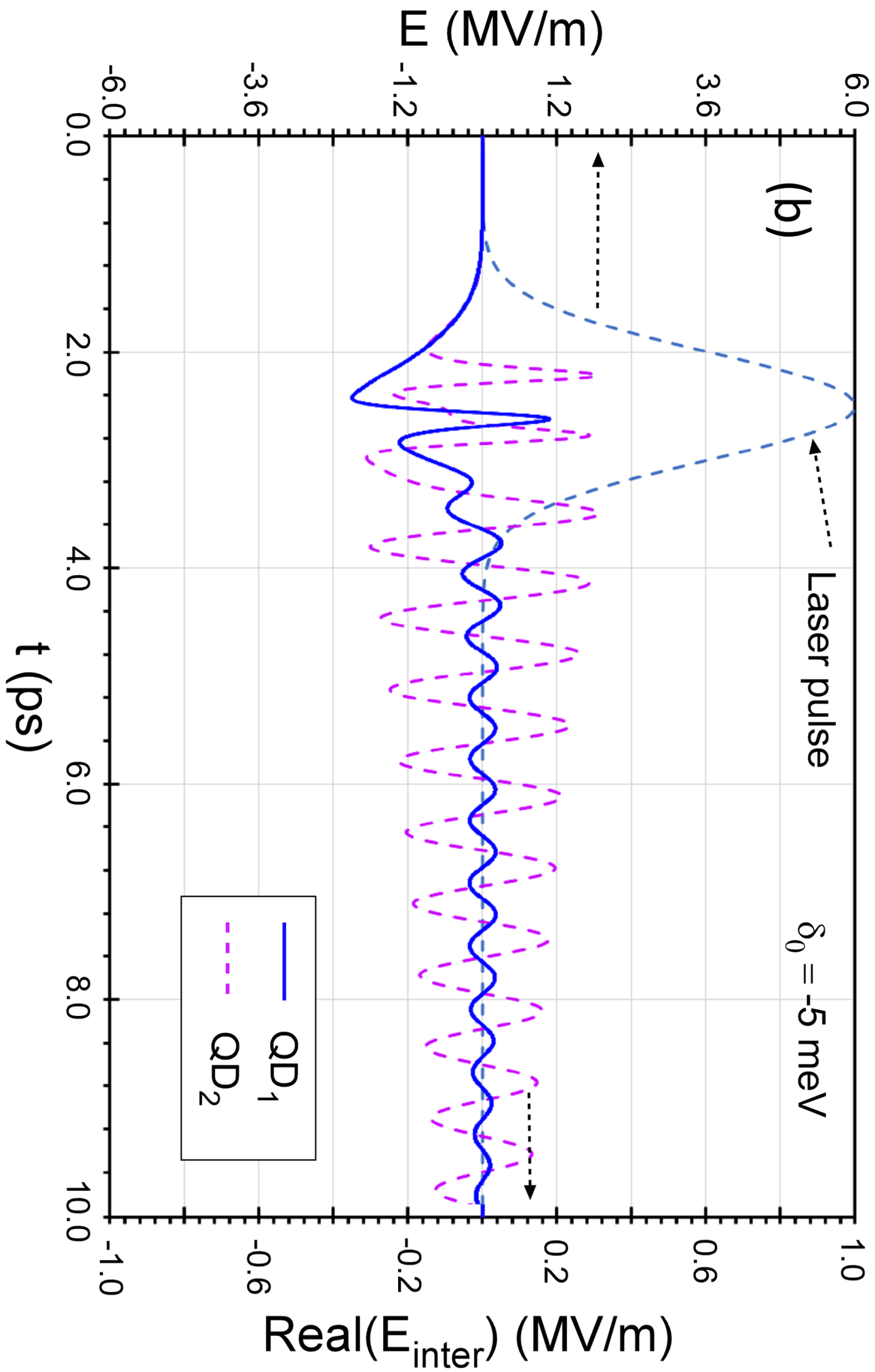

ACCEPTED MANUSCRIPT

This is the author's peer reviewed, accepted manuscript. However, the online version of record will be different from this version once it has been copyedited and typeset.
PLEASE CITE THIS ARTICLE AS DOI: 10.1063/5.0081067

Journal of Applied Physics

AIP Publishing

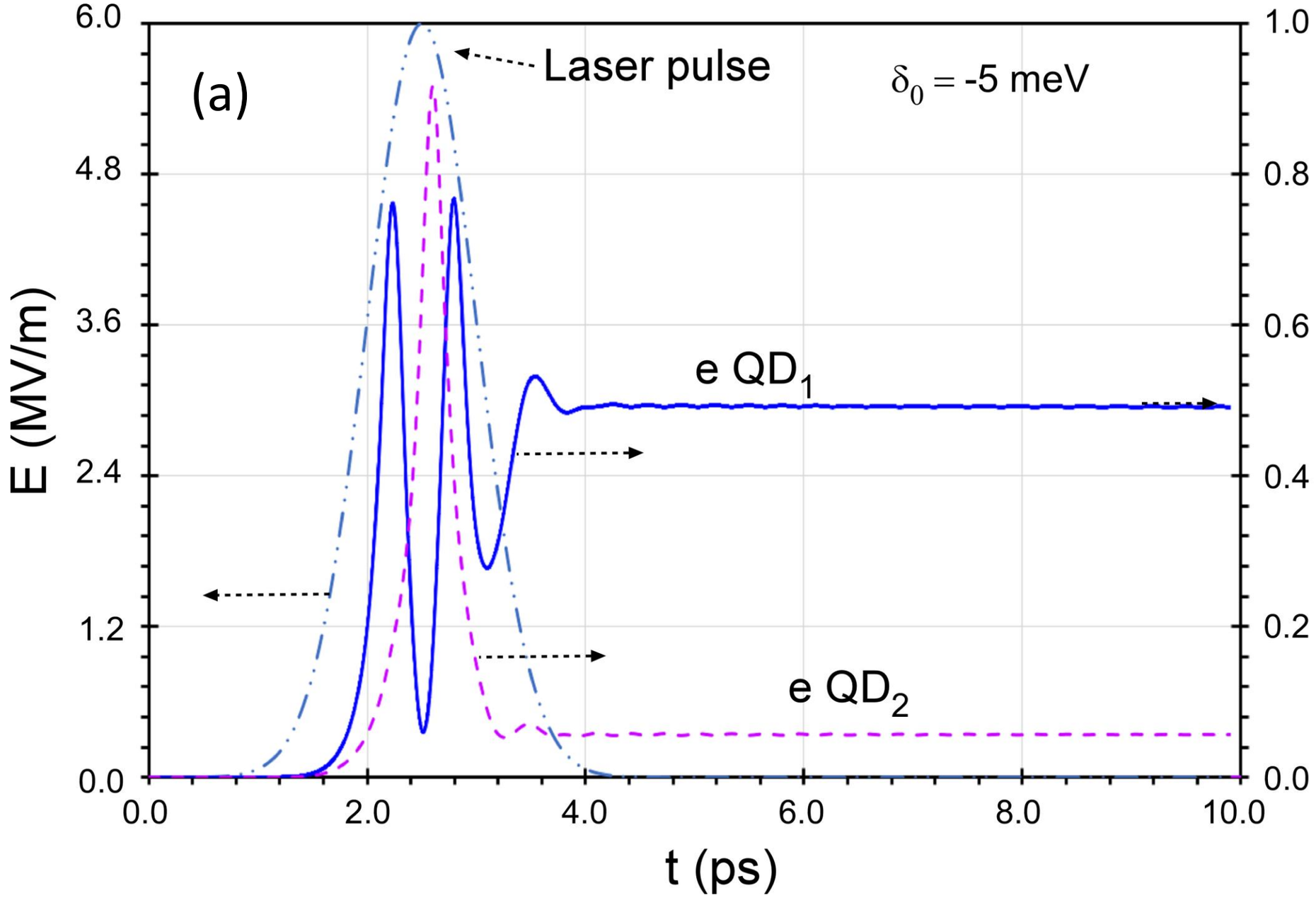

AIP Publishing
Journal of Applied Physics
ACCEPTED MANUSCRIPT

This is the author's peer reviewed, accepted manuscript. However, the online version of record will be different from this version once it has been copyedited and typeset.
PLEASE CITE THIS ARTICLE AS DOI: 10.1063/5.0081067

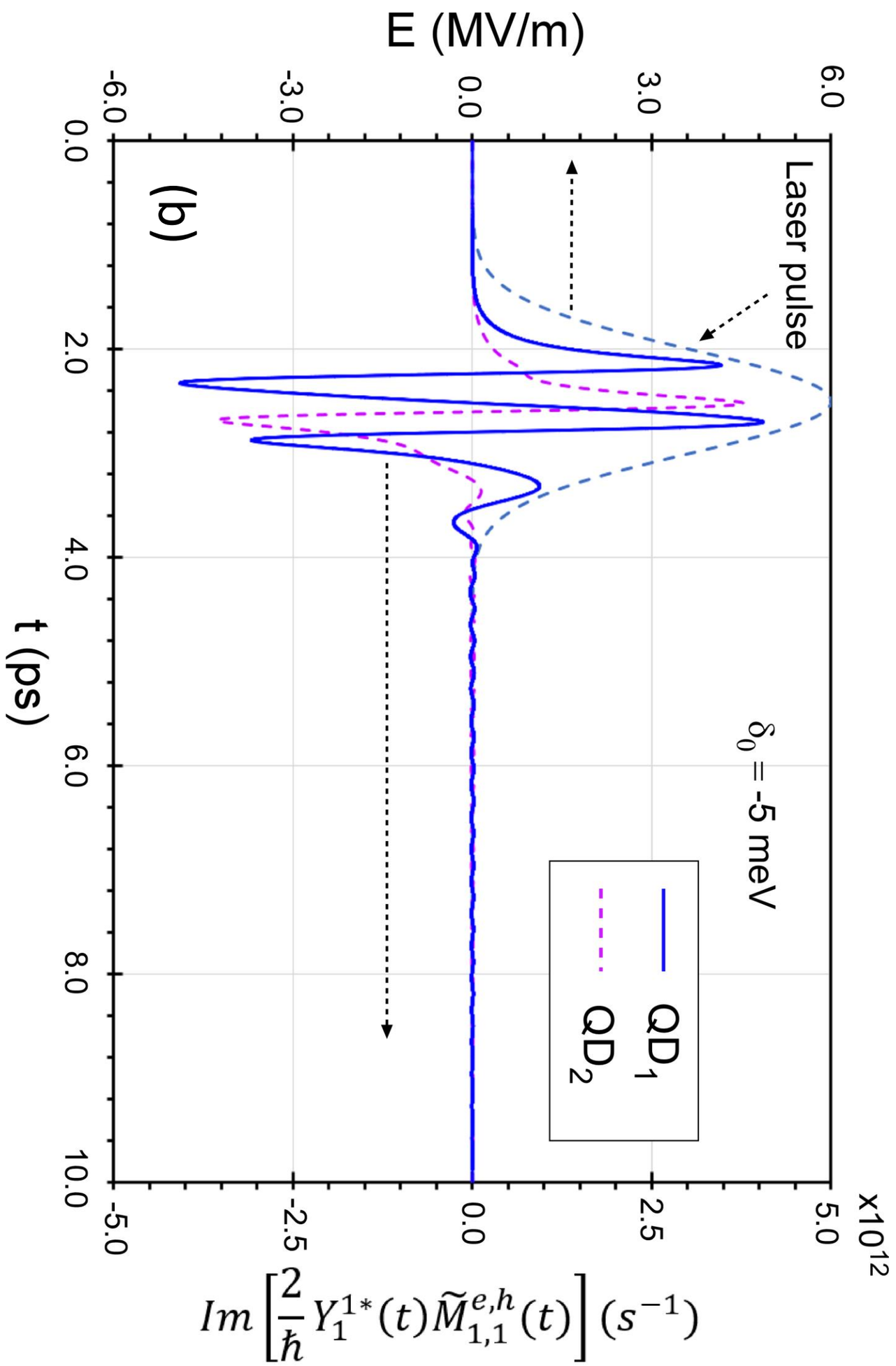

AIP Publishing

Journal of Applied Physics

ACCEPTED MANUSCRIPT

This is the author's peer reviewed, accepted manuscript. However, the online version of record will be different from this version once it has been copyedited and typeset.
PLEASE CITE THIS ARTICLE AS DOI: 10.1063/5.0081067

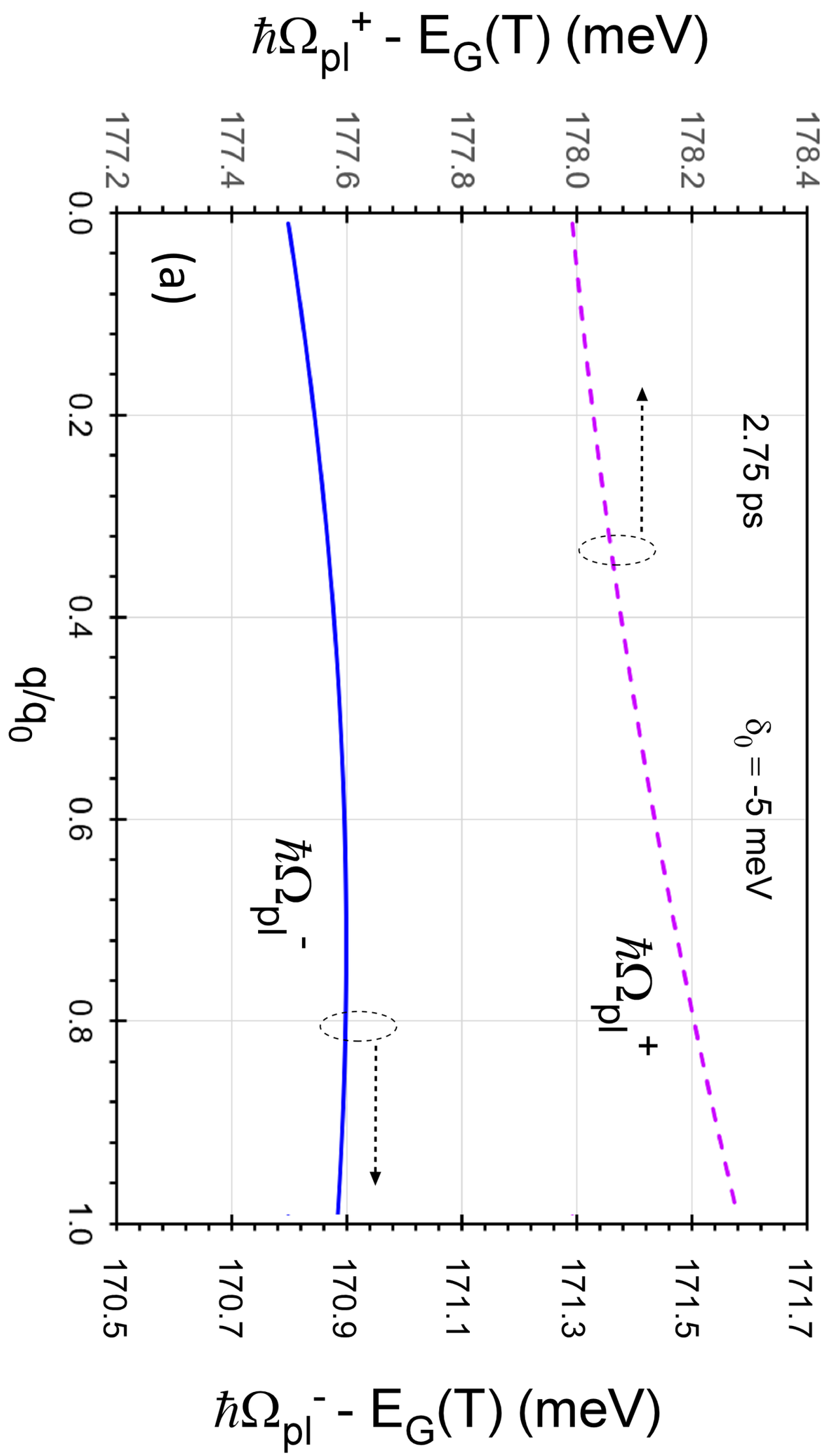

AIP Publishing
Journal of Applied Physics
ACCEPTED MANUSCRIPT

This is the author's peer reviewed, accepted manuscript. However, the online version of record will be different from this version once it has been copyedited and typeset.
PLEASE CITE THIS ARTICLE AS DOI: 10.1063/5.0081067

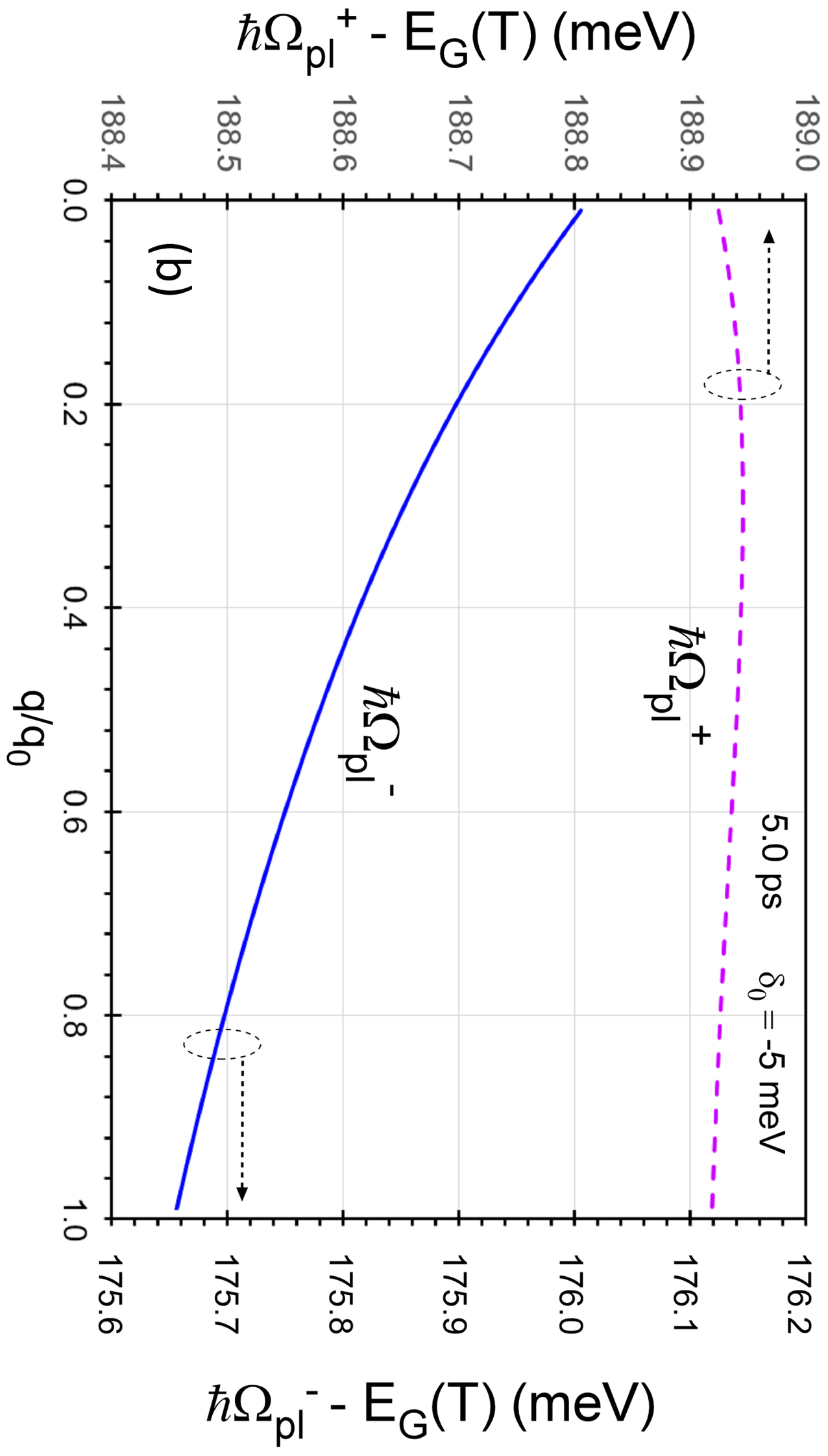

AIP Publishing
Journal of Applied Physics
ACCEPTED MANUSCRIPT

This is the author's peer reviewed, accepted manuscript. However, the online version of record will be different from this version once it has been copyedited and typeset.
PLEASE CITE THIS ARTICLE AS DOI: 10.1063/5.0081067

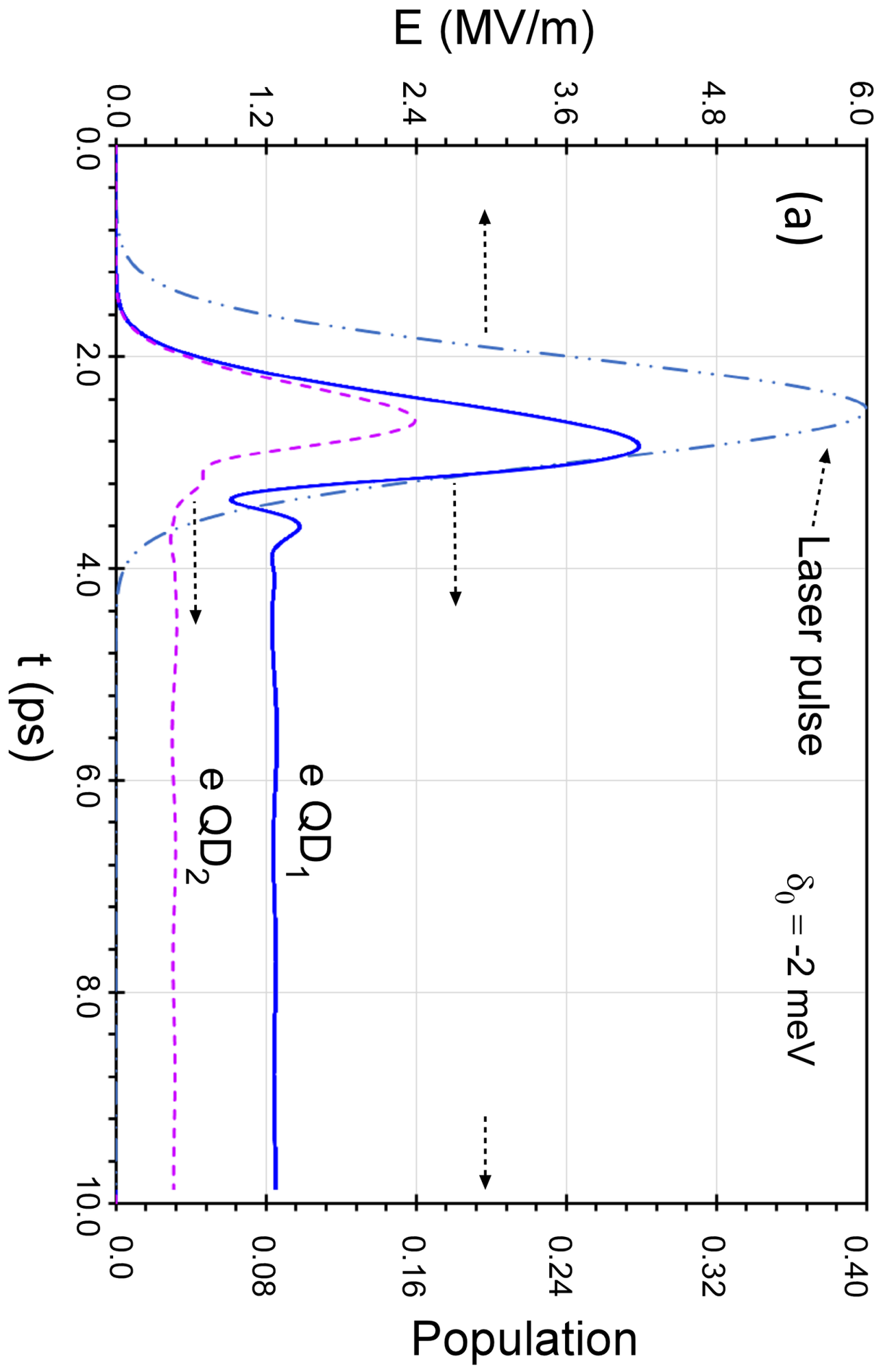

AIP Publishing

Journal of Applied Physics

ACCEPTED MANUSCRIPT
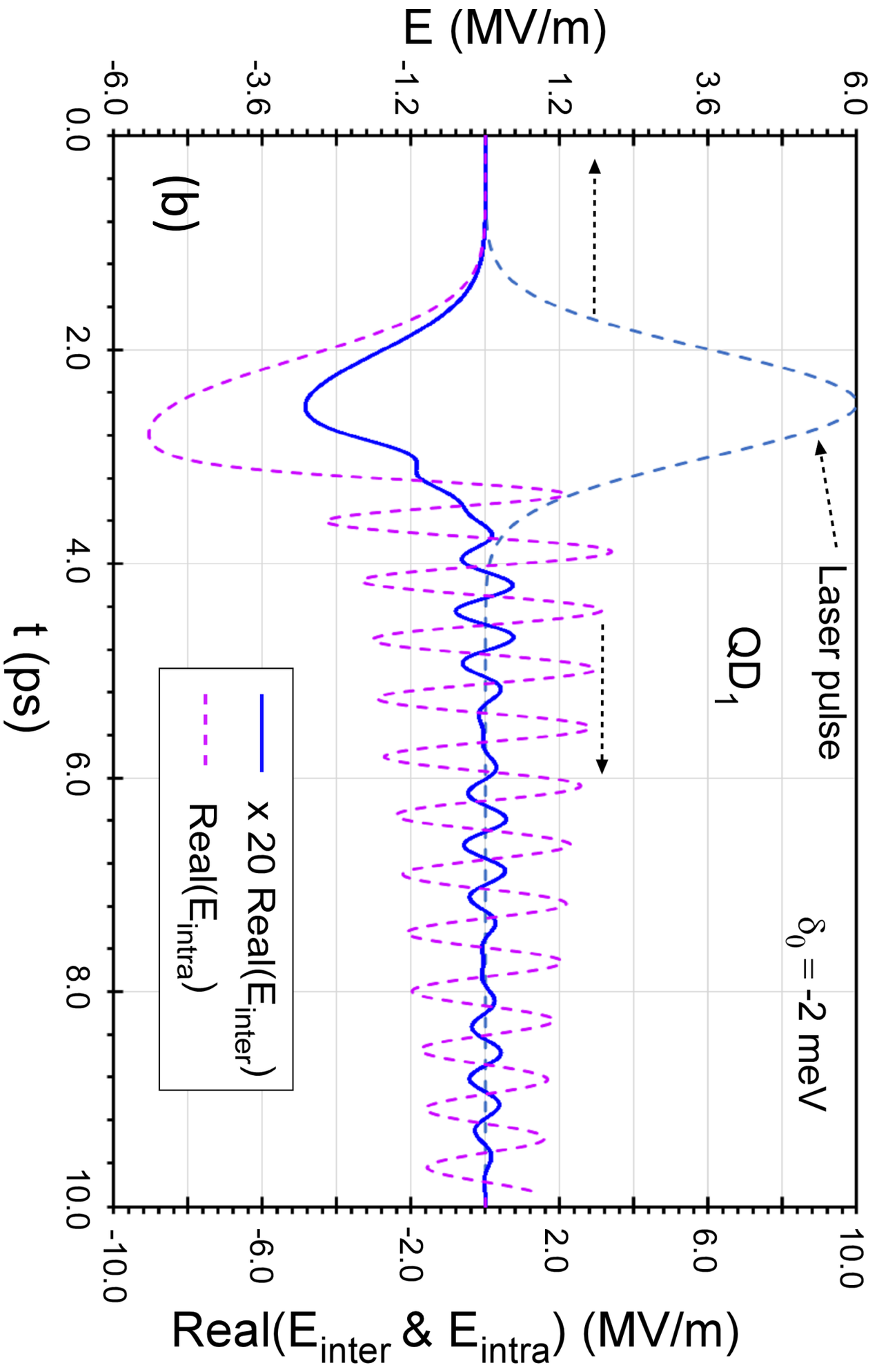
This is the author's peer reviewed, accepted manuscript. However, the online version of record will be different from this version once it has been copyedited and typeset.
PLEASE CITE THIS ARTICLE AS DOI: 10.1063/5.0081067